WEIZMANN INSTITUTE OF SCIENCE

Department of Environmental Sciences and Energy Research

Thesis for the degree

Doctor of Philosophy

חבור לשם קבלת התואר

דוקטור לפילוסופיה

By

Naama Raz Yaseef

מאת

נעמה רז יסיף

הפרדת שטף האוופוטרנספירציה למרכיביו ביער צחיח למחצה (יער יתיר)

Partitioning the evapotranspiration flux of the Yatir semi-arid forest

Advisor

Prof. Dan Yakir

מנחה

פרופ' דן יקיר

September 2008

אלול, תשס"ח

Submitted to the Scientific Council

Weizmann Institute of Science

Rehovot, Israel

מוגש למועצה המדעית

מכון ויצמן למדע

רחובות, ישראל

This work has been conducted under the supervision of

Prof. Dan Yakir

Department of Environmental Sciences and Energy Research
Weizmann Institute of Science
Rehovot, Israel

Declaration

All group members associated with the Yatir Forest flux tower research site have been involved in the maintenance and operation of the flux tower, under the direction of Dr. Eyal Rotenberg. The database of flux and meteorological data is maintained by Dr. Ruthi Ben-Meir. Computation of the gross primary production flux was preformed by Tamar Afik and involved definitions prepared by Dr. Kadmiel Maseyk and Dr. Jose M. Grunzweig. My calculations of throughfall precipitation were based on the relations defined for Yatir by Dr. Yonit Shachnovich. Installation, calibration, maintenance and flux calculation of whole tree transpiration based on Heat Pulse Velocity type sensors and Granier type sensors was preformed by Dr. Gabriel Schiller and Dr. Shabtai Cohen, respectively.
Interpretation and analysis of the data is my own.

All other work presented in this thesis is also my own.

Naama Raz Yaseef

Acknowledgements

This work would not have been possible without the support and encouragement of Prof. Dan Yakir, under whose supervision I chose this topic and began the thesis. Dan has assisted me in numerous ways, starting from early phases of research definition, continuing with problem solving and dead-ends unraveling, until finally teaching me how a scientific essay should properly be written. At the same time, Dan always encouraged to develop my own ideas and provided me with enough space to do so.

I would also like to thank my advisory committee, Prof. Brian Berkowitz, Prof. Avihai Danon and Dr. Shmuel Assouline, for their interest in my work, constructive ideas and advise on where to define boundaries for the scope of the thesis. I have had the benefit of fruitful and inspiring discussions with Prof. Pedro Berliner of the Ben-Gurion University, Dr. Shabtai Cohen and Dr. Gabriel Schiller of the Volcani Institute and Prof. Aaron Yair of the Hebrew University, who was my former advisor and continued to support me during this research. I express my gratitude to Dr. Arie Nadler from the Volcani Institute, who served me as a TDR specialist and guided me through the crucial phases of calibration and installation.

I thank former and current members of our group: Jose, Buckhart, Debbie, Ilia, Leon, Keren, Tamar, Amir and Tamir. They have not only assisted me and educated me in their areas of scientific expertise, but have also made my time more enjoyable. Special acknowledgements are given to Dr. Eyal Rotenberg, who agreed to go over parts of my thesis and has done so with much attention, and for his part in the flux tower, which enabled me to execute my research.

Various people around the department have been indispensable and I am happy to thank them for their help. Here they are, and not necessarily in order of importance: Ruthi, Emanuela, Jaacob, Hagai, Avraham, Neomi, Dalia, Hila, Vadim and Yakir.

I deeply thank my parents, who have always been encouraging and supporting. I couldn't have accomplished this mission without their help and believe in me.

My kids – Ilay, Ronna and Yannay, who have made my life worth living.

And finally, Ofer, my companion for life and my inspiration. Thank you for all.

Summary

Global climate change is predicted to be associated with both reduced total precipitation and increased storm intensities over many regions, including the entire Mediterranean region. The combined effects are difficult to predict and can greatly benefit from studies in dry forest ecosystems exposed to large inter-annual climatic variations. In such ecosystems, the evapotranspiration flux (ET) is the major component of the hydrological cycle and often balance most precipitation (P). Therefore, partitioning ET to its components, plant transpiration (T) and soil evaporation (E), is critical for understanding water availability for carbon assimilation, soil respiration, and water use efficiency, as well as for ecosystem and water management.

We report on a four-year study (2003-2007) in the Yatir semi-arid pine forest in southern Israel (40 years old *P. halepensis*; LAI=1.5; mean precipitation 280 mm yr^{-1}) that showed resistance to seasonal draughts, and carbon uptake capability close to that of the global average for forests (GPP and NEE mean values of 850 and 230 gC yr^{-1} respectively). E was directly measured (bi-weekly 14 sites) using a modified soil respiration chamber (LI-COR). Soil water content (θ) was recorded in three pits with TDRs to depth of 130 cm. These measurements were combined with background, continuous measurements of ET (eddy flux measurements), T (heat-pulse measurements), and meteorological measurements (soil and air temperatures, VPD, radiation PAR or R_n and wind speed).

Large spatial variability in E (daily SD between sites up to ±47%) was correlated best with PAR and θ. The proportion of forest-floor-shaded-fraction (SF) was a function of tree height, canopy width and tree density, and simulating SF provided a basis for estimating E/ET. Seasonal patterns in E and T were differential: E peaked twice - during early and late winter (up to 0.80 mm d^{-1}) and T peaked in spring (up to 1.20 mm d^{-1}). Low E (0.10 mm day^{-1}) was measured during mid winter (daily max. temp. below 15˚C) and low E and T were measured in summer (θ below 10%). E correlated on the seasonal time-scale with environmental parameters: with θ during mostly in the wetting and drying seasons, and with R_n during winter and the dry summer. The partitioning of ET was influenced by precipitation patterns. 82% of rain events were <5 mm, keeping only the upper soil layer θ above ~20% during most of the wet season. In contrast, θ of the root zone (15-130 cm) depended on larger, less

common rainstorms. High soil water holding capacities resulted in increased θ at depth only from mid-winter, but maintained in some cases throughout the dry summer. Accordingly, the E/ET ratio varied seasonally with maximum during early winter, and minimum during spring. Ecosystem water use efficiency (WUE_e) correlated better with the ratio P/RD (RD=number of rainy days) than with P, presumably because P/RD serves as indicator of precipitation patterns. A complete ecosystem hydrological budget was constructed for Yatir indicating that, on average, P was supplemented by vapor adsorption in late summer (5%) and was balanced by interception (11%), soil storage runoff and deep drainage (6%), E (36%) and T (45%).

This study provides the first comprehensive hydrological budget for a semi-arid pine forest. The results suggest that increased storm intensity could at least partly compensate for decreased total precipitation in this region, contributing to the maintenance of relatively high productivity of the forest under the global warming scenarios predicted for this region.

הגשם, המאופיין באזור המחקר בממטרים קטנים ולא רציפים (82% מהאירועים קטנים מ-5 מ"מ), המרטיבים את שכבת הקרקע העליונה בלבד אך מסוגלים לשמור על לחות גבוהה זו (מעל 20%) במהלך כל עונת הגשמים. בניגוד לכך, לחות הקרקע בבית השורשים (15-130 ס"מ) היתה תלויה באירועים נדירים יותר של סופות גשם גדולות. יכולת התאחיזה הגבוהה של הקרקעות גרמה לכך שלחות הקרקע עלתה בעומק החלה לעלות רק באמצע החורף, אך לעיתים נשמרה גבוהה לאורך כל הקיץ. בהתאם לכך, היחס ET/E השתנה עונתית והתאפיין בערכים מירביים בתחילת החורף ונמוכים באביב. יעילות ניצול המים ברמה המערכתית (WUE_e) היה בהתאמה גבוהה עם כמות הגשם השנתית מחולקת במספר ימי הגשם (יחס זה מהווה ביטוי לאופי ולא רק לכמות הגשמים השנתיים). סגירה של המאזן ההדרולוגי הושגה עבור יער יחיר והצביעה על כך שבממוצע, הגשם השנתי התאזן על ידי מים הנקלטים על גבי העלוויה (11%), מים המאוחסנים זמנית בקרקע, אובדים כנגר עילי או כחלול עמוק (6%), מים המתאדים מהקרקע (36%) ובתהליך דיות העצים (45%). תוספת מסויימת לגשם התקבלה על ידי תהליך ספיחה בקרקע היבשה (5%).

המחקר מספק מאזן מקיף ראשוני של המחזור ההדרולוגי ביער צחיח למחצה. התוצאות מציעות כי הגברת עוצמות הגשם יכולה, לפחות באופן חלקי, לפצות על ההקטנה הכללית בכמויות הגשם באיזורינו, דבר המאפשר לשמור על רמות ייצור גבוהות יחסית של היער, למרות תחזיות להתחממות האזור כפועל יוצא של ההתחממות העולמית.

סיכום

שינויי אקלים גלובלים צפויים לגרום להקטנת כמויות הגשם ובמקביל להגדלת עוצמות הגשם באזורים רבים בעולם ובכללם אזור המזרח התיכון כולו. קשה לחזות את ההשפעה המשולבת של שינויים אלו ולכן מחקרים המתבצעים ביערות צחיחים, הנחשפים להבדלי אקלים בין-שנתיים גדולים, עשויים לתרום רבות להבנת המערכת. ביערות צחיחים שטף האוופוטרנספירציה מהווה מרכיב עיקרי במחזור ההדרולוגי ולעיתים מתקרב בגודלו לכלל הגשם. אי לכך, הפרדת שטף האוופוטרנספירציה למרכיביו, דיות מצמחים ואידוי מהקרקע, הכרחי להבנת זמינות המים לצורך קיבוע פחמן, נשימת קרקע, יעילות ניצול המים וכן למטרות תכנון וניהול יערות.

אנו מדווחים על מחקר ארבע-שנתי (2003-2007) ביער יתיר, שהינו יער אורן שתול בדרום ישראל (גשם ממוצע של 280 מ"מ לשנה, מרבית העצים מזן *P. halepensis*, גיל היער כ-40 שנה, אינדקס שטח העלים (LAI) של 1.5), המראה עמידות לתנאי בצורת עונתית וקיבוע פחמן ברמה הקרובה לזו של הממוצע העולמי ליערות (קיבוע פחמן ראשוני (GPP) ויצור נטו ברמה המערכתית ((NEE של 850 ו-230 גרם פחמן דו חמצני לשנה, במקביל). אידוי מהקרקע נמדד ישירות על ידי תא למדידת נשימת קרקע (LI-COR) שעבר התאמה לצרכינו. המדידות החבצעו על גבי 14 טבעות קרקע שיצגו את השונות המרחבית של היער ונערכו פעם בשבועיים במהלך שנות המחקר, לקבלת ייצוג מתאים של עונות השנה. לחות הקרקע נמדדה בשלושה בורות שנחפרו עד לעומק של 130 ס"מ. מדידות אלו השתלבו עם מדידות רקע רציפות של אוווטרנספירציה (מגדל למדידת שטפים), דיות (שיטת הולכת החום) ולמדידות מטאורולוגיות שונות (טמפ' אוויר וקרקע, קרינה, מהירות רוח ומידת הרוויה של האטמוספרה (VPD)).

השונות המרחבית הגדולה שנמדד באידוי הקרקע (סטית תקן של עד 47%± בין 14הנקודות במהלך יום מדידה) קושרה לקרינה ולחות קרקע. שטח החלק המוצל מתחת לנוף היה תלוי בגובה העצים, ברוחב הצמרות ובצפיפות היער, והדמיות של אחוז הצל הווה בסיס לחישוב היחס ET/E כתלות במבנה היער. המגמות העונתית של הדיות והאידוי הראו הבדלים ברורים: האידוי היה מירבי בתחילת ובסוף החורף (עד 0.80 מ"מ ליום) בעוד ששטפי הדיות היו מירביים באביב (עד 1.20 מ"מ ליום). ערכי אידוי נמוכים נמדדו באמצע החורף (0.10 מ"מ ליום, במקביל לירידת הטמפ' היומית המירבית מתחת ל-15°) בעוד ששטפי דיות ואידוי נמוכים נמדדו בקיץ (בעת שהלחות היחסית היתה נמוכה מ-10%). התאמה גבוהה זוהתה בין האידוי ומאפיינים סביבתיים, כאשר לחות הקרקע היתה בעלת השפעה מירבית בתקופות ההרטבה וההתייבשות וקרינת השמש היתה משמעותית בעונה המוגבלת אנרגטית (חורף) ובקיץ. הפרדת שטף האוופוטרנספירציה נשלטה על ידי אופי

Table of Contents

Abbreviations

A	soil adsorption	mm (hr, d, yr)$^{-1}$
E	soil evaporation	mm (hr, d, yr)$^{-1}$
E_s	spatial averaged E	mm (hr, d, yr)$^{-1}$
E_{shade}	averaged E of the shaded collars	mm (hr, d, yr)$^{-1}$
E_{sun}	averaged E of the sun-exposed collars	mm (hr, d, yr)$^{-1}$
ET	evapotranspiration	mm (hr, d, yr)$^{-1}$
GPP	gross ecosystem CO exchange	gr C (d, yr)$^{-1}$
HPV	heat pulse velocity (equal to T)	mm (hr, d, yr)$^{-1}$
I	intercepted precipitation on the canopy	mm
L	ecosystem water losses	mm
LAI	leaf area index	m^2 leaf m^{-2} soil surface
NEE	net ecosystem CO_2 exchange	gr C (hr, d, yr)$^{-1}$
P	precipitation	mm
PAR	photosynthetically active radiation	W m^{-2}
PET	potential evapotranspiration	mm (d, yr)$^{-1}$
P_t	throughfall	mm
R	ecosystem respiration	gr C (d, yr)$^{-1}$
R_n	net radiation	W m^{-2}
SF	forest floor shaded fraction	m^2 shade m^{-2} soil surface
SWL	soil water loss from the soil profile	mm
T	tree transpiration	mm (hr, d, yr)$^{-1}$
T_{a_x}	air temperature at height of x (m)	°C
T_{s_x}	soil temperature at depth of x (cm)	°C
VPD	vapor pressure deficit of the atmosphere	kPa
WS	wind speed at height of 1 m	m s^{-1}
WUE	water use efficiency	gr C / mm H_2O
WUE_t	gross transpiration WUE	gr C / mm H_2O
WUE_e	net ecosystem WUE	gr C / mm H_2O
θ_x	volumetric water content at depth of x (cm)	m^3 water m^{-3} soil

Chapter 1

Introduction

1.1 Climate change and the water cycle

There is a common acceptance amongst the scientific community that human-induced global environmental changes are in motion, a component which includes changes of the climate system. The potential for climate change is driven largely by the rapid alteration of the atmospheric composition that has been underway for the last 200 years of industrial activity. Through the combustion of fossil fuels, the addition of climate forcing gases, including CO_2, CH_4, NO, aerosols and water vapor to the atmosphere have already increased Earth surface temperature, which is expected to increase in approximately 3°C until year 2100, compared to current temperatures (IPCC 2007).

Amongst other changes associated with current and future global warming, the hydrological cycle is expected to be intensified due to higher evaporation rates and larger atmospheric vapor holding capacities (Ohmura and Wild, 2002, Pierrehumbert, 2002). As a consequence, precipitation is often predicted to increase, predominantly in spring, with concomitant decrease in summer precipitation (Groisman *et al*., 2004, Angert *et al*., 2005). Outcomes can be profound, resulting with large floods and increased draught events (Milly *et al*., 2002, Reichstein *et al*. 2002). These predictions require new investigations into ecosystem water balance, in order to better predict how the water cycle will respond to future physical and biological changes.

Water availability, especially in dry regions, has both direct and indirect affects on biomass production, decomposition and long-term carbon sequestration (Jenerette and Lal, 2005, Huxmann *et al*., 2005). The biosphere, upon which humanity is inextricably dependent, is a key element of global change processes. Many properties of the biosphere, including process rates, species distribution and diversity are a function at some level of the climate. There is increasing evidence that parts of the biosphere already show signs of response to recent climate changes (Parmesan and Yohe, 2003). Furthermore, as the biosphere is an important component of the global

carbon cycle, it can feed back on the climate system. If the biosphere is to change in its geographical distribution and mass, the net outcome on regional albedo (effecting surface energy balance) and atmospheric water vapor (effecting regional precipitation, canopy boundary layer energy balance and serving as a major greenhouse gas) are critical parameters when evaluating climate change.

1.2 Ecohydrology and water use efficiency

Biomes characteristics, as well as their evolution in time, are largely defined by the interplay between climate, soil and vegetation. Ecohydrology is a relatively new scientific discipline, developed following the identification of the need to focus on these connections, and can be defined as "the science which seeks to describe the hydrologic mechanisms that underlie ecologic patterns and processes" (Rodriguez-Iturbe, 2000). Such an approach takes under consideration the type of climate, the pedology of the soil and the physiological characteristics of the vegetation. The dynamics of the interactions between these parts of the ecosystems are largely variable and need to be questioned under various spatial and temporal scales.

Although water is not the only limiting factor on growth, it is literally the most influencing one, due to its large impact on vegetation functioning as well as the substantial amounts needed for growth and maintenance. One of the largest challenges of ecohydrology is to explore the effects of water limitation on the productivity of vegetated ecosystems. This is becoming increasingly important under observed and expected drying conditions due to climate change, such as the European 2003 draught (Granier, Reichstein, *et al*., 2007). A specific example of the necessity to connect between all these factors can be given through one of the most basic though crucial issues in vegetated ecosystems - the wilting point, which is the minimal point of soil moisture the plant requires in order not to wilt permanently. Values of the wilting point under field conditions are not constant and are determined by the integrated effects of plant, soil and atmospheric conditions. Plants define the maximum suction pressure, and so even under similar climatic conditions and soil environments, water limitation will occur at a different point for different plant species. Soil moisture also constitutes as a crucial link between the hydrological and the biogeochemical cycles. This dependence includes processes such as decomposition, soil respiration, nitrogen

mineralization, nutrient uptake and weathering followed by solute transport (Parton *et al*., 2001, Huxman *et al*., 2005).

The water and carbon cycles are intrinsically connected in plants, as when stomata open, CO_2 enters the leaf and water transpires from the leaf simultaneously. Water vapor leaves the leaf through the stomata in a rate that is controlled by the gradient of water vapor concentration between the leaf and the atmosphere, the stomata conductance and the features of the boundary layer of the air enveloping the leaf. When environmental signals such as light intensity, temperature, humidity and CO_2 concentration change, metabolic processes and osmotic pressure in the plant respond to it and alter the ionic concentration in the guard cells, which in turn change their water potential, controlling stomatal aperture and development. The relation between the amounts of CO_2 assimilated through photosynthesis to the amounts of water vapor loss through transpiration is often termed plant water use efficiency (WUE). Experiments show a strong linear relation between these parameters, indicating that for a given species at a given environment and climate, WUE is constant under different soil water and CO_2 conditions. Averaged diurnal WUE values for mature leaves are in the range of 1-3 gCO_2/kgH_2O for C_3 plants, 2-5 for C_4 plants and 10-40 for CAM plants (Nobel, 1999). The relation between monthly GPP (gross ecosystem production; photosynthetic assimilation by foliage) and evapotranspiration was shown to be linear for a given biome across a large climatic gradient (1.5 gCO_2/kgH_2O for tundra vegetation up to 3.4 for grassland, forests taking the middle values, Law *et al*., 2002). Strong linkages between the distributions of these two fluxes were observed on a global scale as well (Hetherington and Woodward, 2003).

WUE is expected to be sensitive to the changing climatic conditions, but the consequences are yet uncertain. It is assumed that at elevated CO_2 concentrations, leaf hydraulic conductivity will decrease profoundly and evapotranspiration will decrease accordingly, particularly in dry ecosystems (Beering and Woodward, 1995), possibly resulting in an expansion of the terrestrial carbon sink (Cramer *et al*, 2001), further affecting regional energy and water balances (Field *et al*., 1995). This assumption is sometimes contradicted due to influences such as higher biomass and increased transpiration as a consequence of improved water balance (Schafer *et al*., 2002) and the negative effect of the large annual variability in precipitation and draughts on continuous ecosystems production (Smith *et al*. 2000, Reichstein *et al*., 2002).

1.3 The hydrological cycle

The hydrological cycle describes the continuous movement of all forms of water on, in and above the earth's surface. The water balance or budget for an area over a time period defines changes in the components of the hydrological cycle, and can be quantified as:

$$P = Q + ET \pm \Delta S \pm \Delta\theta \pm \Delta G \pm D \quad (1.1)$$

where P is precipitation, Q is runoff discharge, ET is evapotranspiration, ΔS is the surface storage, $\Delta\theta$ is the soil moisture storage, ΔG is the groundwater storage and D is the deep transfer of water. These variables are normally expressed as depth of water over a given area and time period (for example: mm km^2 yr^{-1}). The water balance equation can be implemented for any defined area, from small plots, to the hillslope scale, the drainage basin and up to continents or the entire globe. It can also be calculated for any time period, but simplest to evaluate for a period over which storage is similar at the start and end points, such as hydrological years or between major changes such as rain events.

Precipitation, the input to the cycle, is largely stochastic in duration and amount at regional scales. Spatial variability increases as climate becomes drier and controlled by convective rain cells far from the center of the storm. The distribution of precipitation is affected by large to small scale topography, influencing wind turbulence and causing redistribution of rain drops. When precipitation encounters a surface, some of it is **intercepted** and accumulates in situ and the rest is diverted as **runoff**. The runoff to rainfall ratio increases with storm intensity, antecedent soil moisture and exposed rocky surfaces. Vegetation increases the amount of water intercepted on the canopy and ground litter, accounting for 10-40% of the annual precipitation (Schlesinger, 1990). During the initial stages of a storm, much of the precipitation is stored on the canopy and on stems, but as the storm continues and these surfaces reach their capacities, excess water drains as **throughfall** and **stemflow** to the forest floor. Drained water from the canopy has a much smaller intensity compared to rainfall and so is more subjected to soil **infiltration**. Once infiltrated, this water becomes **soil moisture** or **groundwater**. Soil moisture is firstly defined by

amounts, rate and pattern of precipitation and secondly, it is controlled by soil characteristics such as depth, structure, soil crust formation, porosity and texture. In drylands, soil moisture is rarely stored between years, as it is rapidly transformed into gaseous phase and returns to the atmosphere. This returning flux is the **evapotranspiration** flux (ET), which is a combined flux:

$$ET = E + T + I \quad (1.2)$$

where E is soil **evaporation**, T is plant **transpiration** and I is evaporation of intercepted water (canopy and rock surfaces). The rate of ET is controlled mainly by two factors: The first is the availability of water for evaporation, which is stored in the upper soil layers and temporarily on canopy surfaces; and for transpiration, for which water in deeper layers can also be relevant depending on root depth. The second is the meteorological conditions (mainly radiation, wind speed and humidity) defining the evaporative ability or the vapor pressure deficit (VPD) of the air in relation to that of the evaporating surface, which is the driving force for ET.

ET can be also defined as the energy employed for transporting water from soil surfaces and inner leaves to the atmosphere, and therefore incorporated in the energy budget:

$$R_n - C - \lambda E = M + S \quad (1.3)$$

where R_n is net radiation, C is the sensible heat flux (loss of heat to the surroundings by conduction or convection from soil, leaves or other surfaces), λE is the latent heat flux lost by evaporation (the product of the rate of evaporation and the latent heat of vaporization of water, λ=2.45 MJ·kg^{-1} at 20°C), M is the net metabolic storage used mainly for photosynthesis and respiration and G is the net physical storage used for heating plant material, both are quite small (less than 5%) and thus are usually neglected. Fluxes are normally expressed in W m^{-2}. As such, the ET component of the hydrological balance, being equivalent to the latent heat component, can be deduced from the radiation balance.

1.4 Soil evaporation

While in humid environments soil evaporation is negligible compared to transpiration, in semi-arid environments it can consist up to 50% of ET or more (Hillel, 1980, Huxman *et al*., 2005). Soil evaporation is the evaporation of water accumulated in pore spaces between soil particles or of thin water films surrounding them. Rates of evaporation are controlled by the rates of energy and mass exchange at the soil-atmosphere interface (Boulet *et al*., 1997, Baldocchi *et al*., 2000). Scientific studies on mass and energy exchange over bare soil have been conducted since the first half of this century (Penman, 1948, Philip, 1957), and today this topic remains an area of active research. These theories initiated many physically-based models (Shuttleworth, 2007, for a review), which evaluate soil evaporation as a function of the product between surface conductance and the humidity gradient. The physical laws controlling these processes are identical for all evaporating bodies, and therefore will be first described in general.

Potential evapotranspiration (PET) can be quantified by the well known and wildly used Penman-Monteith reference crop model. This equation utilizes climatic parameters computed from weather data, not considering the crop or the soil characteristics. PET expresses the evaporating power of the atmosphere at a specific location and time for a hypothetical reference surface of grass, completely covering the ground and supplied with adequate water (Monteith, 1981):

$$PET = \frac{\Delta(R_n - G) + \rho_a c_p (e_s - e_a)/r_a}{\Delta + \gamma(1 + r_s/r_a)} \qquad (1.4)$$

where R_n and G are as above (here in MJ m^{-2} d^{-1}), e_s is the saturation vapor pressure and e_a is the actual vapor pressure (both in kPa) and the different between them represents VPD , ρ_a is the mean air density at constant pressure (kg m^{-3}), c_p is the specific heat of the air (MJ kg^{-1} $°C^{-1}$), Δ is the slope of the saturation vapor pressure temperature relationship (kPa $°C^{-1}$), γ is the psychrometric constant (kPa $°C^{-1}$), and r_s and r_a are the surface and aerodynamic resistances, accordingly (both in s m^{-1}).

The transfer of heat and water vapor from the evaporating surface into the air above the canopy is determined by the aerodynamic resistance:

$$r_a = \frac{\ln[(Z_m - d)/Z_{om}]\ln[(Z_h - d)/Z_{oh}]}{k^2 u_z} \quad (1.5)$$

where z_m is the height of the wind measurements (m), z_h is the height of humidity measurements (m), d is the zero plane displacement height (m), z_{om} is the roughness length governing momentum transfer (m), z_{oh} is the roughness length governing transfer of heat and vapor (m), k is the von Karman's constant, 0.41 (unitless) and u_z is the wind speed at height z (m s^{-1}). Several empiric equations and tables with characteristic values for the derivation of d, z_{om} and z_{oh} exists (Allen *et al*., 1998).

The surface resistance describes the resistance of vapor flow through the transpiring crop and evaporating soil surface:

$$r_s = \frac{r_l}{LAI_{active}} \quad (1.6)$$

where r_l is the stomatal resistance of the leaf (s m^{-1}) and LAI_{acitve} is the sunlit leaf area index (m^2 leaf area m^{-2} soil surface area), approximated as LAI_{active}=½ LAI. Stomatal resistance is either measured or approximated from literature according to crop type, age and condition.

These equations, calculating evaporation from a reference surface, can be utilized in order to calculate actual evaporation as a fraction of PET:

$$ET = K_s \times PET \quad (1.7)$$

where K_s is the surface coefficient, having a wide range of definitions in various researches, which can take (or neglect) under consideration requirements such as soil wetness, soil texture, surface cover, crop type, growing phase and special crop conditions such as plant diseases.

Soil evaporation is characterized by three indicative phases (Hillel, 1972). Initially, evaporation is governed by external atmospheric conditions; rates are maximum, constant and closest to potential (Eq. 1.4). When the thickness of the dry topsoil increases to a point of which the hydraulic gradient in the soil can no longer increase at a rate that compensates for the drying topsoil, the second phase begins in which evaporation rates decrease gradually ("falling rate phase"). The length of this

phase and the rates of evaporation fluxes are controlled by the supply of water from the soil interior to the evaporation site. This process involves transport of liquid water to the evaporating surface (capillary rise, mostly in relatively wet soils), phase change from liquid to vapor and diffusion of vapor from the soil surface to the atmosphere (usually the main mechanism in relatively dry soils). The transfer of vapor and liquid water under combined temperature and moisture gradients is depend upon the soils' water potential and conductive properties, defined by Philip (1957):

$$E = \frac{q_w}{\rho_w} = -D_T \frac{dT}{dz} - D_\theta \frac{d\theta}{dz} - K \tag{1.8}$$

where E is the vapor flux from the soil (m s^{-1}), q_w is the water flux density (kg m^{-2} s^{-1}), ρ_w is the density of water (Kg m^{-3}), D_T is the thermal water diffusivity (m^2 °C^{-1} s^{-1}), T is temperature, z is depth (m), D_θ is the diffusivity of the soil moisture (m^2 s^{-1}), θ is water content (m^3 m^{-3}) and K is the hydraulic conductivity (m s^{-1}).

A better agreement with experimental data is obtained when mass transfer is combined with the transfer of heat:

$$q_h = -\sigma \frac{dT}{dz} - \rho_w \cdot \lambda \cdot D_{\theta\_vap} \frac{dz}{d\theta} \tag{1.9}$$

where q_h is the soil heat flux density, σ is the thermal conductivity including contribution of vapor movement, λ is latent heat of vaporization and $D_{\theta\,vap}$ is the vapor diffusivity. The transfer of vapor in the soil can be defined following Fick's law:

$$q = -D \frac{d\theta}{dx} = -K \frac{d\Psi}{d\theta} \tag{1.10}$$

where q is the flux (m s^{-1}), D is the water diffusion coefficient (m^2 s^{-1}), x is the distance (m) and ψ is the water potential (m). Vapor transfer in the soil is negatively correlated to water content, as gas diffusivity of the soil decreases with increased water filled pores space (Parton *et al*, 2001).

In the third and last phase of soil evaporation, the evaporation flux decreases to a constant and minimum rate. At this phase adsorption from the humid atmosphere to the dry

soil is possible. The process of water adsorption is different from the process of dew: dew formation occurs when atmospheric vapor condenses on the colder soil surface; during adsorption the soil surface temperature can be higher than that of dew point, but the relative humidity inside the pores is lower than that of the atmosphere and vapor molecules interact with the soil solid surface to produce hygroscopic or quasi-crystalline water (Kutilek and Nielsen, 1994). The adsorbed water can later be subjected to evaporation inside the soil and then transported to the soil surface (Eq. 1.10). The magnitude of vapor adsorption on solid surfaces depends on the surface area and is largest for clays (Hillel, 1972) and increases with the depth of the dry soil layer (Katata et al., 2007), as defined by Philips (1957):

$$A = \int_{\theta_t}^{\theta} x d\theta = S\sqrt{t} \tag{1.11}$$

where A is the total water adsorbed (mm), t is the time (s) and S is the sorptivity, which is a function of water content in equilibrium with the relative humidity of the atmosphere and the soil porosity (mm $s^{-½}$).

This flux is usually assumed to be negligible for water utility. However, it has been shown that for bare desert soil during the dry season, adsorption can constitute up to 20% of the R_n budget (Agam *et al*., 2004) and decrease the diurnal amplitude of soil temperature (Katata *et al*., 2007). Recently, it was estimated that water gain from adsorption maintained vital stomatal conductance and transpiration of shallow-rooted perennial grasses during the high water-stress season (Ramirez *et al*. 2007), therefore presumably utilized through some mechanisms by plants.

1.5 Below canopy spatial and temporal variability

The connection between plant, soil and climate systems is further complexed due to its varying nature both in space and time. Such variability is present at some extent in all ecosystems, but is enhanced at dry climates. While most climatic parameters such as solar radiation and temperature are relatively constant between years (excluding gradual climatic changes such as global warming), precipitation, the input to this system, is highly discontinuous and stochastic. Dry climates are characterized by rain pulses with dry conditions prolonging between them, creating a profound seasonal trend. The sporadic nature of the rain showers produces large

annual variability in precipitation pattern and amount, which increases with decreased annual precipitation. As a consequence, it is often insufficient to perform research under annually or seasonally average climatic conditions, as the effect of environmental fluctuations both within the year and between years is of fundamentally important in the quantitative description of vegetation dynamics. Rather, precipitation and its consequence on soil moisture need to be described in terms of frequency and characteristics of events and modeled with tools that incorporate a probabilistic process-based analysis (Porporato *et al*., 2002, Guswa, 2002).

In addition to the large temporal variability, the sporadic nature of precipitation also generates conditions for variability in space. In drylands, significant differences in storm precipitation can be measure even at points less than 100 m apart (Sharon, 1972). In differ to wet climates, in which an extensive and relatively homogeneous vegetation cover exists, the sparse vegetation at dry ecosystems enhances spatial variability (Noy-Meir, 1973). Differences between adjacent vegetated and non-vegetated areas can be extreme, due to differences in incoming and outgoing radiation, temperature conditions, incoming precipitation and surface runoff, pedology, soil moisture and nutrient cycling. These differences contribute to the patchiness nature of dry ecosystems, which, in differ to the sporadic nature of precipitation, often has a reoccurring pattern (Seyfried and Wilcox, 1995).

The usually low LAI typical of dry ecosystems exposes surface variability such as density and type of below canopy vegetation, soil vs. rock surfaces, crust cover, etc. The spatial variability of these characteristics further produce changes in processes connected to the hydrological cycling, such as throughfall precipitation, runoff distribution and soil water content. In addition, low canopy cover produces differences in meteorological variables such as incoming radiation, wind speed and temperature between exposed and non-exposed areas.

Accordingly, up-scaling at these ecosystems is a challenging task at all scales. Causes for this difficulty is mainly due to three reasons: heterogeneity in time and space of the properties that determine processes, variables and rates; non-linearity across scales between processes and variables and the interlinking and feed-backing between the many processes and variables in natural systems.

1.6 Partitioning the evapotranspiration flux

Evapotranspiration from land ecosystems is the main route in which precipitation, the water input of the hydrological cycle, is returned to the atmosphere. ET is an integrated term, composed of linked vapor fluxes (Eq. 1.2). In most researches, ET is treated as a single entity. However, partitioning ET is important for understanding how E and T influence the ecosystem hydrological balance and their interactions with climate. Such partitioning is most critical in water limited ecosystems, in which the E component becomes more and more significant. Therefore, imposing uniformity on the ET flux introduces a limiting factor onto ecosystem research. Implications of flux partitioning are wide, including local water availability, plant growth, carbon assimilation and soil respiration (Law *et al*., 2002; Scott *et al*., 2006; Kurc and Small, 2007; Granier, Reichstein *et al*., 2007). Such information is important for predictions of the WUE and the consequences of ecosystem response to future climate change, deforestation and management decisions. However, due to the close linkage between the fluxes, it is technically complex to partition the two in the field and therefore rarely done or preformed for periods not longer than a couple of days, preventing the long term perspective.

Partition between the fluxes begins with the driving force for ET, controlled by the atmospheric demand for vapor relative to the water content of the soil and the hydraulic conductivity; the latter being intrinsic to the soil when referring to E and to the soil-root-leaf continuum when referring to T. Therefore, while E is a physically controlled system, T is biologically controlled and can be affected by factors such as plant disease, atmospheric CO_2 concentrations and soil fertilization. Semiarid landscapes represent a transitional zone between humid environments, in which woody plants have a large effect on the water budget, and arid ones, in which the total effect on runoff is minimal (Huxman *et al*., 2005). In these areas, the relations between vegetation cover and the water budget is complex and poorly known.

Accordingly, the WUE of the ecosystem will differ from that of the tree component alone, which does not include losses by soil respiration and evaporation. Therefore, ET partitioning can be utilized in order to further examine the WUE index, by dividing it into the soil and tree components. WUE can be calculated for the entire ecosystem, indicating the net balance between assimilation and heterotrophic and autotrophic respiration:

$$WUE_e = \frac{GPP - R}{ET} = \frac{NEE}{ET} \quad (1.12)$$

where WUE_e is the net WUE of the entire ecosystem, GPP (gross primary production) is the photosynthetic assimilation by foliage, R is the respiration combined of soil, stem and foliage efflux and NEE (net ecosystem exchange) is the balance between the two fluxes and is usually measure with the eddy-covariance system. Another scale to be considered is that of the leaf or plant scale:

$$WUE_t = \frac{S}{T} = \frac{GPP}{T} \quad (1.13)$$

where WUE_t is the gross or transpiration WUE, S is sequestration and T is transpiration. Up-scaling leaf measurements in order to assess the WUE of the whole canopy is a major and complicated task. However, WUE_t can be directly calculated if data regarding CO_2 and ET partitioning exists, enabling to differentiate between the sensitivity of each component to environmental conditions.

1.7 Research goals

In light of observed and expected global change, much emphasis has been put in recent years in order to understand feedbacks and effects with the climate system. A major concern in this respect is the biospheres' vulnerability on the one side and our dependence on it, on the other. The water cycle serves as a link between the climate and the biosphere, and is of special importance at water limited ecosystems, in light of predicted climate change. Currently, dry regions constitute approximately 30% of the Earths land surface. Global change is expected to increase both the extent of drylands and the vulnerability of woody plants and forested ecosystems in these regions. Therefore, estimating the resilience and sustainability of these ecosystems is critical for planning and management practices. Notably, a major limitation in eco-hydrological research is the difficulties in partition the evapotranspiration flux into its components, soil evaporation and plant transpiration. Within this context, the basic

objective of our research was to investigate patterns of water loss and utility in a semi-arid forest.

Our research was carried out in the Yatir afforestation ecosystem in southern Israel. This site provides a unique and suitable research system for such research, because of the low tree density and the high bare soil fraction, expected to result with significant soil evaporation. While most studies dealing with climate change effects are carried out in temperate forests, using short-term extreme events such as droughts or heat waves, our study is conducted at a pine forest acclimated to hot and dry condition, enabling to take into account the consequences of long term adaptation and stabilization to such climates.

More specifically, the objectives of this study were to:

1. Evaluate the spatial and temporal variation of soil evaporation in a semi-arid pine forest ecosystem. This includes: (1) develop and verify a methodology to measure E below the canopy, (2) directly measure E and define its patterns.
2. Simulate E based on measured interactions with radiation, soil water content, wind speed, temperature and VPD.
3. Quantify soil evaporation at the ecosystem scale as a function of forest floor surface shaded fraction and its link to canopy architecture (tree dimensions and density).
4. Examine the influence of precipitation pattern (amount, intensity and scatter throughout the season) and the consequent soil water content, on the components of the hydrological cycle in the forest, including that of evapotranspiration partitioning (soil evaporation and tree transpiration).
5. Test the hypothesis that at semi-arid regions, due to ecosystem fitness and acclimation, production can be maintained resulting with high water use efficiency (WUE), but under extreme dry conditions (draught) WUE is decreased.

Chapter 2

Materials and methods

2.1 The research site

The Yatir afforestation is a pine forest established during the 1960s and is currently spread over an area of 28 km^2. The site is located at the transition zone between sub-humid and arid Mediterranean climates, on the edge of the Hebron mountain ridge (Figure 2.1), with a mean altitude of 650 m. The average air temperature for January and July is 10°C and 25°C respectively (Bitan and Rubin, 1991). The hot and dry climate produces very high potential evapotranspiration (annual average of 1600 mm yr^{-1}) in contrast to the low precipitation (annual average of 280 mm, Figure 2.2), defining the climate on the verge between arid to semi-arid (UNEP, 1992). Most of this precipitation is concentrated in the months between December to March and thus an extended rainless period exists between May and November. These meteorological conditions produce two distinctive seasons: a wet winter during which the main plant activity occurs and a hot and dry summer continuing more than half a year. As such, times of maximum ET and maximum PET are not synchronized, enabling some extension of the wet-soil period.

The forest is dominated by the Aleppo pine (*Pinus halepensis* Mill.), with smaller proportions of other pine species, cypress and with little understory vegetation (understory aboveground biomass <0.10 kg m^{-2}). Tree density in 2007 was 300 trees ha^{-1}, and mean tree height was 10 m. Yatir is an open forest – more than 40% of the land surface is exposed, and leaf area index (LAI) is low (~1.50). The surrounding native vegetation, which was the land cover prior to afforestation, consists of sparse shrubland with patches dominated by short shrubs and patches of herbaceous annuals and perennials (total vegetation height of 0.30-0.50 m; Grunzweig *et al*., 2003).

Soils in the research site are shallow (20-40 cm), of Aeolian-origin Leos with clay-loam texture (31% sand, 41% silt and 28% clay; density- 1.65 gr cm^3) overlaying a chalk and limestone bedrock. Sporadically, deeper pits (up to 1.5 m) were located, in which Paleosols where found below 40-50 cm. These are darker soils of clay-silt

texture (9% sand, 44% silt and 47% clay; density- 1.70 gr cm^3) observing large calcite aggregates and cutans (Appendix 1).

While the natural rocky hillslopes of the semi-arid Northern Negev are known to create flash floods, the forested plantation reduces runoff dramatically (lower than 5%, Shachnovich Y., personal communications, Laronne *et al*., 2007). Groundwater is deep (>300 m), decreasing the possibility of groundwater recharge due to negative hydraulic conductivity (Seyfried *et al.*, 2005). Local recharge and deep drainage can be assumed at some depth, as exposed cleavage in the region shows some fractured bedrock.

2.2 Meteorological and soil water measurements

A 19 m flux tower is based at the center of the research site, measuring activity at the ecosystem level of CO_2 (NEE) and water fluxes (ET). In addition, a large suite of meteorological measurements exists. Air temperature (T_a) above the forest canopy was measured with a temperature probe mounted on the meteorological tower. Identical temperature probes were also available for heights of 1, 5, 9 and 13 m. Soil temperatures (T_s) at depth of 2 and 6 cm were measured at six different points around the tower with thermocouples. Net radiation (R_n) was calculated from short and long wave radiation measured above and below the canopy alongside other radiation measurements. In order to measure volumetric soil water content (θ), two systems were integrated at the research site. The first consisted of three reflectrometry sensors (CS616, Campbell Scientific, USA) positioned vertically in the ground and measuring an average for soil depth of 0-30 cm. A specific calibration equation was prepared in the laboratory for these sensors to fit the dense soil present at the Yatir site (Appendix 2). In addition, their high sensitivity to soil temperatures demanded a linked soil temperature measurement, which was carried out at depths of 1, 5, 15 and 30 cm within a close proximity to the CS616 sensors (HOBO H8 loggers, Onset Computers, USA). An integral average of these soil temperatures was then used with the factory defined temperature correction equation. Since 2005, a second system based on TDR sensors (TRIME, IMKO, Germany) was integrated, measuring θ at different depth in three pits (pit 1: 5, 15, 30, 50, 70 and 125 cm; pit 2: 5, 15 and 30 cm; pit 3: 5, 15, 30, 50 and 70 cm; Appendix 3).

GPP was calculated as a residue between NEE and R (see section 1.6 for explanations of terms). While NEE was measured, ecosystem R was calculated as a weighted average between soil (50%), foliage (40%) and stem (10%) respiration (Afik T., personal communication). These respiration fluxes were obtained from relations between measured respiration (during the last hour before sunrise, in which R~NEE), temperature and Q_{10} (temperature sensitivity). Q_{10} for the soil was adopted from Grunsweig *et al*., to be published, and for the foliage and leaf from Maseyk *et al*., 2008.

2.3 Soil evaporation measurements

Measurements of soil evaporation (E) were conducted with a modified LI-COR 6400-09 soil CO_2 flux chamber (LI-COR Inc., USA). Method development and validation are elaborated in Chapter 3.

Chamber-based soil vapor flux was measured at 14 soil collars permanently placed at the Yatir research site. These are 5 cm long and 10 cm wide PVC round collars inserted to a depth of 4 cm in the ground (Figure 2.3). Selection of the locations for collars combined probability sampling (9 collars positioned randomly at the field site) and purposive sampling (5 collars). During the period of E measurements (September 2004 – July 2007) 42 measuring days were conducted. Measurements were carried out between 11:00 and 12:00, which was found to be the time of peak diurnal E fluxes. Parallel to measurements of E, θ was also measured for depth of 0-10 cm next to the soil collars with a mobile TDR (TRIME data pilot, IMKO, Germany). Photosynthetically active radiation (PAR; LI-COR, USA) was also measured over the soil collars.

In addition to days in which the spatial variability of E was measured, six full measuring days representing different seasons and conditions were conducted. During these days, E was measured at two adjacent collars every half hour, from before sunrise until after sunset.

The primary method for perceiving a field averaged value of E was to average the 14 point-measured E per each measuring day. The number of measurements needed according to T-test for the mean (E_{ave}) to be within the range of ±0.01 mm hr^{-1} with confidence level of 95% was calculated according to:

$$N = \frac{t^2\sigma^2}{d^2} \quad (2.1)$$

where N is the required sample size, t is the t-test value for the number of collars measured during the day (n-1) at a confidence level of 95% (2-sided tail of 97.50%), σ is the standard deviation for each measuring day and d is the accepted marginal error, which was defined to be 0.01 mm hr^{-1} (equal to 8.90% of the range of E measurements).

An additional methodology was preformed, taking into account the effect of tree shading on E (discussed in section 4.2.1). The towers' footprint borders where mapped and the areas of shaded and non-shaded surfaces within the footprint were defined. Calculation of the towers' footprint (Gockede et al., 2007) indicated that the largest contribution to the flux during daytime came from an area at a distance of 34 m from the tower and 95% of the recorded flux came from an area within 1,300 m from the tower. An analysis of the wind direction showed that during 64% of the daytime, wind approached the tower from the North-West to South-West sector.

Tree-shaded area within this flux-contributing area was estimated from tree dimensions and the annual pattern of the suns' altitude, determining shadow length. A survey of tree dimensions was conducted at an area of 1500×1500 m within the defined main footprint area (North-West to South-West of the tower), and the tree statistics obtained are presented in Table 2.1. As measurements of E were conducted at ~12:00, daily noontime solar altitude for Yatir was determined utilizing standard equations (Appendix 4). Shadow length was then calculated from crown length, for each day of the year. The shape of the shade created by a single tree was approximately defined as an ellipse, which area was calculated from its diameters: measured average crown width and calculated daily-varying length of shadow. The area of the ellipse was constrained between a minimum limit (area of a circle, sun at zenith) and a maximum limit (length of shadow equaling the averaged distance between trees in order to prohibit mutual shading). Total forest shaded area was calculated by multiplying the latter shaded area with forest tree density. The shaded fraction (SF) was then defined as the ratio between forest floor shaded areas to total forest area. Finally, spatially-averaged E was calculated according to:

$$E_s = SF \times E_{shade} + (1 - SF) \times E_{sun} \quad (2.2)$$

Where E_s is the spatially averaged E, E_{shade} is the averaged E of the shaded collars and E_{sun} is the averaged E of the sunny collars (details in section 4.2.1). Tree architecture and LAI, known to affect shadow density (Kuuluvainene and Pukkala, 1989), were not considered here; presumably, actual measurements of E below trees already incorporate this effect.

2.4 Transpiration measurements

Sap flux, equal to total tree water uptake or transpiration, was measured at the research site by the Volcany Institute utilizing two similar techniques: the heat pulse velocity method (HPV) and the Granier method. Both methods utilize thermocouples and heating probes in order to measure heat pulse velocity (HPV) or heat dissipation (Granier) of the flow in the conductive xylem elements. Utilizing empirical calibrations and knowledge of the cross-sectional area of flow, these measurements are converted to mass flow rate. Variations between trees in the radial pattern of sap velocity and the decline of sap flow toward the heartwood can produce high variation of sap velocity between trees and errors in the estimations of sap velocities based on single point measurements (Cohen *et al*., to be published, Schiller *et al*., to be published). Such variations can occur due to differences between trees in the direction of sun exposure, heterogeneity in soil structure and the resulting rooting systems, soil water content and size and age of the stem. Accordingly, eight trees were measured by each method (not coinciding between methods), representing averaged forest tree size and age. Measurements were conducted hourly for each of the eight trees. Water uptake (L hr^{-1} $tree^{-1}$) was converted to T (mm hr^{-1}) according to tree density (300 trees ha^{-1}) and total daily uptake was averaged between the eight trees.

HPV was measured during 2004–2006 by means of the heat pulse method (Cohen, 1994). This method entails measurement of the propagation velocity of a heat pulse produced by a linear heating device installed in the xylem and measured with a sensor composed of thermocouples installed above it. The 60 mm long HPV probes contained six thermistors each and the heaters (both produced in-house) were inserted into the xylem at a height of 1.30 cm. The calibration coefficient used, which is the

slope of the linear regression between the gravimetrically determined water loss and the calculated sap flow amount, was 0.565 (Schiller and Cohen, 1998). During the summer period, fluxes were below method sensitivity and excluded from the database (Schiller *et al*., to be published). Normalized standard deviation during the measurement period of daily total T between the eight trees was 38% on average, ranging between 11-173%.

Sap flow was measured with Granier type sensors during 2006-2007. This method measures heat dissipation based on measurements of two temperature probes inserted perpendicular into the stem one above the other (Liu *et al.*, 2008). The upper sensor is coupled with a heater powered constantly and the lower sensor measures the unaffected region so that utilizing appropriate calibration equations, the temperature difference between the sensors is used to compute sap flux. 11 in-house built Granier-type sensors were installed at a height of 1.30 m. Granier sensors are more sensitive to flow in comparison to HPV sensors and measured sap flux even during the dry season. Granier sensors are shorter than HPV (20 mm) and needed to be corrected in order to consider all conducting sap wood area. Cohen *et al.* (to be published) measured sap flux to a depth of 44 mm in *P. halepensis* trees at the research site, demonstrating that water transport in the inner sapwood is increased at dry areas as a result of high atmospheric evaporative demand. Accordingly, they calculated a correction factor of 1.72 in order to compensate for the shortness of the sensors. We compared HPV and Granier daily total averaged fluxes measured at the field site during the mutual successful measurement period of March-May 2005 and received similar results (n=13, R^2=0.95, HPV=1.70×Granier). Accordingly, Granier total daily averaged values were multiplied by 1.72 in order to perceive representative fluxes.

2.5 Gap filling the database

In order to compare between monthly to annual fluxes of E, T, ET, NEE and GPP, a complete and continuous dataset was compiled for each parameter, utilizing specific methodologies.

Half hourly gaps of ET, NEE and GPP were filled with averages between the previous and the following half hours. If these values were also missing, averages of the same half hour of the previous and the following days were utilized. The length of

averaging period varied according to the length of missing data period, and correlative half hour values of periods of up to 15 days before and after the gaps were used. Total daily values of ET and NEE and total light hour values GPP were calculated from the continuous half-hour database.

HPV was measured during the period January 2004 - May 2006. However, comparison between HPV, Granier and ET showed that during the period October 2005 – May 2006 the system was not well-functioning, and was eliminated from the database. During the successful measuring period, the system measured at 238 out of 639 days; it did not measure mainly during the summer period, when fluxes were below detection limit, or when malfunctioning occurred at more than 2 of the 8 trees. Schiller *et al.* (unpublished) analyzed the relations between transpiration and VPD, PET and $\theta_{0\text{-}30}$ and found good correlation between them, which were represented by two alternative equations. The first derived total daily HPV from daily total PET (calculated according to Eq. 1.4) and daily averaged $\theta_{0\text{-}30}$ (data obtained from current research) for which R^2= 0.61; and the second derived total daily HPV from daily averaged VPD and daily averaged $\theta_{0\text{-}30}$ with R^2= 0.51:

$$HPV = -0.59 + 0.10 \cdot PET + 0.04 \cdot \theta + 0.02 \cdot (PET - 3.81) \cdot (\theta - 16.93) \quad (2.3)$$

$$HPV = -0.35 + 0.18 \cdot VPD + 0.04 \cdot \theta - 0.83 \cdot 10^{-3} \cdot (\theta - 17.13)^2 + 0.02 \cdot (\theta - 17.13) \cdot (VPD - 1.22) \quad (2.4)$$

[Note: θ in % and not in $m^3\ m^{-3}$ as routinely used in this essay; other parameters are in formerly defined unites]. These equations were utilized in the present research in order to gap fill the transpiration database for the period October 2003 – March 2005, according to the priority: (1) Eq. 2.3, (2) Eq. 2.4, and (3) if both could not be used, total daily T was gap-filled according to the methodology elaborated upon above, utilizing appropriate periods of varying length in order to average daily values of pervious and following days. Comparing between measured and simulated daily values of T showed good agreement and enabled to utilize the simulated values during non-measured days with substantial confidence (Figure 2.4).

Granier type sensors measure T during the period April 2005 – September 2006 for 432 out of a total of 552 days and gap filling was preformed according to the

methodology of average between appropriate periods of previous and following days. A good continuation was also observed between the HPV and Granier techniques; the period April – June 2005 was measured by both systems (Figure 2.4).

Total daily E_s was measured and calculated for the 42 measuring days, and a procedure to gap-fill the non-measured days during the research period was in need. Because E_s values varied largely between seasons, these days were divided into seasons (Section 5.2). Analysis of the meteorological and soil water conditions during each season enabled to define characteristic thresholds for summer (noontime $T_{a\_1}>25°C$ and $\theta_5<0.08$) and winter (noontime $T_{a\_1}<15°C$ or $\theta_5>0.23$); other days were defined as the wetting or drying seasons. Then, seasonal correlation between E_s and existing environmental parameters were tested. A stepwise procedure was applied, and the most appropriate variables to simulate daily E_s were found to be θ_5, above canopy R_n, VPD, T_a and WS. A multi-linear regression equation was fitted for each season (Table 2.2). According to the defined above seasonal thresholds of T_{a_1} and θ_5, the non-measured days were divided into seasons. Then, the seasonal multi-linear regression equations were applied on the meteorological daily noontime values of θ_5, R_n, VPD, T_a and WS to simulate daily noontime E_s. The relation between noontime E and total daily E during the full measuring days was utilized in order to calculate total daily E_s from noontime E_s (R^2=0.91):

$$E_{total\_daily} = 0.39 \cdot \ln(E_{noontime}) + 1.49 \qquad (2.5)$$

A flow-chart of all procedures implemented in order to obtained a continuous database of total daily Es is shown in Figure 2.5.

2.6 Tables and figures

Table 2.1: Statistics (average and standard deviation) of tree dimensions measured during October 2007 in the Yatir forest research site, within the flux-tower defined footprint area.

	Average	Stdev
Tree density (trees ha^{-1})	300	13
Tree height (m)	9.9	1.9
Crown width (m)	4.6	0.7
Height of crown above ground (m)	1.7	0.5
Distance between trees (m)	6.1	2.1

Table 2.2: Seasonal multi-linear regressions describing relations between environmental variables and noontime measured E_s. The number of days (n), correlation coefficient with measured parameters (R^2) and significance (P) are noted for each model; the coefficients (B) and their relative contribution (β%) are noted for each variable. These relations were used in order to gap-fill the E_s database (Fig. 2.4).

	Wetting Season			**Winter**			**Drying Season**			**Summer**		
	n	**R^2**	**P**	**n**	**R^2**	**P**	**n**	**R^2**	**P**	**n**	**R^2**	**P**
	7	0.682	0.04 5	16	0.813	0.03 4	5	1.000	–	14	0.977	0.04 6
	B		**β%**	**B**		**β%**	**B**		**β%**	**B**		**β%**
constant	-6.57E-02			-4.90E-02			-4.22E-02			1.03E-01		
$\theta_{\_5}$	1.22E+00		81	3.20E-01		22	2.07E-01		40			
R_n				4.82E-05		16				-5.05E-05		35
VPD	1.03E-02		19	-1.24E-02		22	-2.41E-03		10	-2.53E-03		24
T_{a_1}				2.31E-03		28	7.56E-04		17	-8.08E-04		26
WS				-8.09E-03		13	3.66E-02		33	-4.27E-04		14

Figure 2.1: The Yatir forest is indicated in a red circle. The site is located at the transition zone between the sub-humid Mediterranean and the arid climates, on the edge of the Hebron mountain ridge, with a mean altitude of 650 m. The research station (a flux tower site and experimental plots) is located at the center of the forest.

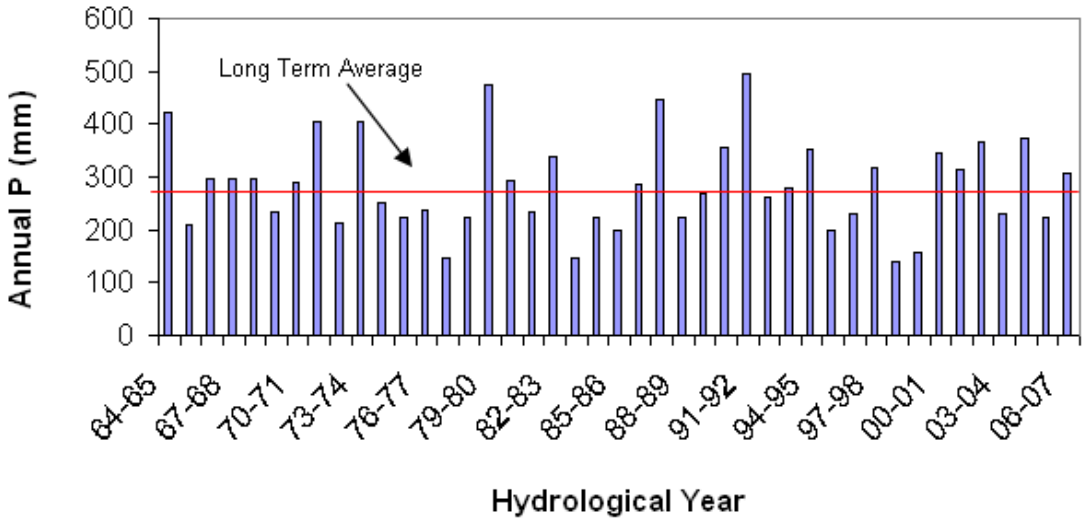

Figure 2.2: Annual precipitation at the Yatir forest site. Long term average was 280 mm, with a large variability around this average.

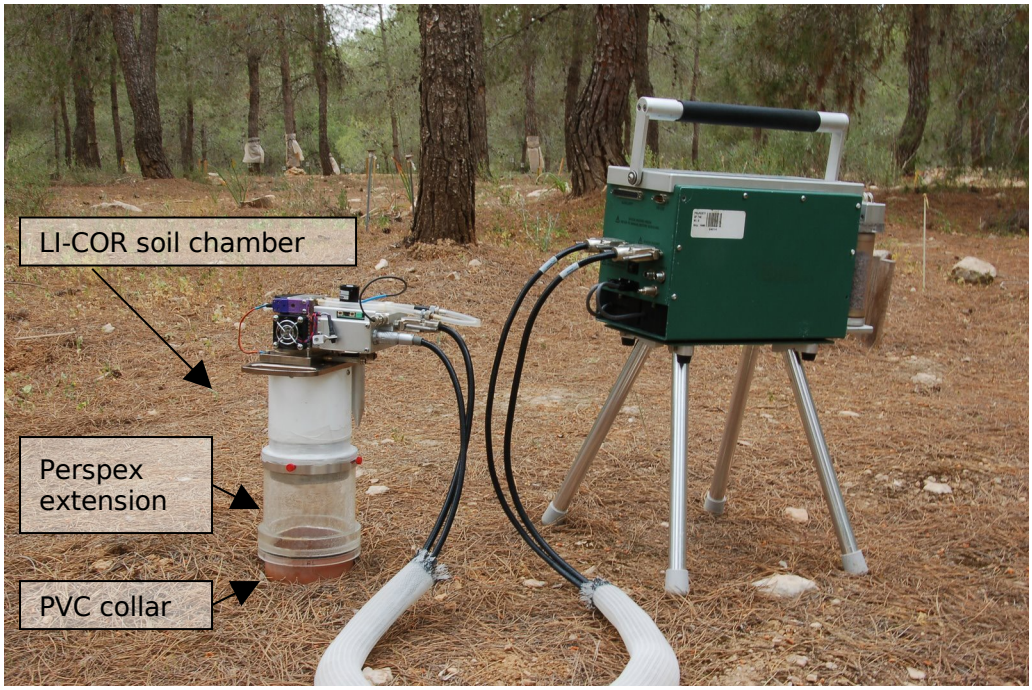

Figure 2.3: Field measurements of soil evaporation were preformed with a modified extended commercial soil chamber. During measurements, the LI-COR 6400-09 CO_2 soil chamber was mounted on the homemade 10 cm Perspex extension, which was sealed onto PVC soil collars permanently installed at 14 different locations within the research area.

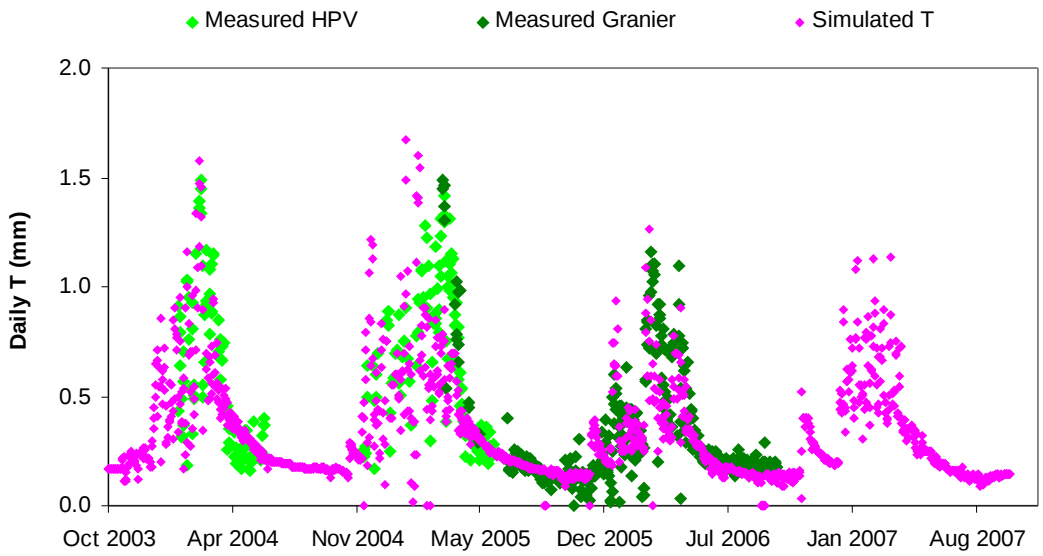

Figure 2.4: Comparison between measured total daily transpiration values and simulated total daily transpiration values (Eq. 2.3 and 2.4). A good agreement between the datasets was observed, enabling to utilize simulated values during non-measured days. A good continuation was also observed between the HPV and Granier techniques; the period April – June 2005 was measured by both systems.

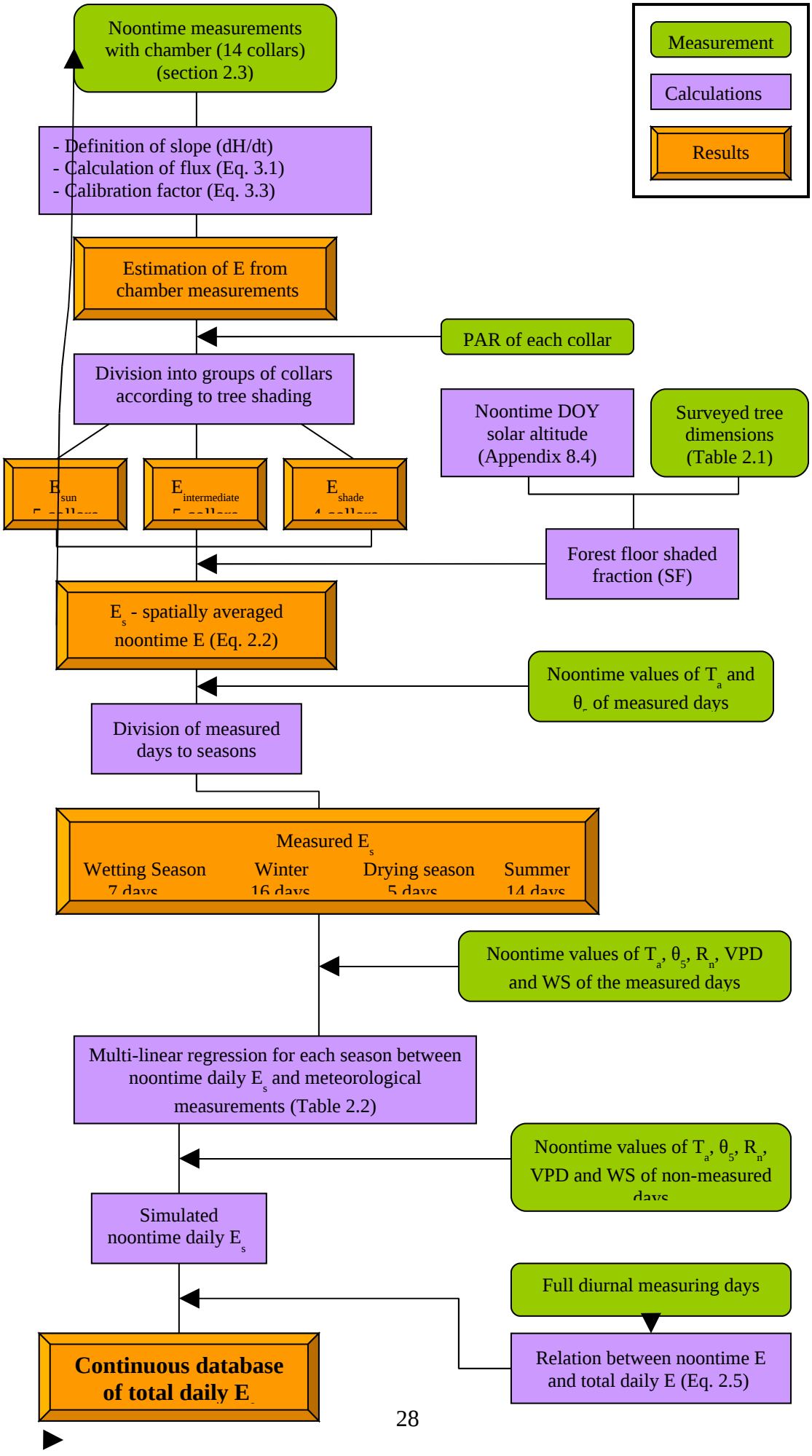
Noontime measurements with chamber (14 collars) (section 2.3)
Measurement
Calculations
Results
- Definition of slope (dH/dt)
- Calculation of flux (Eq. 3.1)
- Calibration factor (Eq. 3.3)
Estimation of E from chamber measurements
PAR of each collar
Division into groups of collars according to tree shading
Noontime DOY solar altitude (Appendix 8.4)
Surveyed tree dimensions (Table 2.1)
E sun
E intermediate
E shade
Forest floor shaded fraction (SF)
E s - spatially averaged noontime E (Eq. 2.2)
Noontime values of T a and θ 5 of measured days
Division of measured days to seasons
Measured E s
Wetting Season
7 days
Winter
16 days
Drying season
5 days
Summer
14 days
Noontime values of T a, θ 5, R n, VPD and WS of the measured days
Multi-linear regression for each season between noontime daily E s and meteorological measurements (Table 2.2)
Noontime values of T a, θ 5, R n, VPD and WS of non-measured days
Simulated noontime daily E s
Full diurnal measuring days
Relation between noontime E and total daily E (Eq. 2.5)
Continuous database of total daily E

Figure 2.5: Flow-chart of all procedures implemented in the process of calculating soil evaporation, starting from field chamber measurement of E and resulting with a contentious database of total daily E_s.

Chapter 3

Measuring soil evaporation utilizing a modified soil chamber - method development

3.1 Introduction

E is often calculated as a residual, where ET is measured with the eddy covariance or the energy balance techniques and T is measured with the sap flow technique (Baldocchi and Vogel, 1996, Rana and Katerji, 2000). Direct methods to measure soil water loss or gain such as microlysimeters and TDR's are used mostly in un-vegetated ecosystems or measure total ET, and they cannot differentiate between water loss paths (Baker and Spaans, 1994, Wythers *et al*., 1999). An interesting methodology to partition ET is based on stable isotopes of oxygen and hydrogen, combining flux and isotopic mass balances (Wang and Yakir, 2000, Yepez *et al*., 2003), but is laborious and is usually conducted for short durations. An additional method utilizes chambers, which measure gas flow within a confined volume of air inside a chamber positioned on the soil surface. The advantage of this methodology is that the measured segment can be specified and a high spatial resolution can be obtained. Accordingly, the chamber method was utilized to measures soil E (Iritz *et al.*, 1997; Stannard and Weltz, 2006), whole tree T (Greenwood and Beresford, 1979; Denmead *et al.*, 1993) or below canopy ET (Dugas *et al.*, 1997; Steduto *et al.*, 2002; Arnone and Obrist, 2003; Mcleod *et al.*, 2004). Disadvantages of these systems are they are usually home made and calibrated, moderately large and immobile. A major criticism on this method is that the chamber alters ambient meteorological conditions and influences the flux rate. This issue is further discussed below.

In this research, vapor soil flux was measured utilizing the fast response of an Infra Red Gas Analyzer (IRGA) connected to a closed soil chamber. This methodology was based on an instrument commonly used in environmental field researches (LI-6400 soil CO_2 chamber), which was modified and calibrated to measure water fluxes. The advantages of this methodology are: (1) The ability to directly measure E at vegetated ecosystems, (2) The mobility of the system, enabling

to account for spatial heterogeneity of E and (3) The usage of a standard and commonly available instrument for soil-atmosphere fluxes. The objectives of this part of the research were: first, to develop a reliable and precise system to measure soil evaporation in vegetated ecosystems, and second, to determine the spatial and temporal variability of soil water loss in a semi arid forest using this system.

3.2 Chamber measurements of soil fluxes

Conventionally, chambers are divided into two groups: steady-state chambers, which are continuously flushed with external air during measurement and closed chambers, which confine the air inside the chamber (Hutchinson and Livingston, 2001). Positioning a soil chamber on the ground immediately changes the ambient conditions within the soil chamber, mainly regarding radiation, temperature, pressure and turbulence. The problem of reduced radiation can be lessened by using transparent chamber materials which enable entrance of most outside radiation (Greenwood and Beresford, 1979, Stannard and Weltz, 2006), and sometimes even enhance it (Steduto *et al.*, 2002). For closed chambers, the foremost distortion is caused by a build-up of gas concentrations inside the chamber, decreasing, the concentration gradients and therefore the fluxes. These effects require short-term rapid measurements (usually less than a minute). Pressure differences between the head space and open atmosphere can also effects measured fluxes (Davidson *et al.*, 2002) while pressure build-up inside the head-space may cause radial diffusion out of the chamber. All of these potential chamber effects usually result in underestimation of the soil flux.

Due to the interest in forest floor soil respiration in recent years, various improvements in chamber design were made that have minimized chamber effects. Technical improvements include suitable chamber dimensions to minimize flux distortion while optimizing flux sensitivity; pre-installation of collars in the soil in order to increase sealing and prevent both radial diffusion and burst of gasses during chamber installation; usage of chamber fans in appropriate speed to reduce concentration build up while avoiding pressure effects; and installation of vents to equalize pressure build up. Davidson *et al.* (2002) summarize results from several modeling, laboratory and field studies using chambers for CO_2 fluxes, and concluded

that closed non steady-state chambers produce an artifact ranging from negligible to 15% underestimation, depending on soil texture and water content.

Reports of validation and measurements of water vapor fluxes with soil chambers are scarce. However, testing the accuracy of such chambers is made easier and more reliable in comparison to other trace gasses due to the possibility of comparing the relatively large water fluxes to the direct and absolute change in soil weight due to change in water composition. The energy balance (Bowen ratio) or soil water budget (e.g. using TDRs) techniques are also used in order to test chamber measurements. While most chamber designs were found to be in good agreement with other methods (Greenwood and Beresford, 1979; Reikosky *et al*., 1983; Dunin and Greenwood, 1986; Pickering *et al.*, 1993; Iritz, 1996; Steduto *et al*., 2002; McLeod *et al.*, 2004), some were found to consistently overestimate vapor fluxes (Grau, 1995; Dugas *et al*., 1997; Stannard and Weltz, 2006), mainly due to rapid fan speed. Others found a need to correct fluxes with calibration factors due to vapor condensing on chamber materials and other designed-related issues (McLeod *et al*. 2004, calib. factor=1.53, Stannard and Weltz, 2006, calib. factor=1.14).

In Summary, previous studies imply that soil chambers are a valid and suitable technique to measure soil water vapor fluxes in the field. Problems of concentration build up and alteration of meteorological conditions inside the chamber can be overcome by chamber design and rapid measurements. While careful testing and calibration is needed, this can be relatively easily achieved.

3.3 Flux estimates from chamber measurements

In this study, measurements of soil E were conducted with LI-COR 6400-09 soil CO_2 flux chamber (LI-COR Inc., USA). This IRGA-based technology measures changes in CO_2 and H_2O concentration over short time periods (1-3 s) with high precision (maximum deviation of ±1 mmol H_2O mol^{-1} air). The chamber and software were originally designed to measure and calculate soil respiration. Therefore, an adaptation of both components was needed for measurement of E. The evaporation process is a transient one; however, for short durations not longer than a couple of minutes, steady atmospheric conditions and energy balance may be reasonably approximated. Such assumption allows the application of a linear fit to the time

evolution in atmospheric gas concentrations (dH/dt, Figure 3.1), from which the flux, F, can be calculated:

$$F = \frac{dH}{dt} \times \frac{v}{s} \times \frac{p}{TR} + \frac{uH}{s} \quad (3.1)$$

Where F (mmol H_2O m^{-2} s^{-1}) is the vapor flux, s (m^2) the soil surface area confined by the chamber, dH/dt (mmol H_2O mol air^{-1} s^{-1}) is the change in the vapor concentrations with time, v (m^3) is the total chamber volume, p (Pa) is the pressure, T (K) is temperature, R (8.31 J mol^{-1} K^{-1}) is the universal gas constant and u (mol air s^{-1}) is the outflow rate through a pressure adjustment hole in the LI-COR chamber, which is negligible in comparison to the vapor flux inside the chamber and therefore neglected in the calculations.

The sensitivity of the above equation to changes or inaccuracy of its variables was assessed. Sensitivity of the flux estimate to temperature was 0.30% / °C, to pressure 1% / kPa and to soil collar height was 8% / cm. As expected and desired, sensitivity of the calculated flux was largest to dH/dt: 26% / mmol H_2O mol air^{-1} s^{-1} (1 mmol H_2O mol air^{-1} s^{-1} comprises less than 3% of the range of field measured dH/dt).

The trend of rising H_2O concentrations inside the chamber (such as the one presented in Figure 3.1) was similar for most measurements, representing different soil and environmental conditions. A curve fitting procedure was preformed and an exponential best fit line was defined (R^2=0.99):

$$y = y_0 + A_1(1 - e^{-x/t_1}) + A_2(1 - e^{-x/t_2}) \quad (3.2)$$

Comparisons of the flux derived from the slope of dH/dt calculated from the linear part and the exponential formula showed a high level of agreement. To simplify calculations, dH/dt was determined from the linear slope on a routine basis.

3.4 Chamber adjustments and testing

The system and analysis procedure were tested and chamber-based flux was compared to balance-based measurements using a calibrated semi-analytical balance with 0.01 gr sensitivity (Sartorius TE1502S, Germany). The IRGA was calibrated before and after each test, against known water vapor and CO_2 concentrations. The tests were preformed on soil samples taken from the upper part of the soil profile at our field site, which were oven-dried at 105°C for 24 hours and packed into containers to fit Yatir upper soil density (1.50×10^3 Kg m^{-3}).

Preliminary tests were conducted under laboratory conditions. Room air temperature ranged between 20-24ºC, RH varied between 40-50% and pressure was 101.50 kPa. Blank sensitivity of the soil chamber was checked on PVC non-reactive surfaces and showed steady concentrations and no flux. Distilled water was added gradually to a dry soil sample and weight was recorded. Evaporation was allowed to take place for a given time, which was followed by gas exchange measurement and another weight determination. This was repeated until θ reached 0.32. Observed gas exchange fluxes were compatible with the changes in θ (Figure 3.2). Adsorption of water by the dry soil was detected for $\theta<0.03$. A highly linear trend of dH/dt ($R^2>0.99$) was observed during the first part of all tests, but the period of the linear change was short (4-6 seconds). It was assumed that this was due to chamber dimensions, originally designed to measure fluxes of a trace gas (CO_2), but rapidly reaching saturation concentrations for H_2O. Therefore, the chamber volume was increased by a 10 cm extension made of transparent Perspex that was properly sealed to both soil collar below and soil chamber above (Figure 2.3). The extension achieved the desired effect and extended the period of the linear trend in dH/dt to 20-50 seconds.

The second phase of method validation was conducted outside the laboratory under outdoor meteorological conditions. These included two drying tests (θ reduction from field capacity down to air-dry) and two wetting tests (θ increased from oven-dried to saturation). The drying tests were run continuously over 15 days and the wetting tests lasted several hours. The tests were conducted during different seasons and hours, to maximize variability of micrometeorological conditions. Estimating E under outdoors conditions produced consistently underestimated fluxes, as compared

to the balance-based results. However, precision of chamber-based measurements was high (less than 5% difference between replicates) in spite of fluctuating meteorological conditions for all flux ranges. The relations between chamber and balance based measurements was linear and constant for the entire range of tests (R^2=0.95, n=54, Figure 3.3) and indicated:

$$E_{balance} = 2.66 \cdot E_{chamber} \qquad (3.3)$$

The three lowest values of E (high-negative) somewhat deviated from this relation. However, values below -0.01 mm hr^{-1} (chamber-based) were not measured at the field, and so did not create a problem. The factor obtained neglecting these points would have increased corrected fluxes in less than 2% and improve R^2 in 1%. In order to account for all possible range of fluxes, these low values were not eliminated.

This empirical relationships provided a practical mean to estimate E without considering or solving the theoretical difficulties in chamber flux measurements. Balance-based results were regarded as an absolute reference and the above equation was universally used in all measurements conducted using the extended chamber.

Based on our test and experience with the modified soil chamber the following procedure was used throughout this study: (a) The LI-6400-09 was operated with the fan working on slow speed and the pump off. (b) The chamber was positioned sideways, open to the near ground atmosphere, until steady state was observed. (c) The chamber and extension were rapidly mounted above a pre-installed soil collar. Foam strips were laid between chamber/extension and extension/soil collar in order to improve sealing. (d) The concentration of H_2O inside the chamber was monitored and recorded every second for 60 seconds. (e) The linear phase of concentration rise was defined, for which the slope (dH/dt) was calculated. The water vapor flux was calculated according to Eq. 3.1 and corrected according to Eq. 3.3.

3.5 Figures

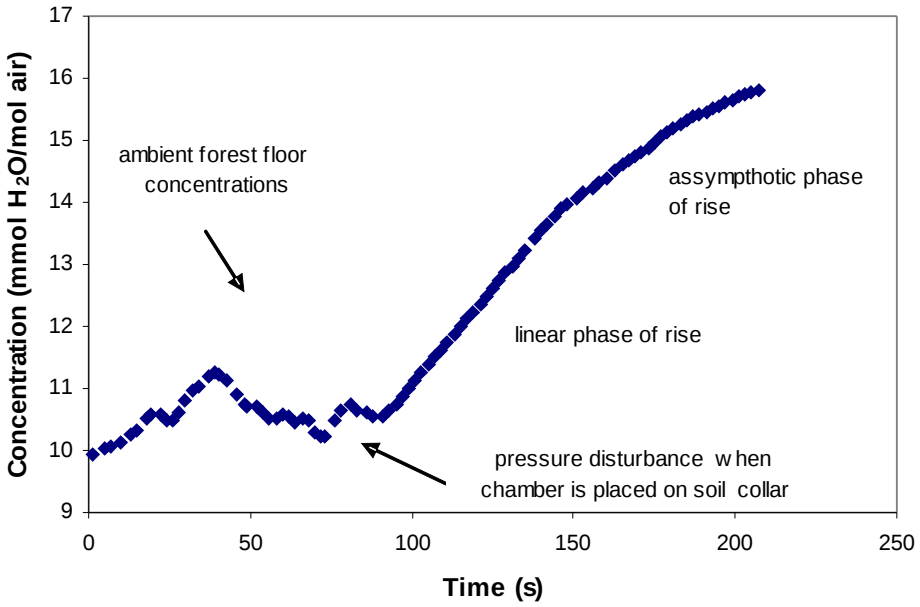

Figure 3.1: A typical sequence of water vapor concentrations measured with the soil chamber. Prior to measurement, the chamber was positioned open on the ground until equilibrium with ambient forest floor conditions was reached. Flux measurements started by placing the chamber on the soil collar, which induced a typical initial disturbance due to pressure change. This was followed by a linear phase of increased water vapor concentration inside the chamber (t~50 s, R^2>0.99). Due to concentration build-up and distortion of ambient meteorological conditions, the linear phase was disturbed after approximately 60 s, followed by a slower asymptotic rise.

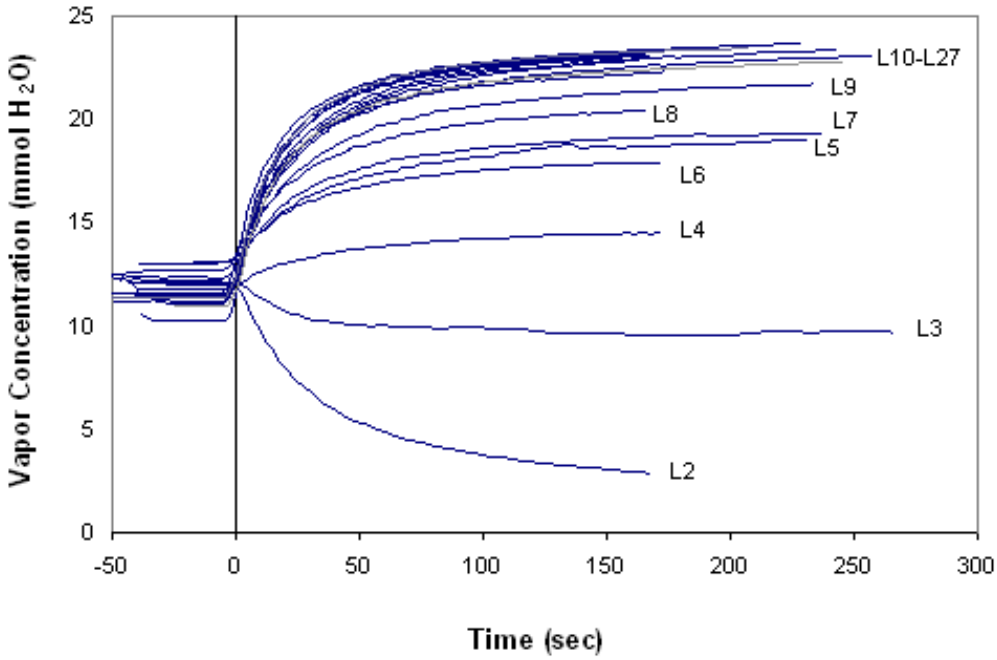

Test	E	θ
	mm hr^{-1}	m^3 m^{-3}
L27	0.142	0.32
L25	0.136	0.22
L22	0.135	0.19
L20	0.135	0.17
L21	0.130	0.17
L23	0.127	0.19
L26	0.123	0.22
L19	0.119	0.14
L11	0.115	0.10
L12	0.110	0.10
L10	0.102	0.07
L9	0.081	0.05
L8	0.068	0.05
L7	0.066	0.04
L5	0.057	0.03
L6	0.046	0.03
L4	0.027	0.02
L3	-0.021	0.01
L2	-0.068	0.00

Figure 3.2: Correspondence between the rising trends of water vapor concentrations inside the chamber (dH/dt) and the soil water content during laboratory experiments (L2-L27). T=0 is the time when the chamber was positioned on the soil sample. Soil water adsorption (negative trend) was measured for $\theta<0.03$. The soil water content and the evaporation flux of each test are noted in the complementary table.

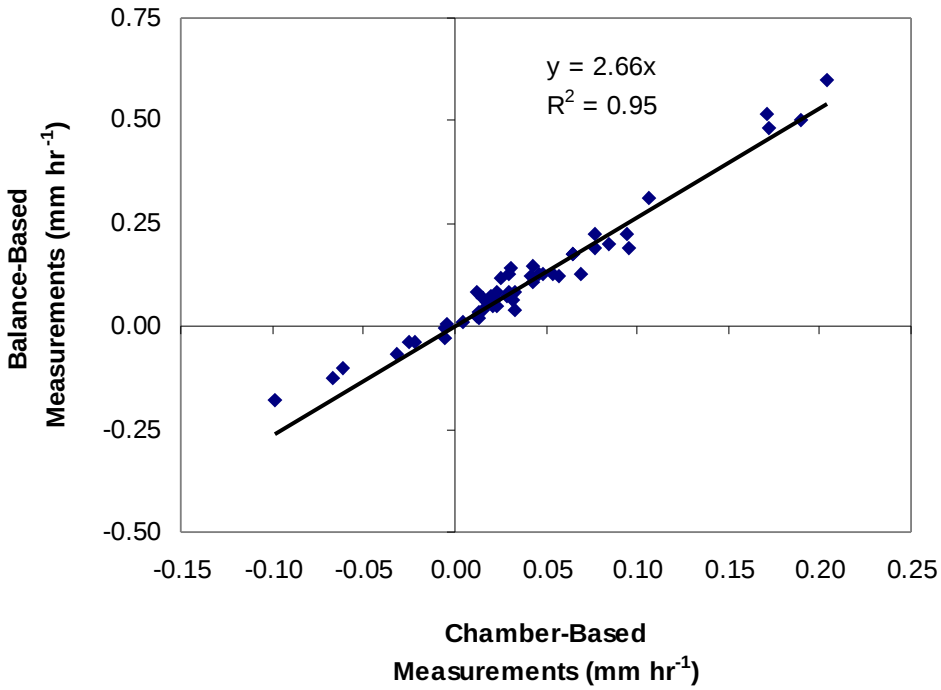

Figure 3.3: Correlation between balance-based and chamber-based measurements of soil evaporation during outdoor tests conducted under variable meteorological conditions (n=54). The three lowest values (high-negative) somewhat deviated from this relation but were never measured at field conditions. The balance technique was considered as a reference and the calibration factor (2.66) was used in order to correct chamber measurements.

Chapter 4

The spatial variability of soil evaporation below the canopy of dry forest

4.1 Introduction

Semi-arid forests and Yatir as a case study are characterized by low tree density that presumably allow sufficient water supply to all trees. In such ecosystems, the fraction of bare soil vs. vegetated areas is relatively large, producing high heterogeneity of surface conditions. The differences in radiation load between sun-exposed and. tree-shaded areas at these high radiation environments is enlarged due to the openness of the canopy (Martens *et al.* 2000). Below-canopy radiation is significant (Morecroft *et al*., 1998, Diawara *et al*., 1991) and maximum spatial variance in PAR was detected for canopy cover of 20-40% (Martens *et al*., 2000). In addition, the bareness of the soil exposes the high heterogeneity of surface characteristics (soil, rocky surfaces, bio-crusts, etc.), consequent being large variance of soil water content at the upper soil layer, caused by variability in runoff production, redistribution and infiltration at the different sites (Yair and Raz Yassif, 2004).

The spatial variability of these factors, which affect the rate of E, is expected to produce large spatial variability of E (Breshears *et al.*, 1998). Despite the significant contribution of E to the ET flux, the issue of the spatial variability of E in vegetated systems is rarely reported. Little is known on the effect of canopy design (tree size and density) on these losses Here, we use the specially developed system to measure variations in E below the canopy and estimate the effect of canopy design on canopy scaled E.

4.2 Results

4.2.1 **The effect of tree shading on E**

Measurements of E showed large spatial variability, and the normalized standard error (SE = standard deviation / √number of measurements × average) among collars during each of the measuring days was in the range of 5-45% (daily averaged E was in the range of 0.01-0.14 mm hr^{-1}, n=42 measurement days, each daily value is an average of 14 collars). We checked for two main potential contributions to the observed variations in E; light intensity in the PAR range and soil moisture. Below the canopy, PAR showed large spatial variability between the 14 measuring points, with SE during each of the measurement days ranging between 10 and 25% (daily averaged PAR was in the range of 182-1079 W m^{-2}). Some of this variability was likely due to changes in cloud cover and variation in solar angle during the 1-1½ hours measuring period.

In spite of the low LAI in this ecosystem, a large fraction of PAR was intercepted by the canopy, producing ratios between PAR above canopy and PAR below canopy of 6 during a typical winter days and of 2 during summer days (Figure 4.1). This partial interception resulted with large variations in soil temperature between shaded and sun-exposed surfaces (Figure 4.1). Spatial variation in θ among the 14 measurement sites was smaller than that of PAR, with SE of 2-13% for θ at depth of 0-10 cm (averaged daily θ in the range of 0.08-0.36). A multiple linear regression combining these two parameters most affecting evaporation partly explained the spatial variability of E (R^2=0.42, P<0.0001):

$$E = 7.91\times10^{-3} + 5.00\times10^{-5}\cdot PAR + 1.93\times10^{-3}\cdot\theta \qquad (4.1)$$

The effect of PAR was greater than that of θ, with standardized coefficients of 0.60 and 0.40, respectively. Accordingly, we used PAR values to divide the collars into three groups: "sun" – receiving sunlight during all daylight hours (5 collars); "shade" – not receiving direct radiation at all (4 collars); and "intermediate" - collars situated in inter-tree gaps and incoming radiation varied during the day from shade to

sun (5 collars). The grouping of soil collars according to PAR showed greatly reduced variability in E, with SE of 21% *within* groups, on average.

Differences in PAR *between* groups was most significant during the high-radiation load summer days, in which "shade" collars received only 8% of the averaged radiation of the “sun” group (Figure 4.2 and Table 4.1). On an annual average, measured incoming radiation for the "intermediate" and "shade" groups was 75% and 30% of the "sun" group, respectively. θ was higher in the "intermediate" group during the wetting period, while at winter higher values were measured in the "shade" group, below trees.

Differences in E between the groups was largest during the transition periods, in which "sun" collars produced fluxes twice as high as those measured at "shade" or "intermediate" collars. During the dry season, albeit overall low fluxes, the high difference in PAR between "sun" and "shade" collars was still reflected in E. Interestingly, although difference in PAR between the groups was gradual and significant, averaged E of "intermediate" resembled that of "shade".

4.2.2 **From point to ecosystem scale fluxes**

The sample size required for an appropriate representation of mean E at confidence level of 95% was evaluated using Eq. 2.1 and varied between 1 and 322 (average of 45) collars. The required collar number increased with the daily SE and was greater than 14 during half of the measuring days. Therefore it was concluded that up-scaling evaporation from point-measured E to canopy scale was not applicative using a normal average of E, and an additional methodology was developed in order to represent ecosystem fluxes.

The division of collars into three groups according to PAR was utilized for the benefit of flux up-scaling, as SE within each group was lower, implying on a relatively constant relation between tree shading and E. Accordingly, an up-scaling approach was implemented based on the relative proportion of the shaded areas (shaded fraction, SF, derivation of values presented in Section 2.3 and Appendix 4). Noontime annual averaged SF was calculated to be 66%, with summertime minimum of 57% and wintertime maximum of 75% (Figure 4.3). Similar results of canopy cover were obtained by Sprintsin *et al*., 2007, for a nearby plot. Maximum SF lasted between September and April, including most of the wet season. The estimated SF

values were then used to calculate the spatially averaged soil E (E_s), according to Eq. 2.2, in which E_{shade} and $E_{intermediate}$ were combined, as differences between them were not significant.

Values of E_s varied between 0.10 mm hr^{-1} during the high θ and high SF season (early to late winter) to 0.01 mm hr^{-1} during the low θ and low SF season (summer). The effect of SF on E_s was such that during the high SF season, the contribution of the high E values measured at the "sun" collars was decreased. During the period of low SF, E_s was approximately an average of E measured at the "sun" and "shade" groups.

4.2.3 **Estimating ecosystem E/ET from forest floor shaded fraction**

The above methodology of characterizing the proportional contributions of sun-exposed and shaded surfaces was further utilized in order to estimate changes in the relative contribution of E to total ET as a result of changes in tree size and density. We utilized measured allometric relationships between tree height and crown width developed for our forest site (Bar-Masada *et al.*, 2006; Grünzweig J., personal communication) to calculated SF for 5 tree dimensions, representing canopy cover from 1 to 100% (Table 4.2). We then estimated the effect of change in SF on E_s for the specific days shown in Table 4.1, according to measured values of E_{sun} and E_{shade} and the calculated SF.

Estimated changes in E_s due to tree growth are presented in Figure 4.4. We found that both tree age (development) and tree density strongly influence soil E, with clear interactions on the seasonal cycle. Tree development influence E to the greatest extent during the wetting period, when E decreased from 0.21 (juvenile trees) to 0.10 mm hr^{-1} (fully grown trees). Increasing tree density extended the period of maximum SF, decreasing the large E rates during the drying and wetting periods (Figure 4.5). At tree density of 600 trees ha^{-1}, distance between trees would be approximately 4.6 m and a full cover of the forest floor (for current tree size) will persist almost all year round, resulting in decreased E from current situation (300 trees ha^{-1}) of 0.14 to 0.06 mm hr^{-1}, during the wetting season.

Annual E and the reflected E/ET ratios were estimated for various canopy cover simulations. E was calculated for each season according to E_{sun}, E_{shade} and SF, the latter dependant on canopy cover. In the Yatir forest, annual E/ET was estimated

to decrease from 0.60 in the juvenile trees phase to 0.40 in the current tree size (40 years old trees, ~300 trees ha^{-1}), and potentially to 0.30 at a full canopy cover. An approximate closure of the forest floor by tree shading occurred at canopy cover > 75%. The non-linear relation between tree height and width was reflected in the relations between canopy cover and SF: SF increased slowly during the juvenile tree phase but was followed by a rapid increase in mature trees due to crown widening, affecting the shaded fraction.

4.3 Discussion

The issue of ecohydrological processes in water limited ecosystems is becoming increasingly important in light of persisting predictions of warming and drying trends in the entire Mediterranean region (IPCC 2007). Results from the Yatir forest site showed that soil evaporation accounted for approximately 0.40 of ET (Chapter 7), putting a strong emphasis on the competition between tree water use and soil water loss. Hence, the effects of changes in tree size and density on E were estimated using a simple modeling approach.

The spatial variability of evaporation in the research site was large, with measured E fluxes between trees double that below trees, on average. These trends were associated with the spatial pattern of radiation and soil water, both affecting the evaporation flux. Tree shading produced variations of up to 80% in PAR between sites. Variations in soil moisture between below trees and between trees sites was attributed to redistribution of localized runoff occurring due to areas of high runoff production (bare soil and rock surfaces) versus areas of high infiltration (at the border of below-crown soil areas, where accumulation of organic matter is large). Canopy interception decreases precipitation below the crown, but stem flow increases it, especially toward the perimeter of the crown (Shachnovich *et al*., 2008). These processes are mainly in the direction of reducing precipitation input below trees (Bredshears *et al*, 1998), consequence being that during the precipitation season, soil moisture is higher at exposed areas in comparison to shaded areas. During the drying season, tree shading enabled to maintained higher θ below trees (Fig. 4.2).

Differences between evaporation measured at the "shade" and "intermediate" collar groups was not significant, allowing us to combine these groups in further

analyses. It is suggested that the reason for this similarity is based on the high energy needed in order to produce E (Eq. 1.3-1.9), for which long and continuous exposure periods are needed, both for wet and for dry soils. The latter conclusion is reinforced by results showing that dry soil evaporation was weakly correlated to short term variations in R_n due to the buffering effect of the dry soil on the rapid changes of energy supply (Stannard and Weltz, 2006).

The large heterogeneity of soil E is particularly important when related to canopy level ET fluxes. Assessments showed that due to the high spatial variability of E, a large number of measuring points (45 on average) was needed in order to represent canopy-scale evaporation as an averaged of measured points with a 95% confidence level. This unreasonable sampling size demanded a development of an alternative up-scaling methodology. We calculated canopy scale E based on the grouping of E measurements according to PAR, showing lower SE within each group; and on the shaded fraction of the forest floor (Eq. 2.2). Simulated results of annual E/ET ratios for different forest design scenarios indicated that tree growth increased both absolute values of SF and the length of period of maximum SF, enabling to decrease evaporation fluxes during the high evaporation season (the wetting and drying seasons), and decreasing water loss by E in 50% during tree growth from 2 to 15 m. A similar effect is caused by increasing tree density, and more than 60% decrease in E during the wetting season is expected between stands of 100 and 600 trees ha^{-1}.

Such simulations can provide a practical management tool to estimate water loss by E within forested ecosystems. We show that this can be conducted based on SF, which in turn can be readily calculated from measurements of tree and crown dimensions. We also demonstrate that soil E in sunny and shaded areas can be characterized during representative days using commercially available equipment. Consequently, different scenarios and combinations of adequate tree type, size and density can be evaluated; therefore enabling to optimize tree water usage and productivity. However, note that the effect of increased shaded fraction on ecosystem hydrology is complicated: as shown elsewhere in this study (Chapter 6), improved water uptake by trees occurs only when water infiltrates to sufficient depth. Other water related processes affected by growth of canopy cover such as canopy interception, below canopy transpiration and overall changes in tree transpiration should also be taken into account.

In summery, our study quantified the spatial variability in soil evaporation at a semi-arid open canopy forest, showing that canopy cover modifies the microclimate beneath trees, including radiation exposure, soil temperatures and soil moisture, all influencing evaporation rates. The spatial variability of E could potentially further influence the spatial pattern of biological processes dependant on water content such as soil respiration (Grunzweig, to be published), microbial activity (Belnap *et al.*, 2005) germination (Aguilera and Lauenroth, 1995) and herbaceous composition (Kurk and Small, 2004).

4.4 Tables and figures

Table 4.1: Noontime values of E for each of the collar groups ("sun", "intermediate" and "shade") which were divided according to PAR, during days representing the different seasons in the research site. Standard error (SE) within each group of collars is noted, as well as daily averaged air temperature (T_{a_1}) and soil water content ($\theta_{0\text{-}30}$).

	T_{a_1} (°C)	$\theta_{0\text{-}30}$		Sun	Intermediate	Shade
Wetting Season 9/11/2006	17	0.13	PAR (W m^{-2})	1154±410	478±100	318±105
			E (mm hr^{-1})	0.210±0.071	0.110±0.022	0.097±0.026
Winter 15/1/2007	11	0.29	PAR (W m^{-2})	458±204	745±275	114±20
			E (mm hr^{-1})	0.051±0.019	0.037±0.016	0.028±0.003
Drying Season 28/3/2007	15	0.22	PAR (W m^{-2})	1351±136	833±216	195±58
			E (mm hr^{-1})	0.129±0.030	0.081±0.007	0.066±0.006
Summer 14/6/2007	20	0.09	PAR (W m^{-2})	1777±1	1687±40	141±2
			E (mm hr^{-1})	0.062±0.015	0.042±0.010	0.041±0.004

Table 4.2: Annual mean, minimum and maximum values of shaded fraction (SF) for various scenarios of canopy cover. The compatible crown width for each value of canopy cover was calculated from the projected tree shadow at zenith. Tree height was then extrapolated from allometric equations for Yatir. SF was determined daily for each canopy cover scenario according to tree dimensions and equations of noontime solar shading.

Canopy Cover (%)	Tree Height (m)	Crown Width (m)	Annual Forest Floor Shaded Fraction (%)		
			Average	Minimum	Maximum
1	2.1	0.7	2	1	4
25	6.8	3.3	38	29	54
50	10.0	4.6	66	57	75
75	11.2	5.6	88	84	92
100	12.0	6.5	100	100	100

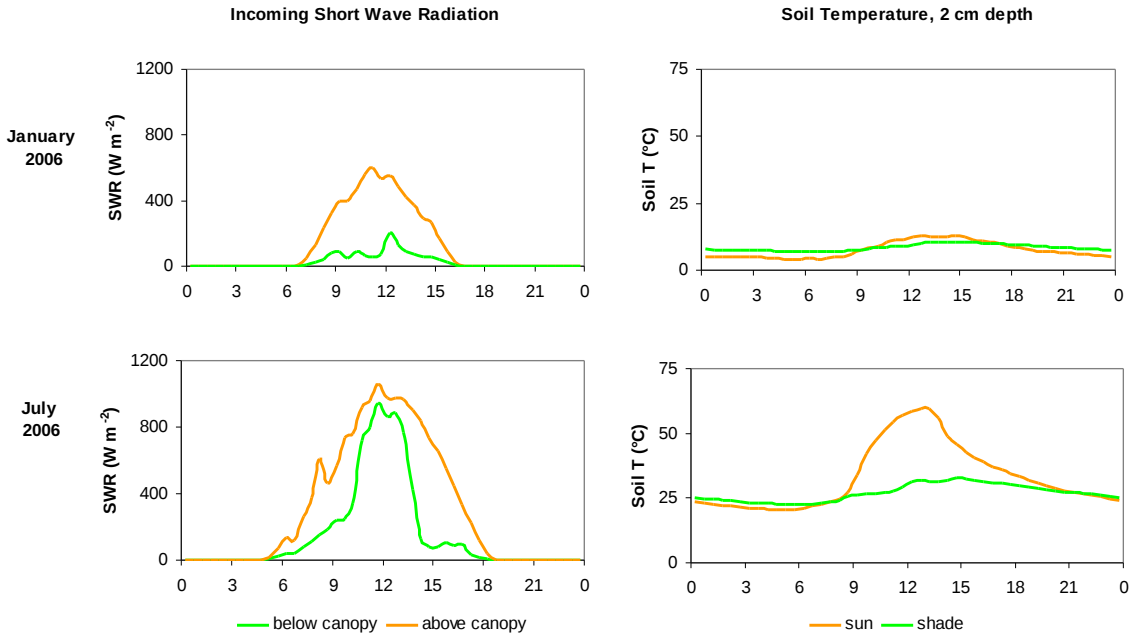

Figure 4.1: Differences in PAR (left) and T_{s_2} (right) above and below the canopy during a typical summers and winters day. Significant radiation penetration in this open, low LAI ecosystem increased variations in the factors influencing soil evaporation.

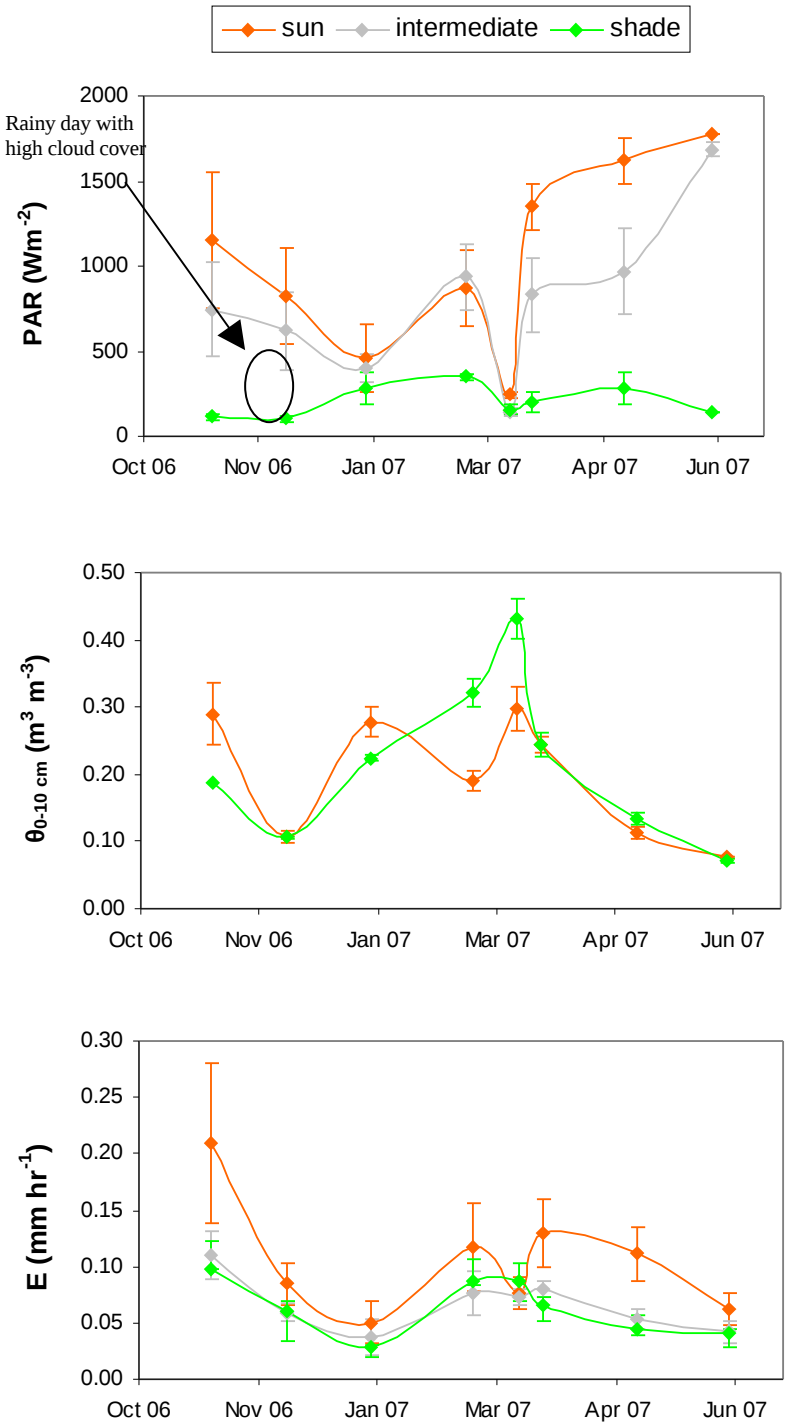

Figure 4.2: Seasonal trends of PAR, θ and E of the three groups of soil collars. SE is noted in bars. In spite of distinctive differences in PAR between the groups, E fluxes were similar in the "intermediate" and "shade" groups. θ was higher in the “sun” group during the rain season and in the “shade” group during the drying season.

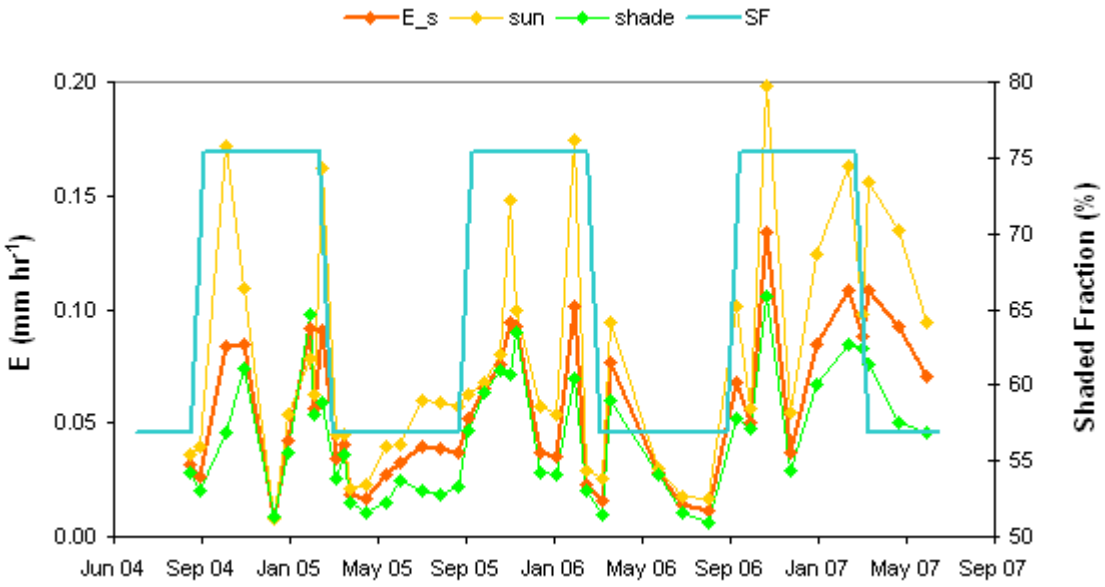

Figure 4.3: Canopy-scale soil evaporation (E_s) was determined according to two factors: the averaged E measured at "sun" and "shade" collar group, and the percentage of forest floor shaded fraction (SF, %). SF varied between 57% (summertime, minimum limit defined as an area of a circle, sun at zenith) and 75% (wintertime, maximum limit defined by the distance between trees, prohibiting mutual shading). During the period of low SF, E_s was approximately an average between E_{sun} and E_{shade}. During the period of high SF, E_s was lower than a simple average between the two groups and the effect of the high E_{sun} fluxes was decreased..

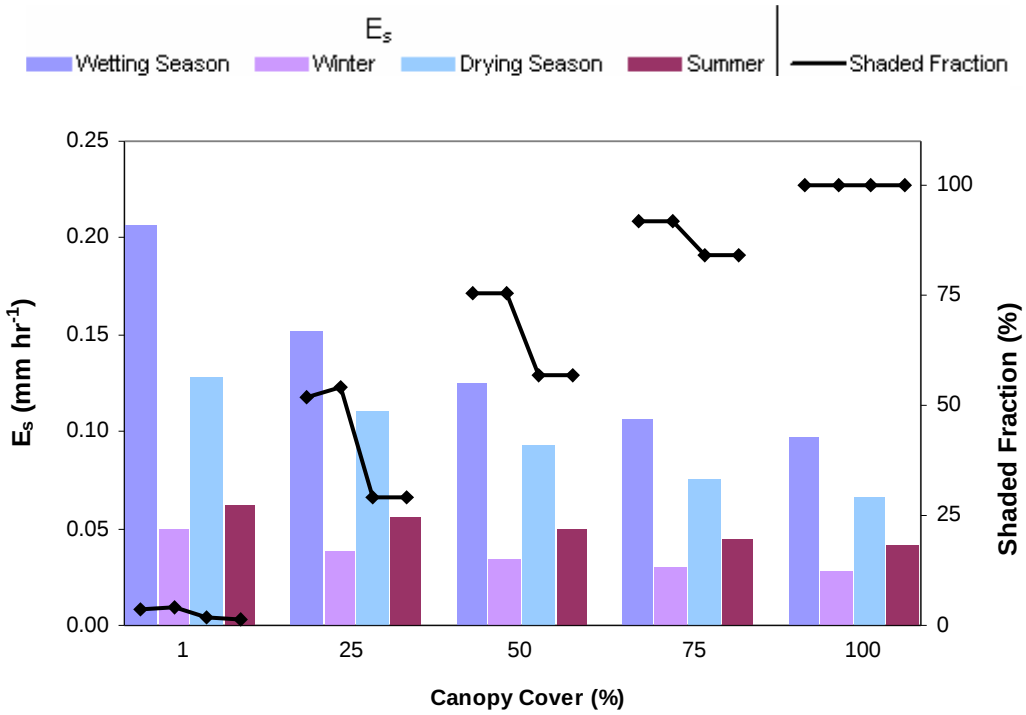

Figure 4.4: The change in spatially averaged soil evaporation (E_s) as a consequence of tree growth while canopy cover increases from 1 to 100%. The annual pattern of noontime daily shaded surface is also shown. Current canopy cover is approximately 50%. In addition to increased SF, tree growth elongated the period of maximum SF so that during the high E seasons (wetting and drying periods), E is suppressed by ~50% during tree growth from a height of 2 to 15 m.

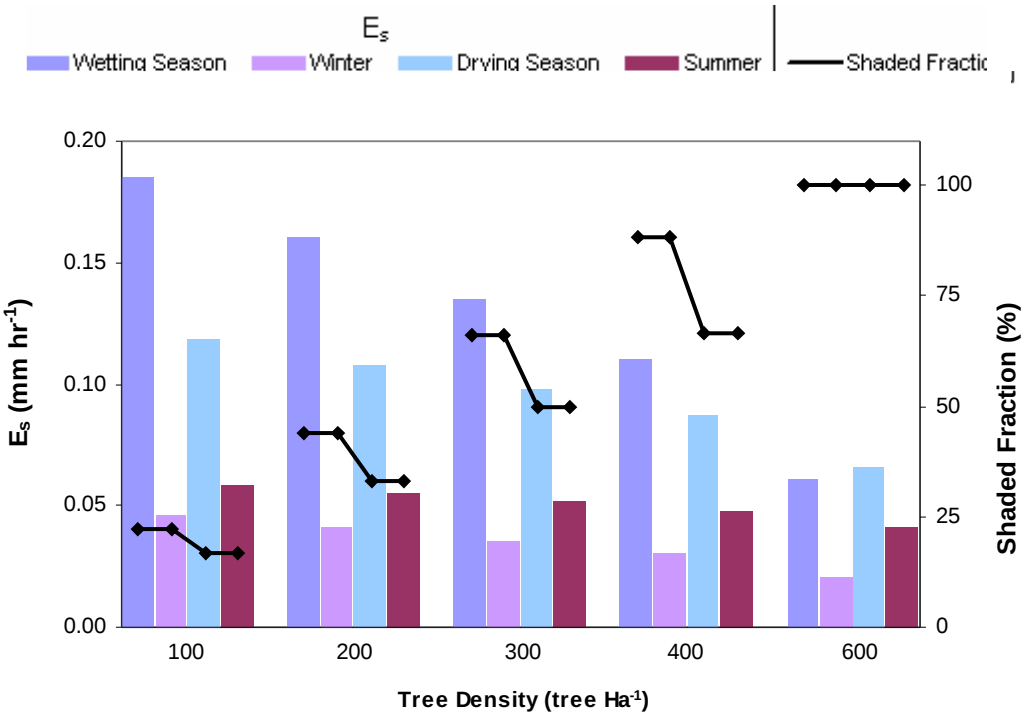

Figure 4.5: The change in spatially averaged soil evaporation (E_s) as a consequence of tree density. The annual pattern of noontime daily shaded surface is also shown. Current density is 300 trees ha^{-1}.

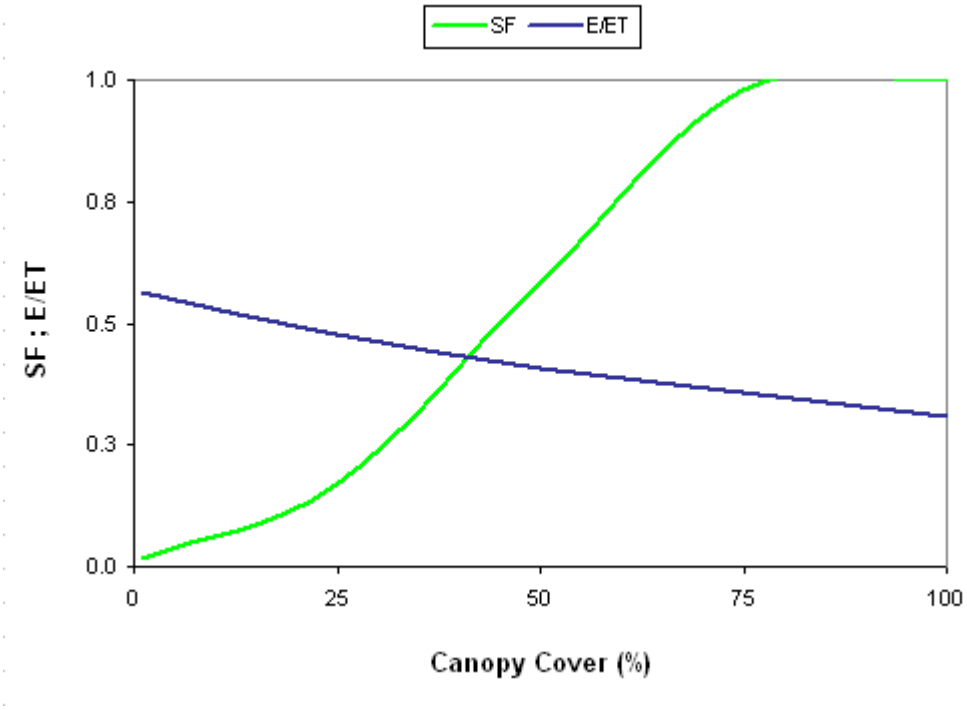

Figure 4.6: The effect of tree development on the water budget. Forest floor shaded fraction (SF) increased moderately during the juvenile phase followed by a rapid increase during the widening phase of tree crowns. Above canopy cover of 75% SF was already near maximum levels. Annual soil evaporation (E) was calculated for each season according to appropriate values of SF, E_{sun} and E_{shade}. At full canopy closure, annual E is not expected to decrease below 85 mm, accounting for 0.30 of total ET at Yatir.

Chapter 5

Temporal patterns of soil evaporation

5.1 Introduction

The response of vegetated ecosystems to the environment is a key issue intensively investigated by means of measurements and models on short and long time scales, especially due to the need to understand how vegetation will respond to projected scenarios of climate change (Granier *et al*., 1999, Law *et al*., 2002, Gervois *et al*., 2008). Still, there is a demand to improve the parameterization of these processes (Garratt, 1993, Grelle *et al*., 1997), implying on the insufficient understanding of ecosystem functioning and sensitivity to climate.

The Mediterranean climate is characterized by high seasonal variability, with rapid and strong changes occurring during the transition periods between the hot and dry summer months and the wet and cold winter months. Strong diurnal oscillations are also characteristic, especially at the arid and semi-arid regions, between the hot sunny hours and the cold nights. These transitions are accompanied with seasonal and diurnal variations in metrological conditions such as incoming radiation, air and soil temperatures, relative humidity, precipitation, soil water content and wind speed. Accordingly, a strong temporal variability in soil evaporation fluxes is expected. Precipitation events at these regions are highly sporadic, producing large annual variability in soil water content and therefore inter-annual differences of soil evaporation patterns are also to be expected.

Of special interest are the conditions prevailing during the long dry summer season. During this rainless period, values of potential evapotranspiration are high, reducing soil water contents to low and constant levels. Therefore, the processes producing soil evaporation and the mechanisms allowing for maintenance of plant activity during the dry season are in question.

In this research, fluxes of soil evaporation were measured at various days and seasons, spreading evenly during the three measured years, allowing for the investigation of diurnal to annual variability of soil evaporation.

5.2 Results

A clear diurnal cycle was observed during the days in which E was measured continuously (6 days in which E was measured at two collars every half hour, Figure 5.1 and Table 5.1). In summer, E ranged between null in the mornings and afternoons to a daily maximum of 0.04 mm hr^{-1} at noontime. During the wetting and drying seasons, the diurnal cycle was more noticeable and maximum noontime E fluxes of up to 0.20 mm hr^{-1} where measured. The diurnal cycle was not of a smooth bell-shape but rather had a sharp increases and decreases affected by instantaneous meteorological conditions, with peak E rates normally between 11:00-12:00. The trend and values of measured diurnal E fit well both T and ET and a good closure of the budget (ET=E+T) was achieved for most of these days. During four of the six days, leaf scale gas exchange was measured simultaneously by Maseyk, K. showing similarity of trends between leaf scale and whole tree T. Leaf scale gas exchange was not scaled to tree or canopy fluxes and therefore not shown here. However, this data was important during a day in which compatibility between the fluxes was not achieved (9/6/2005) and both E and T were low in comparison to ET. T fluxes were even lower than E and showed no daily fluctuations. Leaf gas exchange observed a similar trend, possibly reflecting some aboveground stress effect due to abnormal meteorological conditions (this was a "Hamseen" day).

Compatibility between E and ET included adsorption events, expressed in negative values of these fluxes. Soil adsorption of vapor, observed during laboratory testing on dry soils (Figure 3.2) was measured at the field during two of the three summer days in which E was measured continuously (28/9/04 and 9/6/05, Figure 5.2), in the hours close to sunrise and sunset. The adsorbed fluxes measured were small (-0.04 and -0.05 mm for the two days, respectively), but were not negligible when related to the overall E fluxes during these days (0.28 and 0.14 mm). During these (and other) summer days, a good agreement was observed between the diurnal trends of atmospheric RH and θ (Figure 5.2). This agreement directed to the physical process causing soil water adsorption (Section 1.4): transport of moisture from the moist atmosphere (nighttime RH>75%) to the dry air within the soil pores (daily averaged θ_5<0.05). A diurnal amplitude in θ down to a depth of 30 cm was measured during the dry period (April – October), with amplitude decreasing with depth. However,

calculated contribution of adsorbed water from these amplitudes (difference between daily maximum and minimum θ values equaled 0.016, 0.004 and 0.003 m^3 m^{-3} for depths of 5, 15 and 30 cm, respectively) were higher than measured E. It is assumed, that although these TRIME TDRs are not supposed to be affected by soil temperature (Appendix 3) some effect exists, enlarging the actual diurnal cycle of θ.

Adsorption was not observed during one of the summer measured days (13/9/2004), even though high RH and low θ conditions occurred. Kosmas *et al.* (2001) indicate that adsorption is characterized by high oscillation of RH (daily amplitude of maximum-minimum values >25%). At our research site, nearly all days of the year have diurnal amplitude of RH higher than that specified and at summertime it is ~50%. The demand for high daily amplitude of RH for the occurrence of adsorption fitted our results: during the day in which adsorption was not measured the amplitude of RH was 40%, while it was 70 and 55% for the others.

A good simulation of half hour E values was achieved incorporating half hour meteorological variables into multiple linear regression equations. The parameters used were the same as for the simulation of noontime daily values (θ_5, R_n, VPD, T_a and WS) and a specific multi-linear regression was constructed for each day ("specific regression", Figure 5.3). Simulated values fitted well measured values ($0.81<R^2<0.95$, $P<0.05$), including adsorption events, and calculated total daily E with a cumulative error smaller than 2% (in comparison to measured values). Simulated peak E values were slightly lower than measured peak E values. However, the utility of these regressions was low as they were fitted for specific days, and so an additional regression, combining half hourly data from all six full measurements days, was constructed ("general regression", Figure 5.3, $R^2=0.62$, $P<0.05$):

$$E = -0.013 + 0.082 \cdot \theta_{0\text{-}30} + 2.680 \cdot 10^{-5} \cdot R_n + 0.004 \cdot WS \qquad (5.1)$$

where E here indicates simulated E by the general regression equation. The standardized contribution of each of the variables ($\theta_{0\text{-}30}$, R_n and WS) was 49, 38 and 13%, respectively. T_a and VPD were deleted from the simulation due to co-linearity with other parameters. Predictions by this regression for days in which E was not measured were not successful and values were often unacceptably low (therefore

adopting the methodology elaborated in section 2.5 to gap fill the measured E database).

Based on noontime measurements of E (on 42 days evenly spread measured days), the seasonal trend was characterized by high fluxes during the wetting and drying periods (maximum daily fluxes of 0.20 mm hr^{-1}, Figure 5.4) and lower fluxes during mid-winter and summer (maximum daily values within the range 0.01-0.04 mm hr^{-1}). Low fluxes were measured during mid-winter, when temperatures were low (T_{a_1}<15°C) and during the dry summer season (θ_5<0.08). High fluxes were measured when high soil water content (θ_5>0.23) at the upper soil layer was combined with relatively high air temperatures (T_{a_1}>15°C), i.e. the transition periods. Accordingly, daily measured values were divided into four typical seasons and a multi-linear regression was assembled for each season utilizing meteorological parameters (Table 2.2). A stepwise procedure enabled to choose the most appropriate variables between the given meteorological parameters (θ_5, R_n, VPD, T_a and WS) for each season. R^2 between measured and simulated values was high for most seasons: wetting season = 0.68, winter = 0.81, drying season = 1.00 and summer = 0.98. During summer θ was irrelevant as soil moisture was constantly low and the relative contribution (β%) of R_n was highest. During the wetting and drying periods θ had the largest affect on simulated E and during winter it was T_a.

The variability of the seasonal trend of E between the three measured years was low, and a similar annual pattern was kept, in spite of differences in precipitation, between the three hydrological years.

5.3 Discussion

Evidence from atmospheric general circulation models suggests that the climate is sensitive to variations in evaporation from the land surface (Schmugge and Andre, 1991, Yang *et al*., 1998), therefore depending upon the accuracy and sensitivity of the parameterization inputs of land surface processes in these models. In light of the large contribution of E to ET, especially in dry systems, models' improvement is dependant upon the efficiency of predicting soil evaporation from environmental and meteorological variables. Various models, due to lack of sufficient field data, simplify soil evaporation and derive it as some function of PET and θ (Granier *et al*., 1999, Chen and Dudhia, 2001). Comparison between evaporation values derived from these types of models and evaporation values measured at the Yatir field site showed very low compatibility, with modeled fluxes overestimating even rates of total ET.

The methodology developed in this research enabled to measure and study temporal patterns of soil evaporation. Observed results showed trends of E had high variability between seasons. Therefore, the effect of the meteorological conditions was checked by producing best-fitted multi-linear regressions and simulating measured E values. The pattern of measured E had noticeable diurnal cycles, with peak daily values around noon time and compatibility to measured trends of T and ET. The annual cycle showed typical seasonality, with high fluxes during the wetting and drying periods (up to 0.80 mm d^{-1}). A decline in fluxes occurred after the short wetting season, with respect to decreasing values of R_n and T_a, until minimum values of ~0.10 mm d^{-1} were measured during mid-winter (T_a<15°C). Low fluxes were measured also during the dry and long summer period (θ_5~0.05). The observed seasonal trend was similar between the three measured years alas the large annual variability in precipitation patterns and amounts between the years. This issue will be discussed in the following chapter.

A good seasonal correlation (Table 2.2, $0.81<R^2<0.95$, $P<0.05$) was obtained between measured and simulated values of E. Simulations utilized data of R_n, T_a, VPD, θ_5 and WS, with varying partial contribution between seasons. However, similar to their impact on the spatial variability of E, the variables most effecting diurnal and seasonal cycles of E were θ and R_n (or, alternatively, R_n as indirectly expressed in T_a),

with the first (θ) more significant during the water limiting period (wetting and drying season) and the latter (R_n and T_a) more significant during the energy limited period (winter) and the dry summer, for which θ was non-relevant. Wind speed was also found to influence diurnal changes of E. However, its effect was variable between hours of days and between days of the same season, therefore making it difficult to usefully incorporate in a general equation.

During the hours before sunrise and after sunset of the summer season, soil adsorption was observed. Measured negative fluxes did not balanced the positive fluxes of E measured during the daytime hours (~0.05 mm adsorbed and 0.14-0.28 evaporated, varying between measured days) but whole nighttime E was not measured in this research, and therefore total adsorption amounts could not be estimated. The few researches focusing on this process measured soil adsorption during the summer period at various dry Mediterranean sited to be within the range of 0.70-1.44 mm d^{-1}, varying according to site characteristics, mainly soil texture and canopy cover, and accounting for up to 70% of total daily bare soil E fluxes (Kosmas *et al.*, 2001, Verhoef *et al*., 2006, Ramirez *et al*., 2007). Ninari and Berliner (2002) reported on lower nighttime condensation values: 0.13-0.23 mm for a bare soil in an arid site in southern Israel during the summer season. The latter values are still higher than total daily summer E fluxes reported here (0.10-0.20 mm d^{-1}). This could be attributed to differences in soil texture and meteorological conditions, but also to the reported negative effect of trees and plants on adsorption amounts (Kosmas *et al*., 2001, Ramirez *et al*., 2007). To conclude, these values indicate that the mechanism of adsorption can be responsible for 30-70% of the total daily summer E fluxes, in correspondence with earlier studies.

Global circulation models often disregard processes occurring in dry regions and especially those relevant to the dry season, during which soil water content is below wilting point (i.e. adsorption), thus contributing to the insufficient parameterization of evaporation from land surfaces (Boulet *et al*., 1997). The reliance of simulated E during all seasons on more than one variable also indicated the need for more sophisticated parameterization of evaporation processes of dry regions.

5.4 Tables and figures

Table 5.1: Environmental condition during the full measuring days. Daily sums of measured E, T and their ratio with ET are also presented. Adsorption (A) is included in the net total daily sums (E).

	13/9/2004	28/9/2004	3/3/2005	14/3/2005	20/4/2005	9/6/2005
$\theta_{0\text{-}30}$ ($m^3\ m^{-3}$)	0.09	0.08	0.22	0.33	0.13	0.10
R_n max ($W\ m^{-2}$)	678	624	577	680	682	760
VPD max (kPa)	3.31	5.99	2.53	0.68	3.19	2.43
T_{a_1} average (°C)	20	28	19	9	20	20
WS average ($m\ s^{-1}$)	0.61	0.61	0.68	0.68	0.66	0.57
E total ($mm\ d^{-1}$)	0.10	0.14	0.57	0.78	0.23	0.09
A total ($mm\ d^{-1}$)		-0.04				-0.05
T total ($mm\ d^{-1}$)			1.14	0.78	0.64	0.16
ET total ($mm\ d^{-1}$)	0.25	0.35	1.90	1.61	0.96	1.13
E/ET (%)	38	39	30	49	24	8
T/ET (%)			60	49	67	15
(E+T)/ET (%)			90	97	91	22

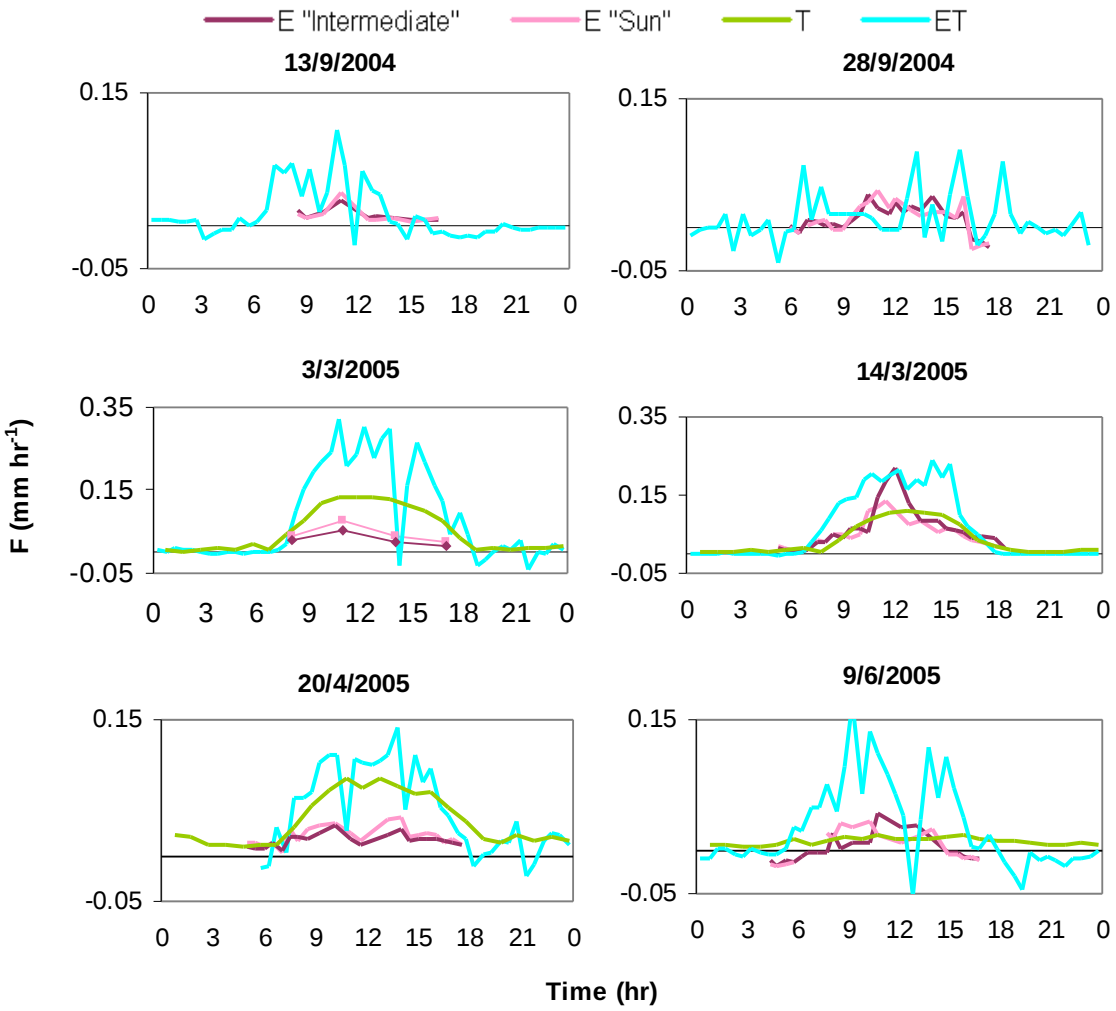

Figure 5.1: Whole day measurements of T (1 hr values, average of 8 trees, HPV), E (half hour values, two adjacent soil collars, soil chamber technique) and ET (half hour values, flux tower). T was not measured during the first two campaign days. Measurements showed high compatibility of diurnal trends between flux components (see Table 5.1 for total daily values). Low compatibility was observed during 9/6/2005.

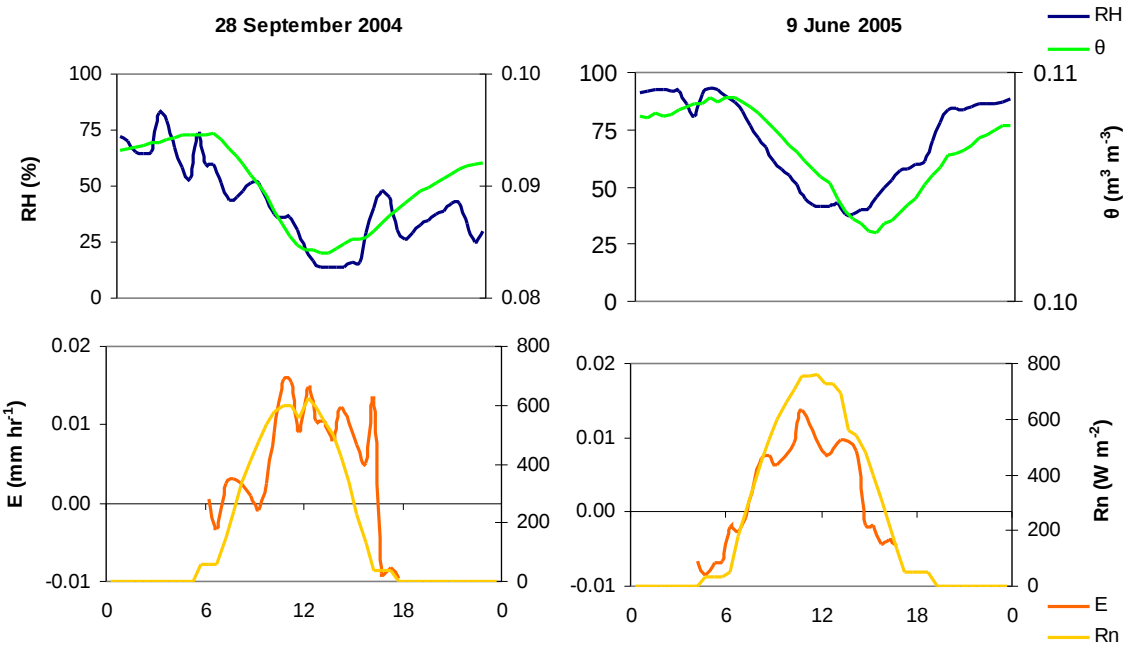

Figure 5.2: Days of measured soil adsorption. Negative fluxes of soil evaporation (E) were measured before sunrise and after sunset (represented in R_n) during two of the full measuring days. A good agreement was observed between atmospheric relative humidity (RH) and the trend of water content in the soil (θ), implying on equilibrium of water vapor concentration between the air within the dry soil pores and that above the soil: adsorption was measured during hours of high RH and θ and evaporation was measured during hours of low RH and θ.

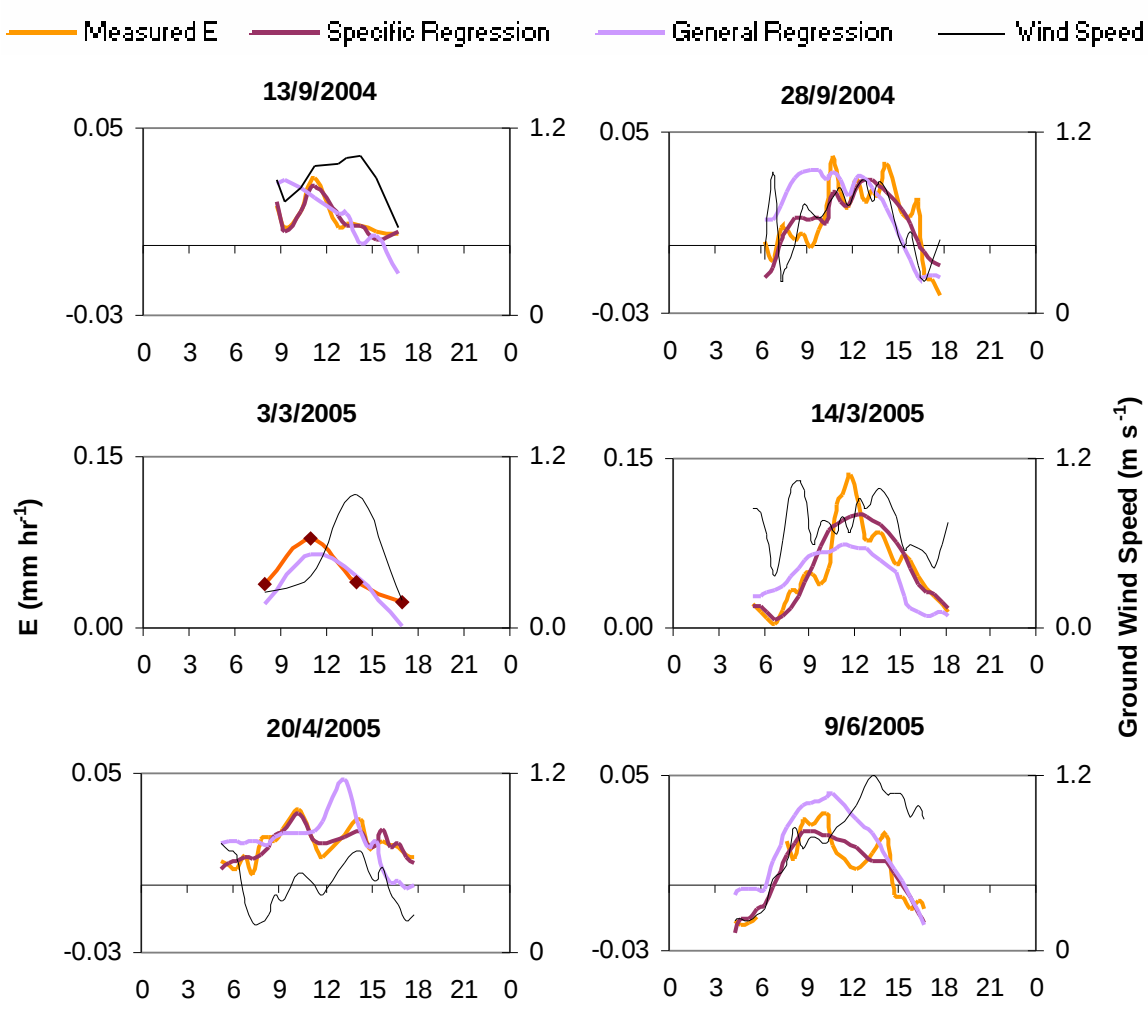

Figure 5.3: Half hour values of measured and modeled diurnal cycles of E. Measured E is an average of two soil collars (Figure 5.1). A linear regression was applied separately for each of the days (Specific Regression) and for the combined data from all days (General Regression). Both regressions described well measured values utilizing environmental variables, including soil water adsorption events. Wind speed is also shown; its effect on E was variable between days.

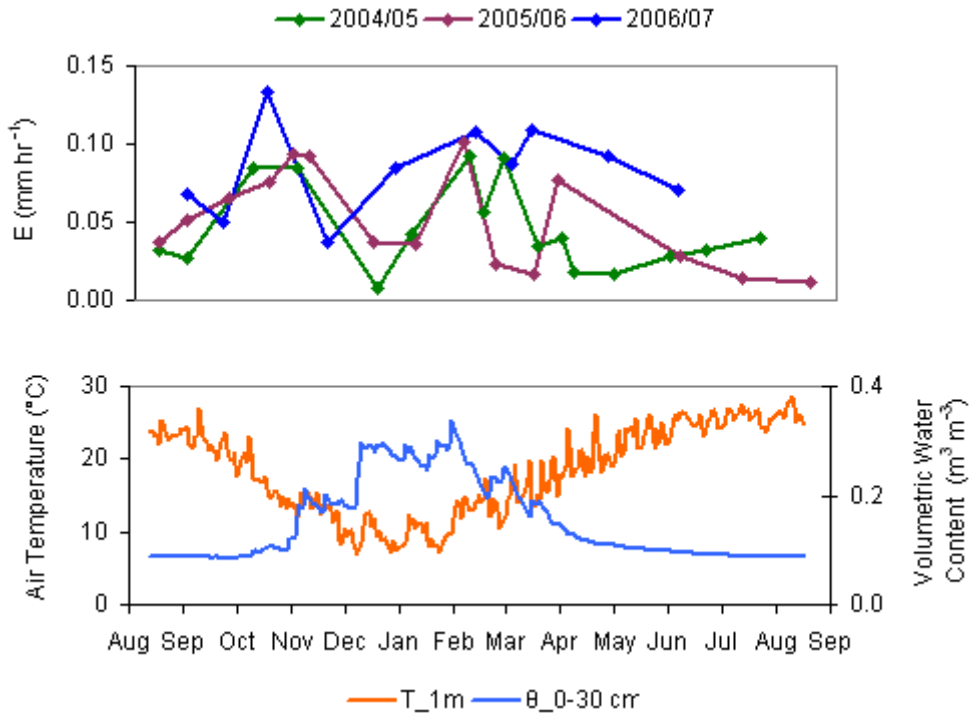

Figure 5.4: Seasonal trend of measured E_s (upper graphs), air temperatures and soil water content (lower graph). Similarity between years was large: peak rates were measured during early and late winter (combination of high soil water content and temperatures) and lower rates were measured during mid winter (low temperatures) and summer (low soil water content).

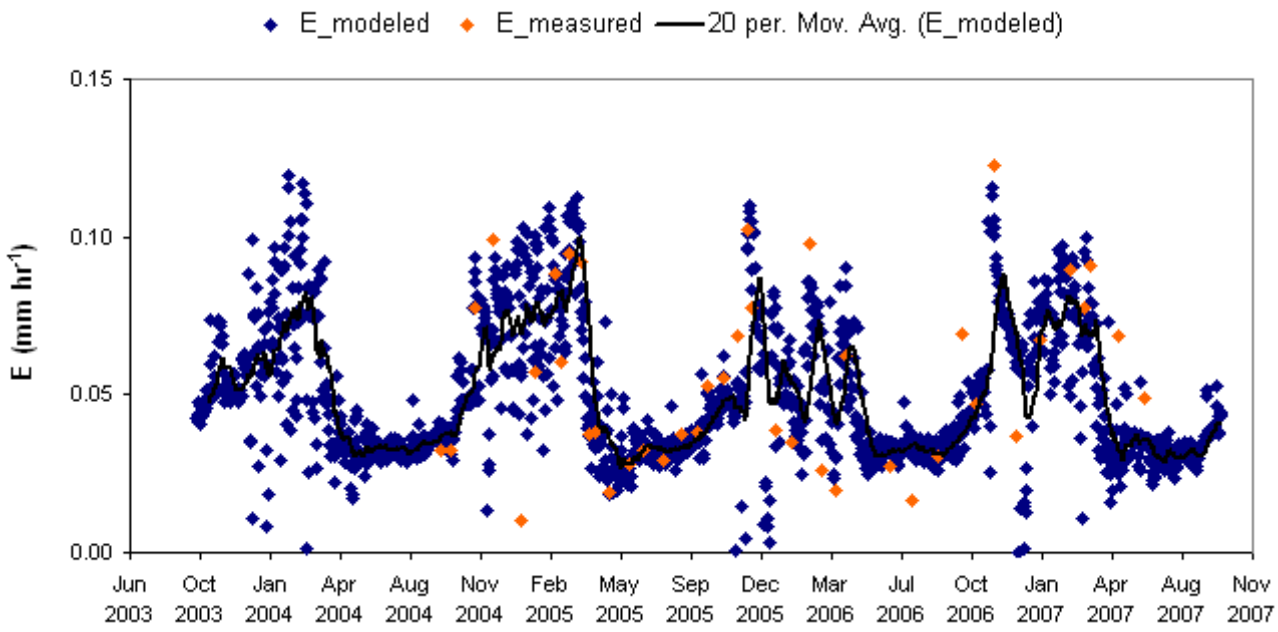

Figure 5.5: Noontime measured values of E_s (approximately equaling to daily maximum fluxes and representing field spatial variability) and modeled E. Modeled E values were calculated from multi-linear regressions obtain separately for each season based on environmental parameters and measured E_s. Datasets show reasonable compatibility and thus were used in order to gap-fill the measured values.

Chapter 6

Resolving the water balance of the Yatir forest

6.1 Introduction

Semi-arid ecosystems are primarily water-controlled environments. While temperature, radiation and often nutrients are sufficient for the existence of biota continuously throughout the year, water is a strong limiting factor most of the time (Noy-Meir, 1973). Precipitation in these climates is characterized by convective cells, which produce discontinuous rain showers (Sharon, 1972). The distribution of storms throughout the year and the resulting soil moisture content at different depth can have a significant effect on the partitioning between water evaporated from the soil and water that is available to plants.

Precipitation, the input to the water balance (Eq. 1.1), is distributed into runoff, recharge and evaporated water, the latter further partitioning into soil evaporation, tree transpiration and intercepted precipitation (Eq. 1.2). The distribution between these components is controlled by the nature of the precipitation and by the surface characteristics of the ecosystem encountered by the precipitation. Therefore, knowledge regarding precipitation patterns and amounts, the canopy structure and density and the soil characteristics (crusts, depth, texture, density, etc.) is necessary in order to understand processes of runoff, infiltration and subsurface flow (Hillel, 1972).

In dryland ecosystems, ET is the largest part of the water balance and usually accounts for approximately 90% of the rainfall (Zhang *et al*., 2001). In these warm and water-limited systems, water uptake by vegetation is dependant on the unavoidable losses by soil evaporation, runoff and drainage (Noy-Meir, 1973). In most vegetated dryland ecosystems, the latter components (runoff and drainage) are relatively small, further enhancing the control of soil evaporation on plant water availability. Therefore, partitioning ET into its components - soil evaporation and tree transpiration, is of great importance. Such partitioning is necessary in order to understand the biotic and abiotic factors influencing the pathways, amounts and

efficiencies in which water is distributed within the ecosystem. Partitioning the water flux will also contribute to the understanding of vegetation responses to variations in environmental conditions, and ultimately, their productivity (Law *et al.*, 2002, Small and Kurk, 2003, Huxman *et al.*, 2005).

Water use efficiency (WUE; the ratio between CO_2 assimilation and H_2O loss, Sections 1.2 and 1.6) is a center point between the water and carbon cycles, making it an important parameter to study in order to investigate plant and ecosystem response to environmental change. WUE integrates a complex of plant and ecosystem factors and can be determined for different scales, such as for the entire ecosystem or for the tree component alone. Partitioning of the ET flux can be further utilized in order to partition the WUE into these two components, which are expected to differ one from the other. Often, it is the later (tree component - WUE_t) that is needed in order to understand ecophysiological processes in detail, but rarely does enough information exist in order to specify it.

Accordingly, the nature of the precipitation and the characteristics of the soil in the research site were investigated, in order to define their effect on the distribution between the components of the hydrological balance. Soil water content at different depth was of special focus, as it serves as a crucial parameter in the ecohydrology of the forest. Further, ET partitioning was combined with parallel efforts in our study area to partition net ecosystem carbon exchange (NEE) into the tree gross primary productivity (GPP) and soil respiration (R), in order to understand forest functioning and sensitivity to change.

6.2 Results

6.2.1 **Precipitation pattern and amounts**

Long-term annual precipitation average in the Yatir forest for the period 1964-2008 was 280, with a large standard deviation of 87 mm (31%) between years (Figure 2.2). During the five years of research (2003-2008) annual P was below average (268±73 mm), with three dry years and one wet year (Table 6.1). Analysis of the precipitation temporal distribution during this period showed that the wet season (defined from the first storm above 10 mm until the last storm above 5 mm) was

relatively short and lasted about a third of the year. The number of rainy days was 33 and the number of storms (continuous precipitation with breaks no longer than 24 hrs) was 25 per year on average. Most storm events were small and insignificant: 41% of the storms were smaller than 5 mm and contributed only 11% of the annual rainfall (Figure 6.1). The largest contribution to the annual rainfall was from storms of 10-20 mm (30%). On average, only six such storms occurred each year during the research period, and so their timing throughout the wet season can be expected to have an important effect on the ecosystem. Accordingly, rain intensities were low (1.6±1.7 mm hr^{-1}), with 70% of the rainy hours with intensities below 2 mm hr^{-1} and 92% of the rainy hours with intensities below 4 mm hr^{-1}. Occasionally, events with rates of up to 18 mm hr^{-1} were recorded

Due to the sporadic nature of the precipitation events in these climates, in which long breaks during the storms are observed, the rain storms were further divided into shower events (continuous precipitation with breaks no longer than 1 hr). Categorization of shower size showed that almost half of them were smaller than 1 mm and cumulatively produced only 5% of annual precipitation (Figure 6.2). While the number of storms per year was quite conservative during four out of five years of measurements (27-29 storms per year), the number of showers varied by twofold. A clear negative correlation was found between annual P and the total number of showers. In other words, high annual P was associated with significant and continuous storms and dry years with many small showers.

Not all precipitated water reaches the surface, as some is intercepted on the canopy. Storm throughfall (P_t) was calculated according to the relations defined by Shachanovich *et al*. (2008) for Yatir (P_t=0.94P-0.76), who also indicated that P_t has large spatial variability within the forest. According to these relations, P_t was calculated to consist 89% of P (Table 6.1).

Shachanovich *et al*. (2008) measured stem flow in the Yatir research site and defined it to be only 1.4% of P_t. Similar findings were reported by Gelfand I. (personal communications). Accordingly, this component was neglected in our research.

6.2.2 Soil water content and infiltration

Measurements of volumetric soil water content showed that $\theta_{0\text{-}30}$ reacted immediately to first autumn rains, followed by a wet season during which soil water content was kept well above 0.30 (Figure 6.3). Spring drying lasted approximately 2 months and was characterized by an exponential decay. Following was a long period of dry condition in which $\theta_{0\text{-}30}$ decreased to a constant value of 0.09 during all summer months.

The variability in P between years during the research period provided a first approximation of the effect of precipitation pattern and amount on the soil water content at the research site: while total amounts of P influenced the length of the wet soil season, the distribution of storms defined the value of θ. For example, during 2003/4 and 2005/6 annual precipitation amounts were similar (231 and 224, respectively), but the rain season of 2003/4 was short and condensed (79 days), while during 2005/6 it was much longer (120 days) and breaks between rain events lasted more than 10 days. The overall length of the wet soil period (defined according to $\theta_{0\text{-}30}>0.10$, Table 6.1) was similar for both, but while for 2003/4 θ was kept high most of the winter, during the drought year of 2005/6, long dry spells between medium to small storms caused the soil to dry down to near summer values.

The distribution of soil water with depth was obtained from TDRs installed vertically at three pits in the research site, measuring θ down to a depth of 125 cm. Results show that the shallow soil layer (θ_5, representing the soil layer of 0-10 cm) was kept continuously wet throughout a long part of the year (November – May, $0.10<\theta_5<0.30$), and that the inter-annual variability of θ_5 was low, in spite of the large precipitation variability (Figure 6.4). Inter-annual variability in the patterns and values of θ increased with soil depth. During the wet season of the low precipitation year 2005/6, θ_{30} barely increased from summer values, but in wetter years an increase in θ was observed down to depths of 50 cm. The association of θ with P at this depth was not direct - increase in θ_{50} did not express the noisiness of the storms but rather had a smooth seasonal trend with high values of θ prolonging from February until May. Only during the high precipitation year of 2004/5 was an increase in θ recorded at depths of 70 and 125 cm. Here, the drying process began late (maximum levels of θ_{70} until May and of θ_{125} until June), and prolonged through the whole summer until November of the following hydrological year. The annual pattern of wet-soil

occurrence at different depth averaged for the research period is presented in Figure 6.5.

Subsurface flow was observed, expressed as a short and intense peak in θ recorded below a hillslope but not above it (Figure 6.6). During the wet year of 2004/5 both sites experienced increase in θ at depth of 70 cm, during the dry year of 2005/6 water did not infiltrate to this depth at either sites and at the two other years an increase in θ_{70} was observed below the slope and not above it, and interpreted as subsurface flow.

Soil infiltration was not recorded during storms smaller than 2 mm even at the depth of 5 cm. During larger storms, infiltration rates were estimated from the averaged lengths of periods between measured precipitation and observed increase of θ at different depths (half hour increments of both P and θ). At the depth of 5 cm soil moisture increase was observed approximately 3 hours after the beginning of the rainfall, at 15 cm depth it was measured 5-10 hours after the rains and at depths of 30 cm 10-20 hours after rains, depending on antecedence soil moisture. Calculated infiltration rates according these time periods and depths were within the range of 15-30 mm hr^{-1}. As mentioned, at deeper soil layers (50-125 cm), infiltration rates were so low that θ was not synchronized with storm P. Depth profiles showed that θ was higher at deeper layer than at shallow ones during the drying periods, but not during the rain season, as would be expected for rapid infiltration (Figure 6.7). Low infiltration rates could be explained by the soil texture and density in the research site (clay-loam texture, density of 1.65 gr cm^{-3}, Appendix 1), implying characteristics such as highly compacted soil and tendency to swell.

In light of these results, precipitation amounts needed in order to infiltrate to various soil depths were calculated according to:

$$P_s = H \cdot \left(1 - \frac{\rho_b}{\rho_p} - \theta_m \right) \qquad (6.1)$$

where P_s (mm) is the amount of precipitation needed in order to saturate a layer and for the wetting front to advance to the next deeper layer, H (mm) is the layer height, ρ_b (gr cm^{-3}) is the bulk density, ρ_p (=2.65 gr cm^{-3}) is particle density and θ_m is the minimum soil water content measured at each layer. Soil porosity was calculated by

the term $(1-\rho_b/\rho_p)$. The calculated cumulative saturation water depth (Table 6.2) was the expected amount of precipitation needed in order to increase θ from its minimum values at end of the summer to field capacity. Using Eq. 6.1 and the observed distribution of storms size, we estimated that only 6% of the storms were sufficiently large to infiltrate below 20 cm. It seems, therefore, that under the observed precipitation in the study site, the superficial soil layer presented a significant barrier to infiltration, particularly at the end of summer or during dry spells within the precipitation season (such as those of 2005/6). Even a larger barrier to infiltration takes place below 40 cm, at the boundary between the upper Leos soil and the deep Paleosol (Appendix 1). The relatively lower density of the Paleosol resulted with high calculated porosity (0.45) and accordingly, high amounts of water holding capacities (approximately 90 mm for the layer 40-60 cm), for which only rare precipitation events enable infiltration below this depth. The large cumulative water holding capacities of the soil layers above 50 cm also explain the non-synchronization between the seasonal trend of θ at deeper layers (50-125 cm) and the timing of the storms.

6.2.3 Soil water loss

Daily soil water loss from the soil profile was calculated according to:

$$A = (\theta - \theta_m) \cdot H \qquad (6.2)$$

$$B = A_d - A_{d+1}$$

$$\begin{cases} B \le 0 & \text{Ø} \\ B > 0 & SWL = \sum_{l=1}^{l=6} B \end{cases}$$

The term A calculates the amount of water in each soil layer (θ_m and H are as above). The term B calculates changes in water amounts between consecutive days for each layer where d is the day of year (DOY). The term SWL (soil water loss, mm d^{-1}) calculates cumulative loss of water from the whole soil profile (0-125 cm) where l is the number of the TDR sensor, representing a soil layer. The results are summarized in Table 6.3.

The proportional contribution of the upper layer (0-10 cm) to the annual SWL was the largest (~50%), except for the year 2004/5 in which significant accumulation

of water at depth was observed and the proportional contribution of the layers below 60 cm significant (above 20%). As mentioned, during this year deeper layers continued to dry out until the beginning of the following year. Accordingly, soil moisture storage ($\Delta\theta$) was calculated from the SWL at these depths from October 2005 until an increase in soil water associated with the 2005/6 rain season was observed. Calculations defined $\Delta\theta$ = 22 mm, accounting for 13% of the SWC budget of 2005/6. The drying process at of the deep layers following the high precipitation year of 2004/5 was still observed during 2006/7, and the calculated $\Delta\theta$ between 2005/6 and 2006/7 was 14 mm, accounting for 8% of SWL during 2006/7. No soil water storage between hydrological years was observed afterward.

SWL was compared to ET measured by the eddy covariance technique at the flux-tower system and showed compatibility between trends (Figure 6.8; R^2=0.73, ET_{tower}=1.14×ET_{SWL}, 10-days averages). During the wet season compatibility was better, and fluxes of SWL were lower in ~13% than ET fluxes. During the dry season, SWL was approximately half of ET (averaged fluxes of SWL~0.15 mm d^{-1} and ET of 0.30 mm d^{-1}), except for the summer of 2004/5 (high SWL as a result of the still occurring drying process of deep layers).

6.2.4 ET partitioning

The contentious database of daily fluxes of T, E and ET during the research period is presented in Figure 6.9. The seasonal trend of ET and T differed from that of E (Figure 6.10 A): while E peaked during early and late winter (the drying and wetting transition periods), T had a more pronounced annual trend and gradually rose from low summer values with peak fluxes during spring, in correspondence with peak photosynthetic activity. Comparison between the separate fluxes of E+T and ET measured by the tower were comparable in trend and less in magnitude.

The partial contributions of E and T varied seasonally (Figure 6.10 B): the contribution of E was strongest during early winter (Oct., E/E+T=65%) and gradually decreased towered late-winter (Mar.-May, E/E+T=34%). During the summer, the contribution of E and T was equivalent. This pattern could be explained by the distribution of soil water content with depth (Figure 6.11). The seasonal trend of E was synchronized with θ at a depth of 5 cm, while that of T was well synchronized with θ at a depth of 30 cm, which is the depth of maximum tree root density. And so,

while θ_5 increased early in the season (November, Figure 6.5), θ_{30} began to increased at January and peak annual T fluxes were synchronized with peak θ_{30} (March – April). Accordingly, the highest E/ET ratios were observed during early-winter, when E fluxes were high and T fluxes low. During late-winter and spring, E fluxes were comparable in size to those of early-winter, but E/ET was small due to high T fluxes.

Inter-annual variations of E and T could also be explained by soil water content distribution with depth. Due to the relatively constant annual pattern of θ_5, variability of annual E was low (8%, Table 6.4), while a larger standard deviation in T (18%) was observed between years, associated with inter-annual variations in soil water content at depth. The annual ratio of T/E+T reacted accordingly and were explained better by precipitation pattern and the resulting soil water at depth, and less by annual precipitation amounts: 2004/5 was a relatively wet year (P=377 mm) and θ increased during the wet season to at least 125 cm, producing high T/E+T ratios (58%). 2003/4 was a relatively dry year (P=231 mm); however, the rain season was condensed (148 mm during 27 days), which most likely also increased precipitation penetration depth in the soil (the deep soil moisture system was not yet available at that time), creating T/E+T ratio equaling to that of 2004/5, albeit low annual P. The following two years differed in precipitation amount (P=224 for 2005/6 and P=308 for 2006/7), but both were characterized by small to medium sized storms, in which θ did not reach the deep soil layers. This presumably enhanced soil E and limited tree water uptake, with resulting T/E+T ratio of 52-54%.

6.2.5 Water use efficiency

Daily fluxes of NEE and ET, both measured by the eddy covariance methodology at the flux tower, are presented in Figure 6.12, together with daily fluxes of GPP and T. Positive values of these parameters represent fluxes from the ecosystem to the atmosphere (transpiration, evaporation and respiration) and negative values represent fluxes in the opposite direction (water adsorption or carbon assimilation). Trend of GPP was continuously negative, as appropriate for a year-round photosynthetically-active forest. Summer fluxes where low, with typical values of -1 $gCO_2\ d^{-1}$. Fluxes increased gradually toward the spring season and peak annual fluxes varied between years in the range of -5 to -10 $gCO_2\ d^{-1}$. The trend of GPP was well synchronized with that of T. The inter-annual trend of NEE showed positive

values (carbon release) during summer with typical values of +0.5 gCO_2 d^{-1}. Fluxes increased gradually toward the spring season and annual peak fluxes varied between years in the range of -3 to -6 gCO_2 d^{-1}. The trend of NEE was well synchronized with that of ET.

Correlations between monthly sum values of these fluxes, representing the water use efficiency of the gross tree component (WUE_t=GPP/T) and the net ecosystem component (WUE_e=NEE/ET) are presented in Figure 6.13 A. (Remark: for convenience and compatibility with customary reporting, when discussing WUE the signs attributed to flux directions were eliminated). While for the tree component a relatively good linear correlation between GPP and T was observed during all seasons (WUE_t=6.90 gCO_2/kgH_2O, R^2=0.77) for the whole ecosystem a significant difference in the ratios of NEE and ET was observed between the wet season (WUE_e=1.64 gCO_2/kgH_2O, R^2=0.67) and dry season (no correlation detected). Accordingly, the seasonal trend of WUE_t was more pronounced than that of WUE_e (Figure 6.13 B). Water use of the entire ecosystem was most efficient during the wet period (Dec-Apr, WUE_e = 1.90 gCO_2/kgH_2O·month) and "wasteful" during the dry period, when carbon emission by soil respiration was larger than tree carbon uptake. Water use efficiency of the tree component was high all year, with a slight maximum during the spring season (Apr-Mar, WUE_t = 9.5 gCO_2/kgH_2O·month). Variations of monthly values between years were larger for WUE_e than that of WUE_t (normalized standard deviation of 82% and 34%, respectively).

The annual values the carbon fluxes are presented in Table 6.5. Three of the four study years showed good correlation between P and WUE_e (Figure 6.14). 2003/4 deviated from this trend with WUE_e higher than "expected" according P. This was a dry year (231 mm) but most rains were concentrated during a short season (30 rainy days), producing high T (134 mm, probably enabled by deep infiltration) and relatively low R (555 gCO_2, probably caused by the short wet soil season) and resulting with relatively high WUE_e (0.9 gCO_2/KgH_2O) in relation to the low P. When this precipitation pattern was taken under consideration, by dividing annual P with the number of rain days (RD), WUE_e "lined up" with those of other years (R^2=0.93). As apposed to WUE_e, WUE_t during this year was the lowest of all measured years; the high T fluxes (relative to the low P) were not accompanied by high GPP.

6.3 Closure of the hydrological budget

After defining the trends, sizes and characteristics of the various components of the hydrological cycle, the balance between inputs and outputs needs to be treated. The hydrological components were finally defined according to the averaged values of annual fluxes during the four year research period (Table 6.6 and Figure 6.15): P=285, I=31 (11%), ET=267 (94%), T=129 (45%) and E=102 (36%), all in mm yr^{-1} and accompanied percents are of P values. Interception (I) was calculated from the difference between measured P and calculated P_t (Table 6.1). The ET flux was quit successfully balanced by its components (Eq. 1.2: ET=I+T+I; 267~262 mm yr^{-1}).

Differences between P and ET (15 mm yr^{-1}, 6% of P) were attributed to various losses defined in Eq. 1.1 and as follows. Surface storage (ΔS) was not accounted for here and is non-relevant on an annual basis in dry regions. Similarly, groundwater storage (ΔG) was considered non-existing due to deep depth of the water table. Soil moisture storage ($\Delta\theta$) between years was observed during two of the five years investigated (calculated to be 22 and 14 mm for 2004/5 and 2005/6, respectively) but was utilized during the following years and therefore existed only temporarily. Surface runoff (Q) was measured in different studies to be low - approximately 3% of P on annual basis (Shachnovich Y., personal communication). Deep drainage (D) was not directly measured in Yatir. These fluxes ($\Delta\theta$, Q and D) cumulatively account for the annual difference between P and ET and therefore generally treated as losses (L). The definition of $\Delta\theta$ as "loss" is only on an annual basis; this reservoir is probably returned to the system at the following year/years: during years that followed high-precipitation years, ET was higher than P (Table 6.6; annual P of 2002/3, preceding the first year of research, was 373 mm). Soil adsorption was not included in the annual budget as it cancels out on a daily basis. However, as previously discussed, it is estimated that this process accounts for approximately half of the summer fluxes. During the months July to October, conditions in favor of soil water adsorption exist: a combination of dry upper soil (θ_5 below 0.10) and large daily amplitude of RH (above 40%). The cumulative E flux during these months was 23 mm and accordingly, we estimate A to be in the order of 10-15 mm.

3.4 Discussion

The hydrological cycle plays a major role in the complex interactions between soil, vegetation and atmosphere. Models that have been developed in an attempt to quantify fluxes within the soil-plant-atmosphere continuum (SPAC) rely on soil water conditions, as it regulates above ground humidity, photosynthetic and respiratory activities (Rodriguez-Iturbe, 2000, Guswa, 2002). In dry ecosystems, soil water is the single most important factor controlling ecosystem functioning; plant activity is in many cases restricted to the wet season and is largely decreased during dry years (Porporato *et al*., 2002, Granier *et al*., 2007). The inter-annual variations in environmental conditions during the five study years presented an opportunity to investigate the influence of precipitation patterns and amounts on soil water distribution and the resulting effect on ecosystem activity.

Forested canopies behave as dual-source systems, as its vegetation and underlying soil surface contribute, in differing but significant amounts, to the mass and energy exchange between the biosphere and the atmosphere. Therefore, an understanding of evapotraspiration from forests requires knowledge of the individual processes that control water and energy fluxes within the forest. However, not many studies of ET partitioning are reported. Amongst the existing researches in arid and semi-arid forest ecosystems, variation between the ratios of E/ET ranged between 10-80% (Huxman *et al*., 2005, Kurpius *et al*., 2003, Yepez *et al*., 2003, Williams *et al*., 2004, Stannard and Weltz, 2006), but mainly below 30%.

The Yatir forest is situated in a semi-arid climate zone, and as such, its sustainability is questionable. The forest, however, shows an ability to overcome draught years even with annual P lower than 150 mm, and, measurements of CO_2 flux show that it is capable to maintain yearly average NPP close to that of the global average for forests (Grunzweig *et al*., 2001 Law *et al*., 2002), resulting from high carbon uses efficiencies (Maseyk *et al*., 2008) and presumably resulting from efficient mechanisms of water distribution and utility.

What then enables to maintain tree productivity in the Yatir forest? First, the concentrations of all annual P during winter, when PET rates are lowest, minimize evaporation during this period and maximize the accumulation of water in the soil. In other ecosystems with similar annual P but with a bi-modal P trend (which include summer rains), infiltration rarely exceeds 15 cm (Kurc and Small, 2003, Scott *et al*., 2006). Second, while most precipitation events in the research site were found to be

small (82% of showers below 5 mm), usually at least one large storm (>60 mm) or a number of medium consecutive storms occurred, allowing for deep infiltration. Such a situation existed even during the very low precipitation year of 2007/8 (98 mm during 9 days; total annual P of 201). Deep infiltration will occur only when rains concentrate during a short period, enabling to overcome the dense and fine soils in Yatir with its high barrier of water holding capacities (calculated to be 64 mm for the upper 20 cm). The effect of these storms on the ecosystem is important, as based on root density distribution, water uptake by plants is largely below a depth of 10 cm (Jackson *et al.*, 1996), while above this depth most water evaporates rapidly to the atmosphere (Boulet *et al*., 1997, Huxman *et al*., 2005). Therefore, this mechanism is more favorable for plant types with deep rooting systems such as trees, in contradictory to grasses or short shrubs. In such situations of deep infiltration, accumulation of moisture at deeper soil layers begins late in the season followed by a slow drying process, presumably maintaining water available for plants throughout the whole summer season. In our research site, the average soil profile is not deeper than 40 cm. At specific pits deeper profiles were exposed, in which high soil water content was measured below 50 cm even at the end of the summer (θ>0.20). The spatial occurrence of such pits at the forest scale is not estimated to be large. However, it can be assumed that the maintenance of relatively high soil water content throughout the year implies some equilibrium with the adjacent bedrock or of soil lenses inside the fractured bedrock, presumably enabling utilization by occasional deeper roots. And third, as shown by Maseyk (2006), efficient utility of the limited amounts of water was obtained by the trees at the Yatir forest through various mechanisms such as shifting the timing of the active season, applying protection mechanisms and decreasing summer stem and foliage respiration, therefore enabling high levels of productivity and maintaining activity even during the dry summer season.

This research enabled to define the components and processes of the hydrologic balance for Yatir. P had a high inter-annual variability (normalized standard deviation of ±25% between research years) and characterized by small, in-contentious rain showers. Interception was calculated to be ~11% of P, decreasing even more the already-low inputs. Interestingly, this value fits well our analyze of precipitation showers, which show that 11% of total precipitation was contributed from showers smaller than 2 mm; observations of soil water content changes at

shallow depth (θ_5) indicate that these showers hardly increase soil moisture. ET accounted for most of P (94%) and accordingly, losses out of the system (runoff, deep drainage and temporal soil water storage) were small. Actual losses were estimated to be even less than 6% of P, because calculations of the losses included soil moisture storage between years, which was utilized during the following years and therefore canceled out on time scales longer than one hydrological year. During years following high precipitation years (2002/3 and 2004/5, annual P of 373 and 377 correspondingly), ET equaled and even slightly exceeded P. At these years, soil water loss (SWL) was shown to be relatively high throughout the summer season and deep soils continued to dry up during the early winter of the following hydrological year, therefore contributing to ET from precipitation of the preceding year. Our measurements and simulations enabled to estimate soil evaporation to be in the range of 102±8 mm yr^{-1}. Adsorption was estimated to add ~15 mm (5% of P) but is canceled out on a daily basis, not to say on annual scales. Based on annual averages for the research period, a good closure of these components was obtained (Figure 6.15), according to the general hydrological balance equation (1.1) and the components of the ET flux (Equation 1.2).

However, on a monthly scale, comparison between the sum of the individual fluxes E+T and the total ET measured by the flux tower (Figure 6.10A) indicated some inconsistencies in magnitudes: during the end of summer and early winter (Oct.-Dec.), E+T was larger by ~25% than ET, while during other months the sum was lower by ~25% than ET. During the rain season, a difference of about 12% can be expected since ET includes canopy intercepted precipitation which should not be incorporated in the E+T flux. It is noted that flux-tower measurements during precipitation events are problematic, usually resulting with recorded fluxes lower than actual ET, therefore complicating such comparison during rainy days. In addition, intercepted precipitation does not apply for the dry summer months and cannot explain higher ET fluxes during this season. The end of summer deviations may be at least partly explained by events of atmospheric moisture adsorption. Such events were often observed in this period, but not incorporated in the simulations of seasonal E, which were based on noontime measurements (see Figure 2.5). Notably, in summer ET was high not only in relation to E+T but also in relation to the independent SWL budget. This may indicate to possible overestimation of ET by the tower flux measurements during this season. Inter-comparisons of flux estimates with

independent methodologies are a key to identifications of uncertainties and to further refinements of the hydrological budget in this system.

Precipitation pattern, controlling soil water content, was detected as a basic and significant variable for the understanding of ET partitioning. While the small but common rain showers characteristic of semi-arid regions enabled to persistently keep high moisture level during more than half a year, large storms resulting with deep infiltration into the root zone were less common, and only during the second half of the rain season enough water accumulated at these depth. Accordingly, E was water limited during the summer but energy limited during the winter and produced peak fluxes during the wetting and drying periods combining wet soils and high radiation situations. As opposed to that, T fluxes were still restricted by low water supply during the first half of the wet season and merely began to rise during mid winter, parallel to the increase in soil water content at depth of maximum root density (~30 cm). The larger inter-annual variability of T in comparison to that of E goes with the notion of large inter-annual variations in precipitation pattern, resulting with variations of soil water content at depth.

Clearly E and T had a variable contribution to the ET flux and could not be simply estimated from a constant ratio. The highest contribution of E was observed during early-winter (October-December), when E/ET sometimes reached values of 0.80-0.90. Increase in T fluxes at late-winter produced E/ET ratios of 0.27-0.37 and during summer, E and T were approximately equivalent in their contribution. The relatively high E/ET ratios measured at the Yatir forest reflect the combined effects of an open forested canopy and small and sporadic precipitation events.

Precipitation pattern was also observed to effect ecosystem functioning, indicating that vegetated dry systems are more sensitive to rain intensity then they are to total amounts of P. For example, although based on limited data, our analysis (6.14) indicates that when annual WUE_e is compared to the ratio P/RD (where RD denote number of rainy days and the ratio serves as an indicator of precipitation pattern and intensity), all values seem to "line up" along a common best linear best fit line. This is not the case when WUE_e is compared directly with P. Note that in 2003/4 P was relatively low but most precipitation was concentrated in relatively few intensive events resulting with deep infiltration that enhances T and produced high WUE_e in comparison to the low P, but not in comparison to the high P/RD. A concerning issue was raised when looking at the WUE_t component, which during this year was lowest

of all measured years (Table 6.5). Low WUE_t was a result of high T fluxes which were not accompanied by high GPP fluxes, presumably indicating on some above ground physiological stress effect due to the overall low P amounts and/or short wet season (for comparison, 2003/4 and 2006/7 had identical P/RD ratios, but the latter received more annual precipitation and produced larger WUE_t values).

Current climate change models and some observations of climate change in the Mediterranean region predict a decrease in P, but likely associated with intensification of the hydrological cycle (i.e. fewer but larger storms; Groisman et al., 2004, Angert *et al*., 2005, IPCC 2007). Our results indicate that increased storm size, and the consequent deeper soil penetration, may at least partly compensate for the decrease in P and help maintain the relatively high forest productivity observed (except when the forest is over stressed by factors other than soil moisture).

6.5 Tables and figures

Table 6.1: Annual totals of precipitation characteristics during the research period. Rain season - from the first storm above 10 mm until the last storm above 5 mm. Wet soil season - the period in which soil water content (0-30 cm) was above 0.10.

The annual precipitation average for the research period was close to that of the long term average (Figure 2). Throughfall precipitation (P_t) was approximately 89% of precipitation. Variability of annual P, number of showers and length of the rain and wet soil seasons was large between these consecutive years.

	2003/4	2004/5	2005/6	2006/7	2007/8	Average
Precipitation (mm)	231	377	224	308	201	268
Throughfall (mm)	203	340	198	275	178	239
No. of days with rain	30	31	42	40	23	33
No. of storms	27	27	28	29	15	25
No. of showers	55	47	84	72	65	65
Length of rain season (days)	79	131	120	139	66	107
Length of wet soil season (days)	192	246	193	208	114	191

Table 6.2: Soil properties of the different soil layers. The depth of the TDR sensor is noted in brackets. High water content was measured in the deep layers even at the end of summer. Water holding capacity and cumulative saturation water depth were calculated (see text).

	Layer depth (cm)					
	0-10 (*5*)	10-20 (*15*)	20-40 (*30*)	40-60 (*50*)	60-87 (*70*)	88- 125 (*125*)
Layer height (H, mm)	100	100	200	200	275	375
End of summer water content 0-30 cm (θ_m, fraction)	0.05	0.10	0.15	0.21	0.23	0.26
Bulk density (ρ_b, gr cm^{-3})	1.65	1.56	1.60	1.47	1.58	1.60
Water holding capacity (W_c, mm)	38	41	79	89	111	149
Cumulative saturation water depth (W_s, mm)	33	64	113	159	207	258

Table 6.3: The contribution of each soil layer to annual SWL (in mm). The periods of 2004/5 and 2007/8 are incomplete. 2004/5 was a high precipitation year, infiltration was deep and most soil water loss was from the deep layers. During the two full data years, the shallow layer produced approximately half of the soil water loss budget.

Soil Layer / Year	Period	Soil water loss (mm)						
		0-10 cm	10-20 cm	20-40 cm	40-60 cm	60- 87 cm	87-150 cm	Sum
2004/5	Mar - Sep	49	18	11	27	50	40	196
2005/6	Oct - Sep	93	22	6	10	21	14	166
2006/7	Oct - Sep	101	35	13	21	21	11	201
2007/8	Oct - Sep	60	20	12	20	20	11	143

Table 6.4: Annual sums of T and E and their partial contribution. Values of ET are specified in Table 6.6.

Year	T	E	E/(E+T)	E/ET
	mm yr^{-1}		%	
2003/4	134	99	0.42	0.42
2004/5	156	112	0.42	0.33
2005/6	111	93	0.46	0.41
2006/7	115	106	0.48	0.40
Average	129	102	0.44	0.39
N stdev (%)	16	8	7	11

Table 6.5: Annual values of WUE_e (NEE/ET) and WUE_t (GPP/T). RD is the number of rain days per year (Table 6.1) indicating rain intensity.

Year	P/RD (mm $yr^{-1}d^{-1}$)	GPP gCO_2 yr^{-1}	NEE gCO_2 yr^{-1}	WUE_e gCO_2 / kgH_2O	WUE_t gCO_2 / kgH_2O
2003/4	7.70	776	221	0.93	5.77
2004/5	12.16	1173	361	1.06	7.68
2005/6	5.33	677	166	0.74	6.74
2006/7	7.70	872	232	0.89	7.58

Table 6.6: The components of the hydrological budget for the Yatir forest during the research period.

mm yr^{-1}	P	I	ET	L
2003/4	231	28	235	-4
2004/5	377	37	343	34
2005/6	224	26	227	-3
2006/7	308	33	263	45
Average	285	31	267	18
Stdev	72	5	53	25
% of P	100	11	94	6

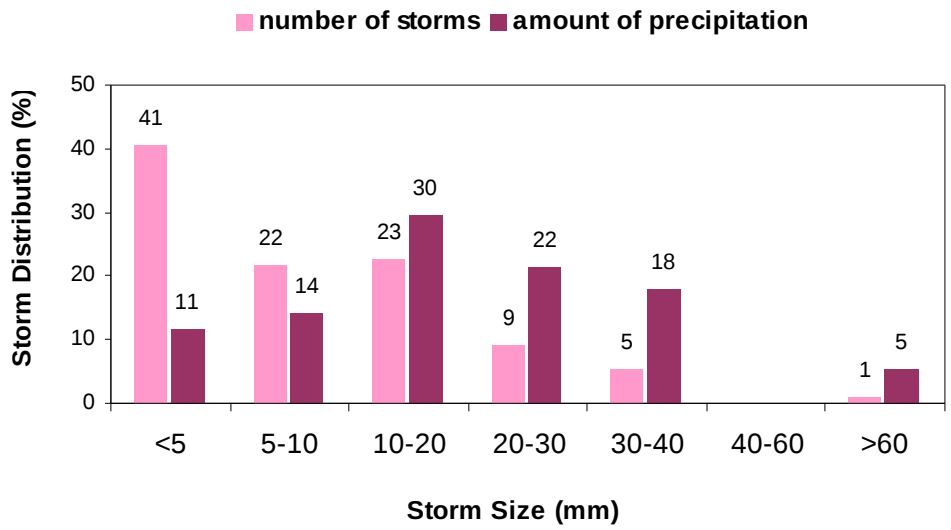

Figure 6.1: Distribution of storm size and amounts during the research period (values in % of total). Division into storms was preformed when breaks between events were longer than 24 hours. Most storms were smaller than 5 mm. One large storm (above 60 mm) contributed 5% of the total rain amount during this period.

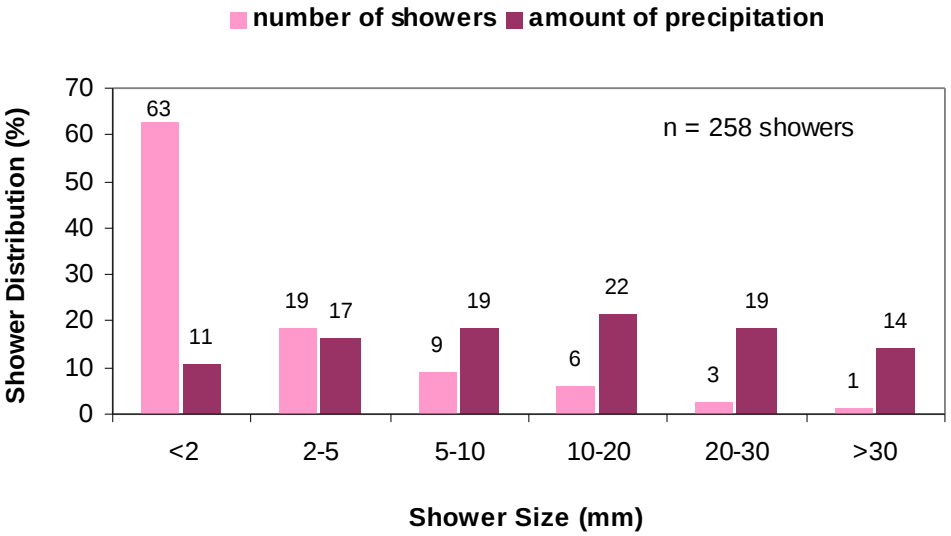

Figure 6.2: Distribution of shower size and amounts during the research period (values in % of total). Division into showers was preformed when breaks between events were longer than 1 hour. Showers below 2 mm were combined into one category, as their contribution to soil water content was not observed.

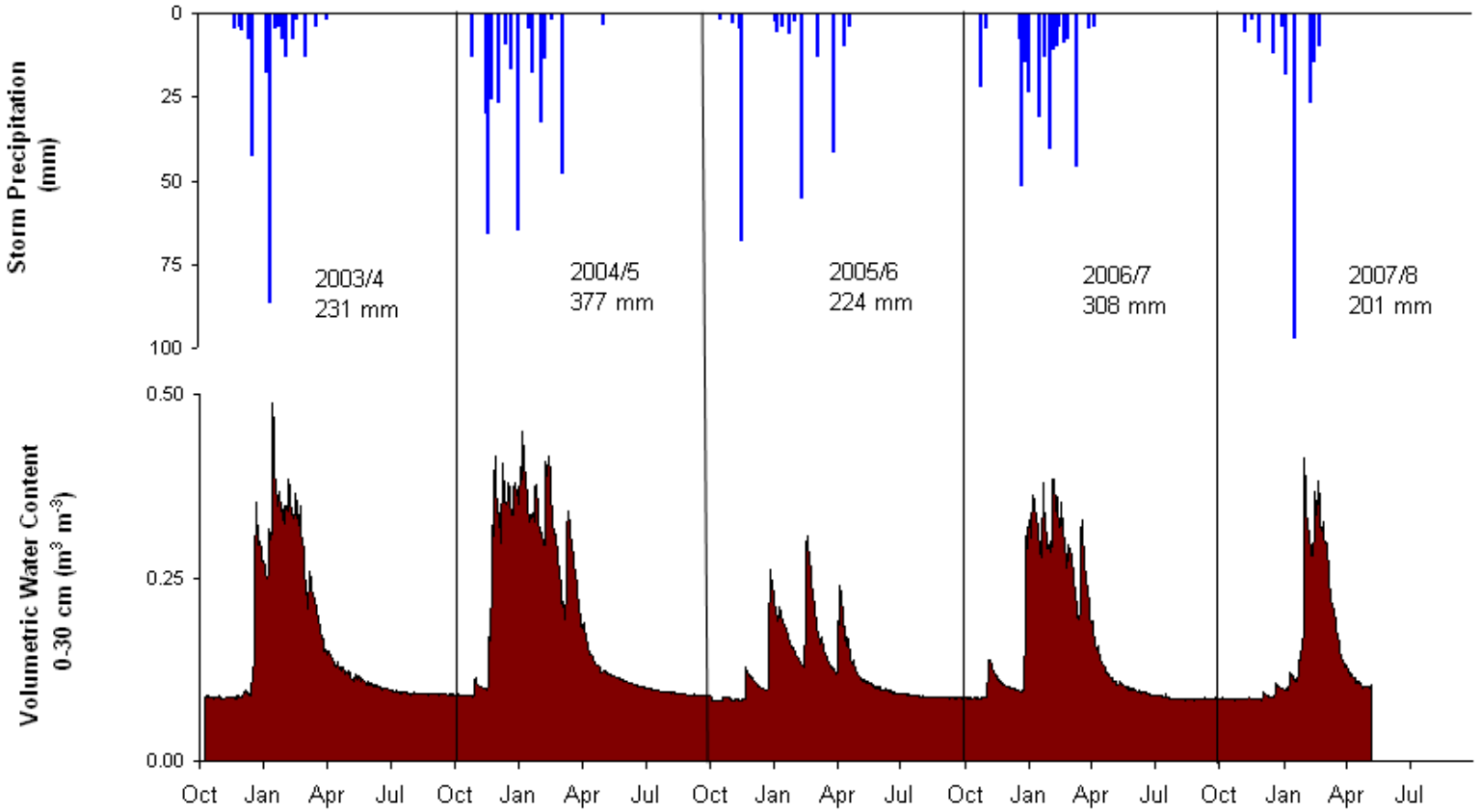

Figure 6.3: Storm precipitation and soil water content (average of three SC616 sensors measuring average soil water content for depth 0-30 cm). Trends of soil water content showed an almost mirroring view of precipitation patterns

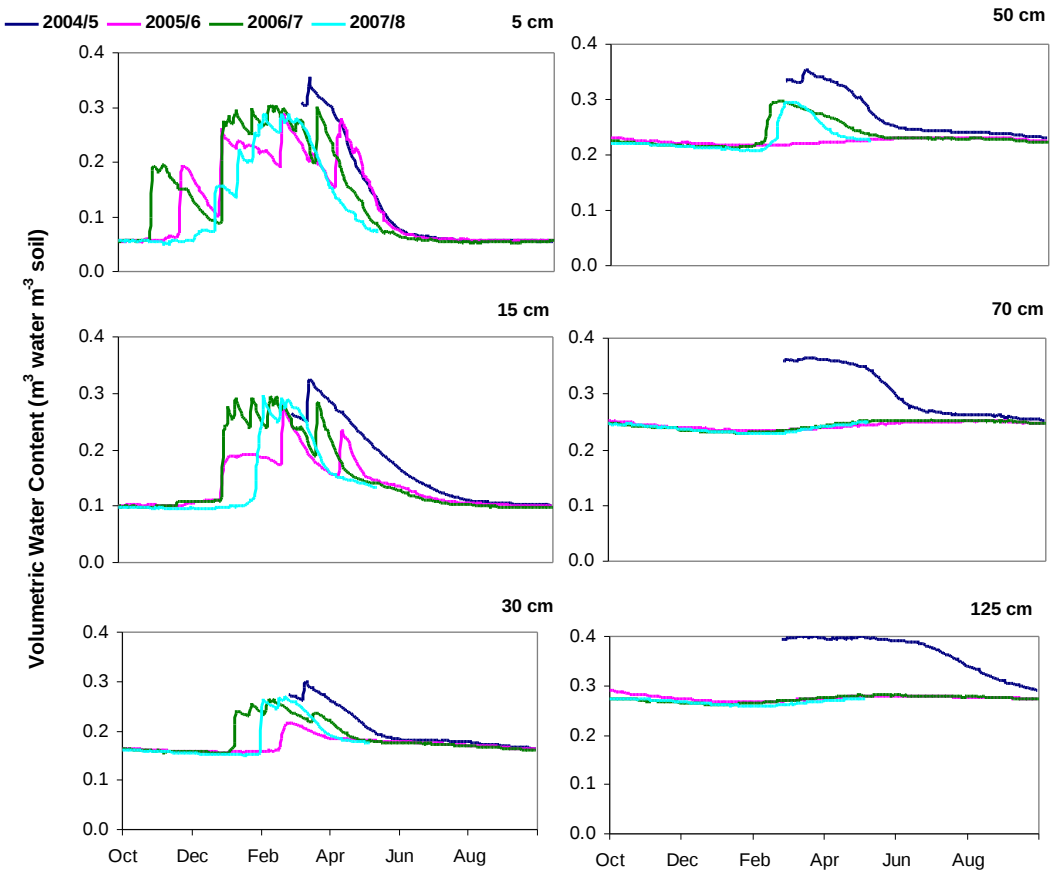

Figure 6.4: Soil water content measured at different soil depth during the research period. Soil water content of the shallow layer (θ_5) were similar albeit difference in precipitation between years. Annual variability increased with depth. Only during the wet year of 2004/5 did water infiltrate below 50 cm, and water storage between years was observed. While at the shallow layers (down to 30 cm) θ reacted immediately to rains, at deeper layers the annual trend was not synchronized with precipitation and maximum values were measured near the end of the rain season.

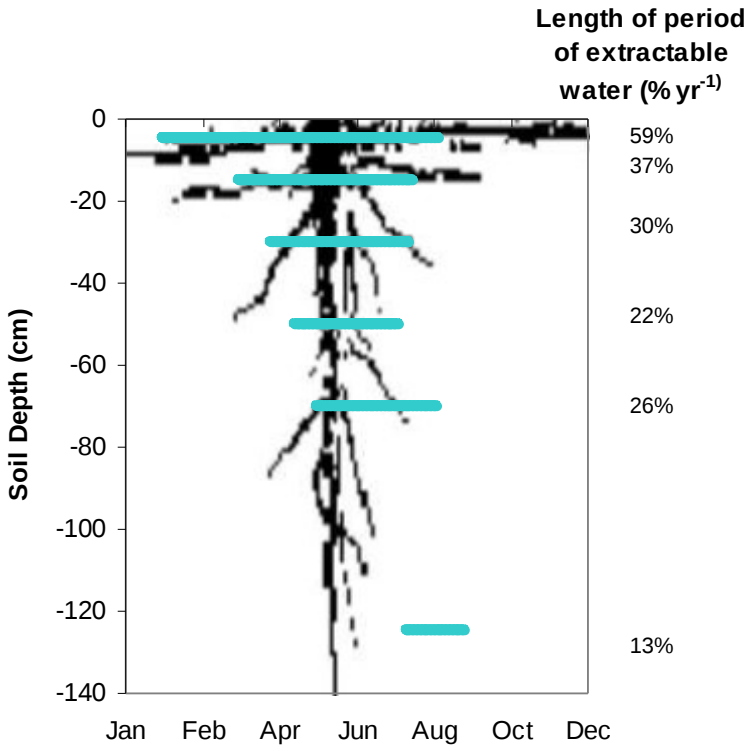

Figure 6.5: The seasonal pattern of soil moisture at different depth averaged for the research period. Extractable water content was defined above thresholds typical for each layer (θ_5>0.10, θ_{15}>0.16, θ_{30}>0.19, θ_{50}>0.25, θ_{70}>0.27 and θ_{125}>0.30). Rooting pattern with depth is shown for general reference and not to scale.

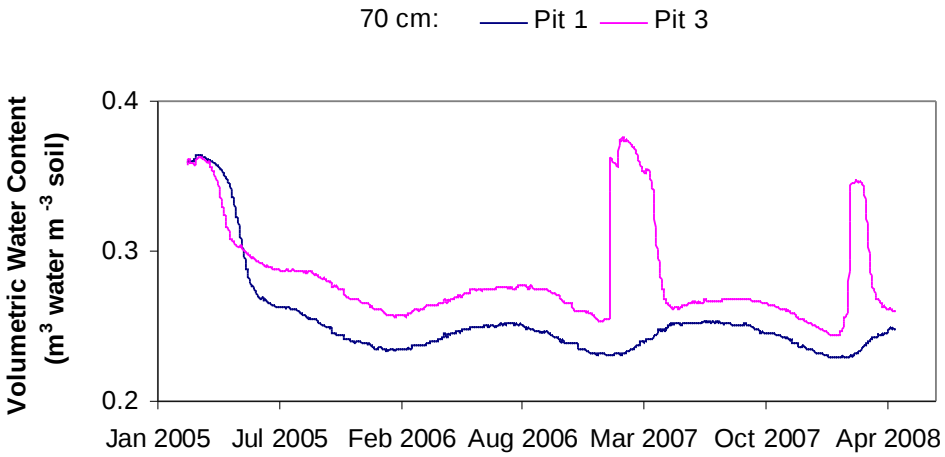

Figure 6.6: Soil water content at depth of 70 cm at pit 1 (planar area above the hillslope) and pit 3 (planar area below the hillslope). During the wet year of 2004/5 both sites experienced increase in θ, during the dry year of 2005/6 water did not infiltrate to this depth and at the other years subsurface flow was observed at the lower part of the slope.

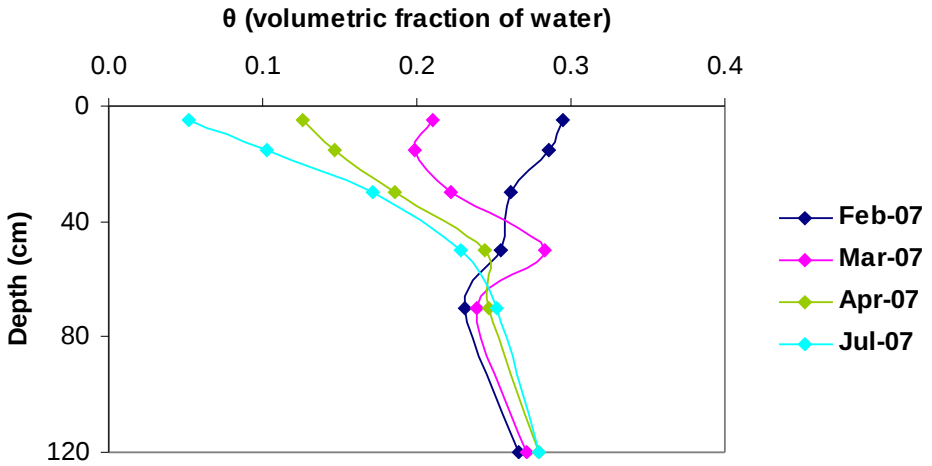

Figure 6.7: Profiles of soil water content representative of different seasons. Change in soil water content below depth of 70 cm was minimal. During mid-winter (February) the shallow layer was still wetter than deeper ones. Only at the beginning of the drying season (March), water infiltrated to layers below 50 cm, while the upper soil horizons begun to dry out.

A

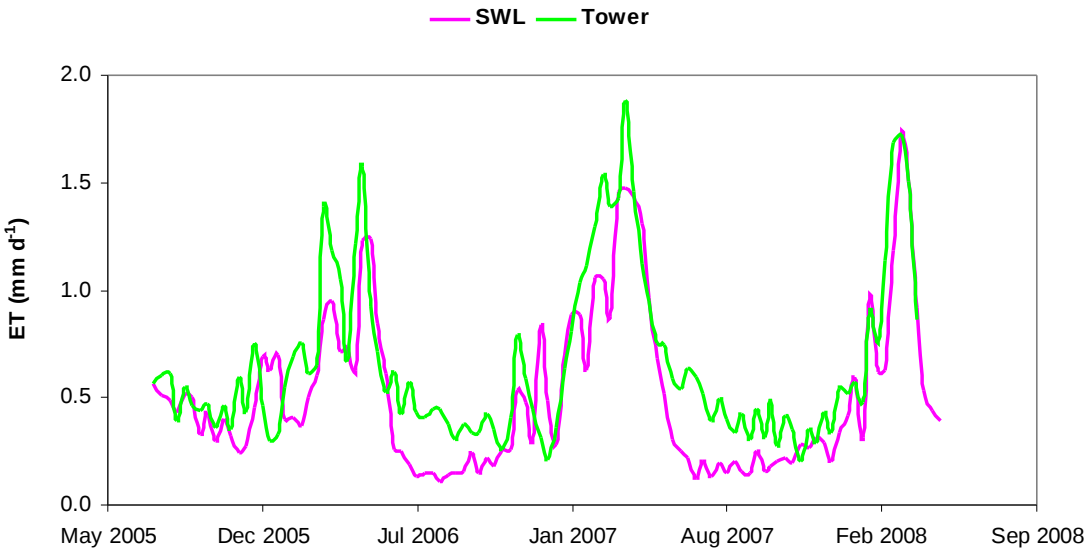

B

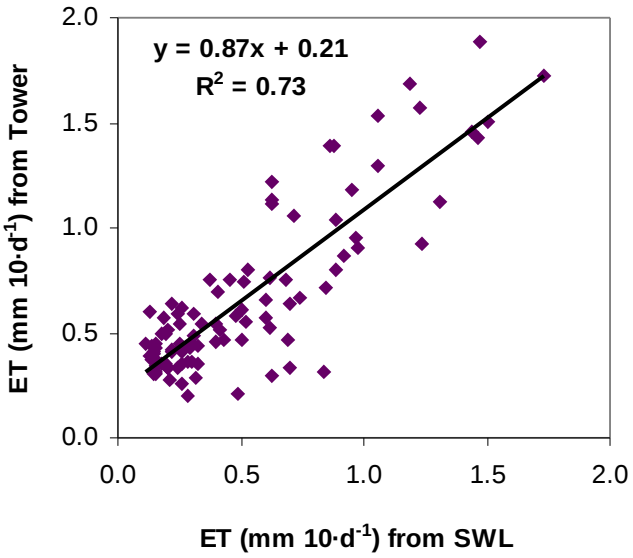

Figure 6.8: (A) Time sequence of water flux measured by the flux tower (ET) and calculated from soil water balance (SWL). 10-days averages showed good agreement. ET was higher than SWL mainly during the summer. (B) The linear correlation between the ET and SWL, including summer values.

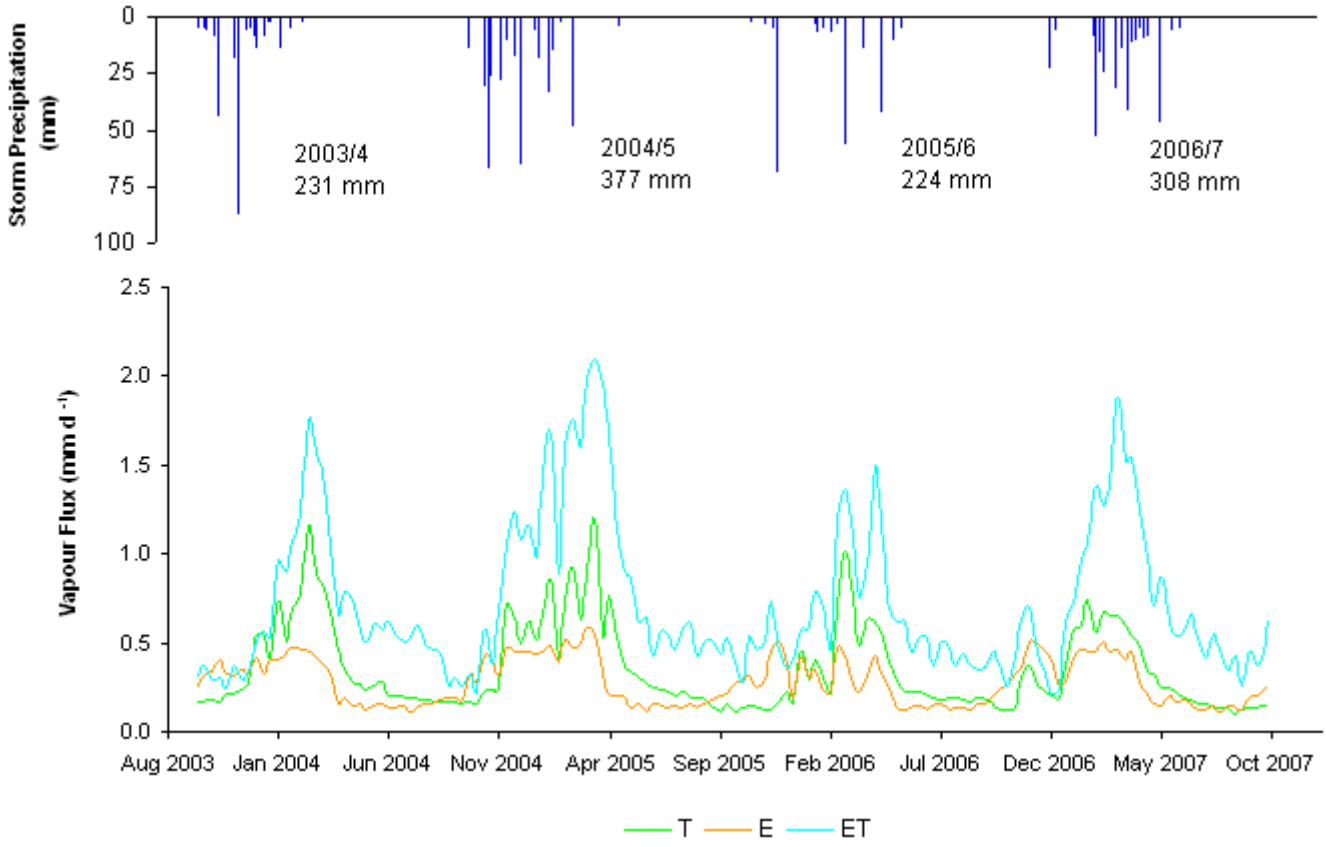

Figure 6.9: Storm precipitation (upper graph, total annual precipitation is noted) and 10 day averages of daily total fluxes of E, T and ET (lower graph). T and E differed in their seasonal trend: while peak E fluxes were measured during early and late winter, T begun to rise at early winter and peaked during late winter to early summer.

A

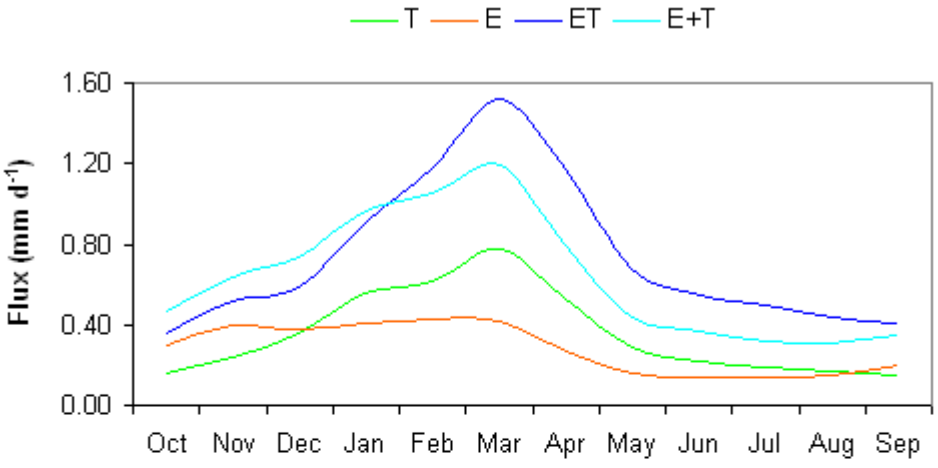

B

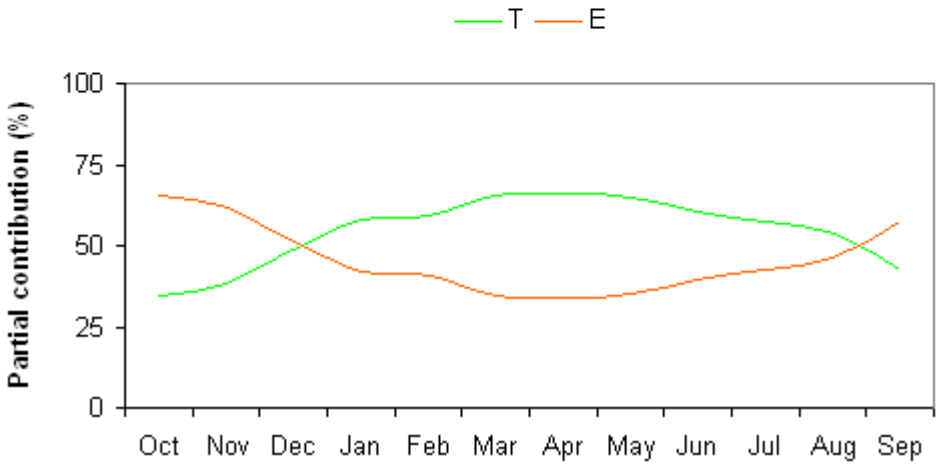

Figure 6.10: (A) Monthly averages of T, E, ET (measured by the flux tower) and E+T (combined fluxes of the two independently measured fluxes). The combined flux (E+T) was higher in ~25% than ET measured by the tower during early winter and lower by the same magnitude during the rest of the year (treated in the discussion). (B) Monthly averaged ratios of T/(E+T) and E/(E+T). The contribution of E to the ET flux was most pronounced during early winter (65%) and gradually decreased towered mid-winter (34%).

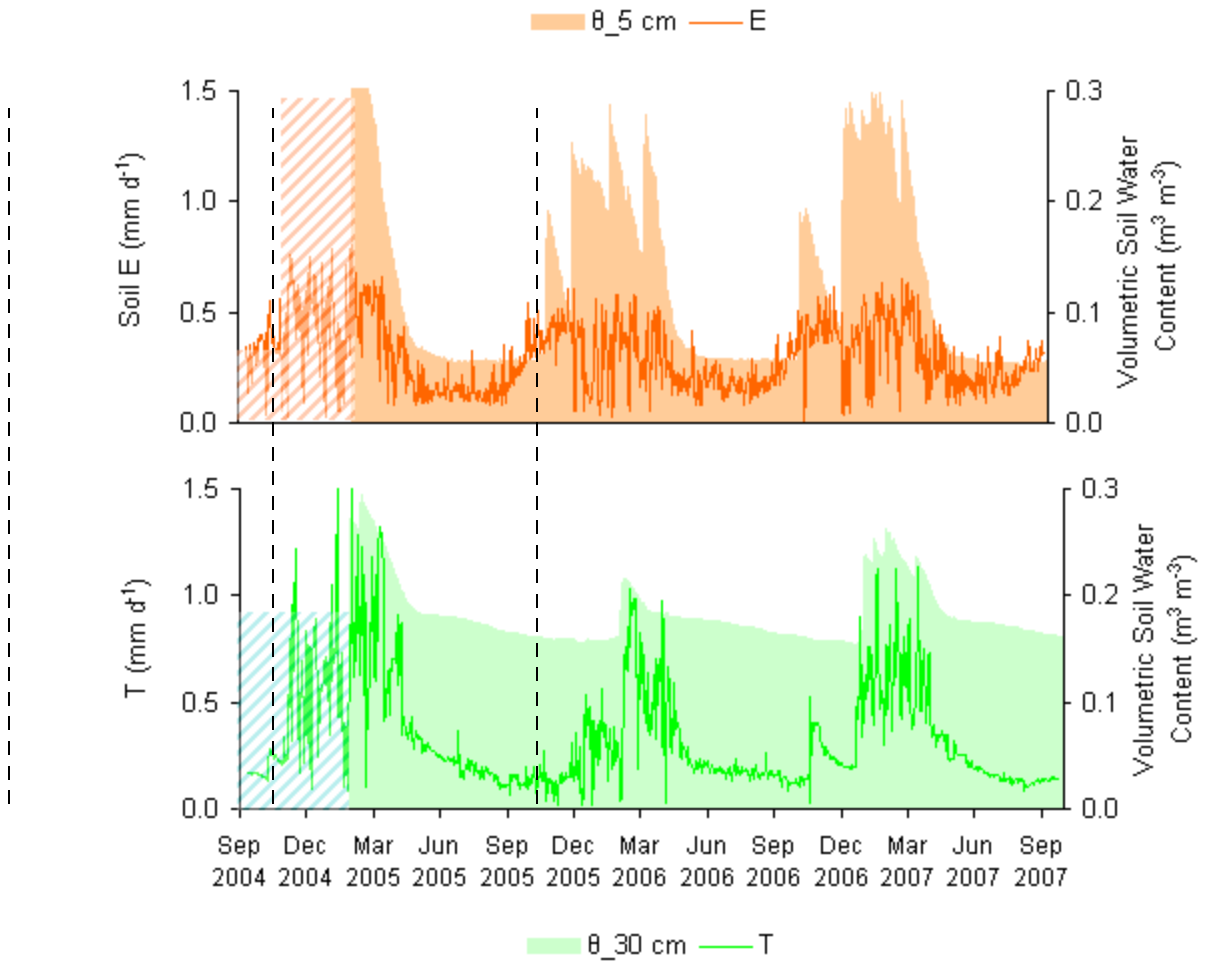

Figure 6.11: The trend of E was synchronized with soil water content at the shallow depth (5 cm, upper graph), while the trend of T was synchronized with soil water content at depth of 30 cm, where highest root density was observed, showing the control of soil water distribution on ecosystem water availability and functioning.

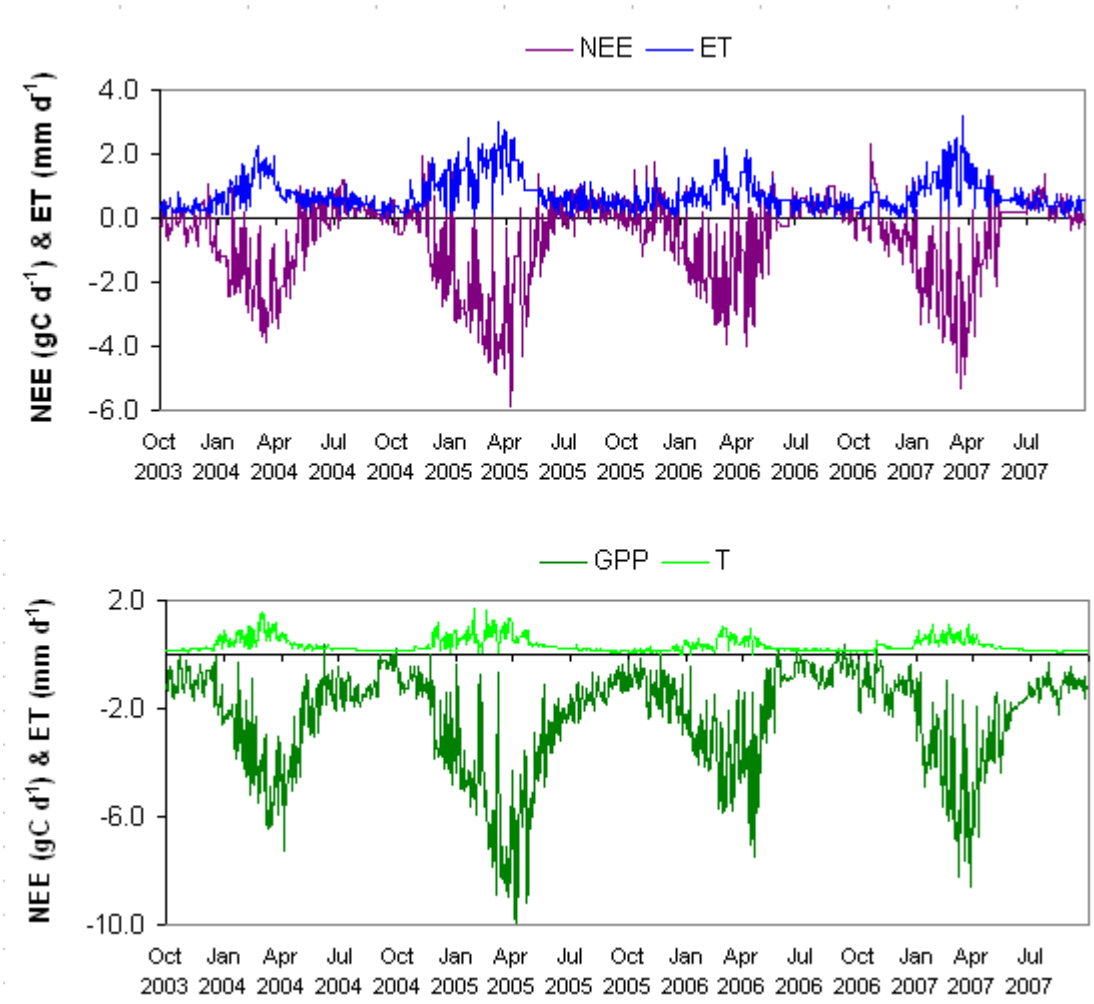

Figure 6.12: A good correlation was observed between fluxes of water release and carbon uptake. The lower graph is of the tree component: tree transpiration (T) versus gross primary production (GPP). The upper graph is of the whole ecosystem: vapor fluxes of evapotranspiration (ET) versus carbon fluxes of net ecosystem exchange (NEE). Negative values represent ecosystem uptake.

A

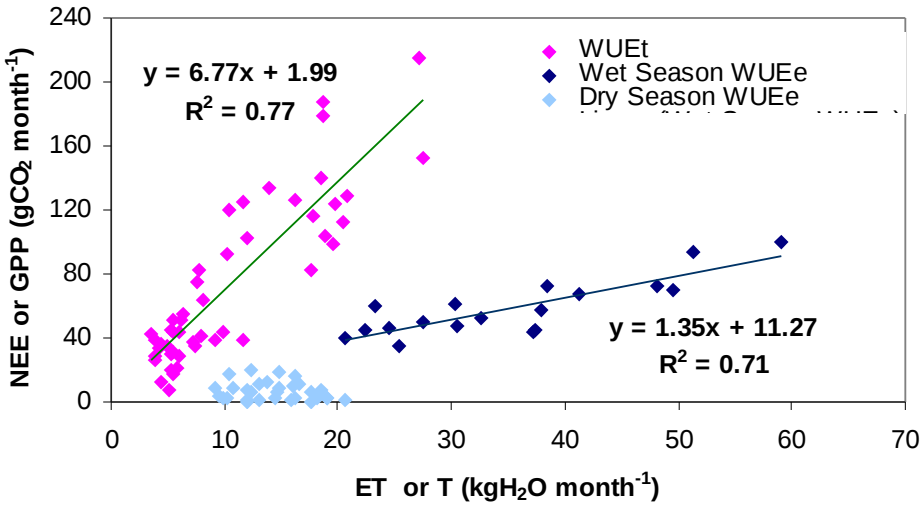

B

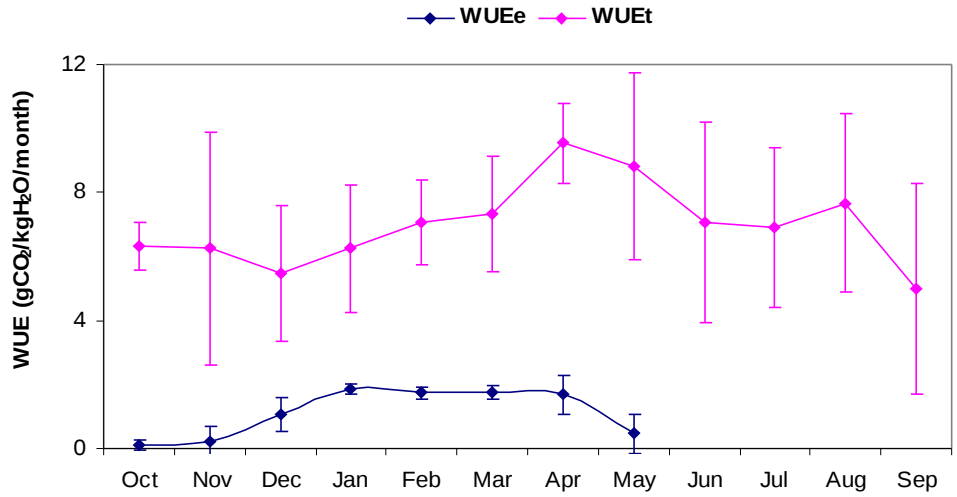

Figure 6.13: (A) The relation between monthly sums of GPP vs. T (representing the tree component - WUE_t) and of NEE vs. ET (representing the whole ecosystem - WUE_e). Good correlation was observed except for NEE and ET during the dry season, in which R was high and controlled NEE. (B) The annual trend of WUE. Monthly values of WUE_e and WUE_t, averaged for the four year research period and their standard deviation (bars) are presented. Water use of the entire ecosystem was most efficient during the wet period (Dec-Apr) and "wasteful" during the summer period, when carbon emission by soil respiration was larger than that of tree carbon uptake. Water use of the tree component was high throughout the year, with a slight maximum during the spring season (Apr-Mar); deviation in the trend between years was larger than that of WUE_e.

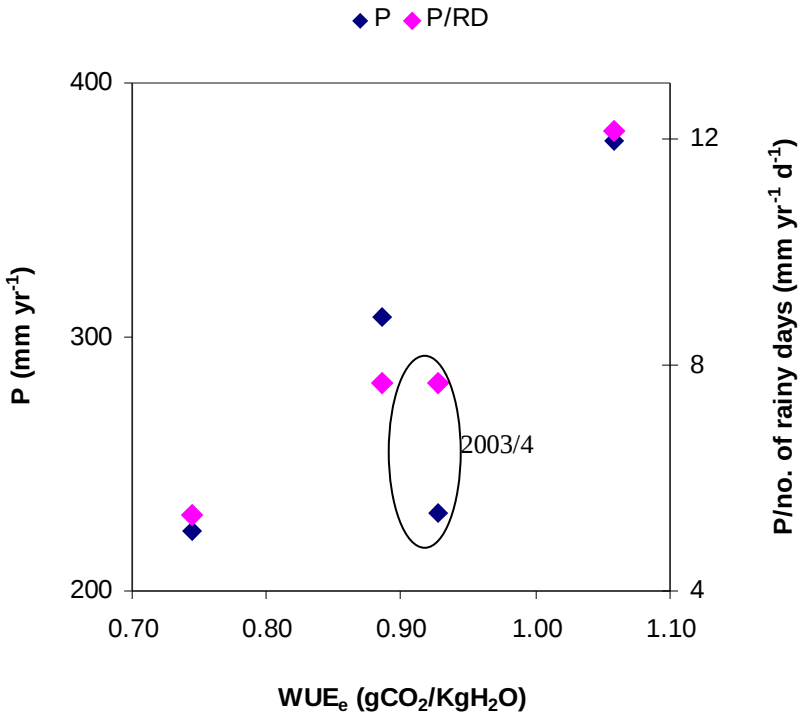

Figure 6.14: Annual values of WUE_e in relation to annual precipitation and annual precipitation divided by the number or rain days (RD, values presented in Table 6.1). Three of the four study years showed good correlation between P and WUE_e; 2003/4 deviated from this trend with values higher than "expected" according P. This was a dry year but most rains were concentrated during a short season, probably enabling deep infiltration, producing high T and low R and resulting with relatively high WUE_e. The ratio P/RD, serving as an indicator of rain pattern , produced better correlation with WUE_e (R^2=0.93).

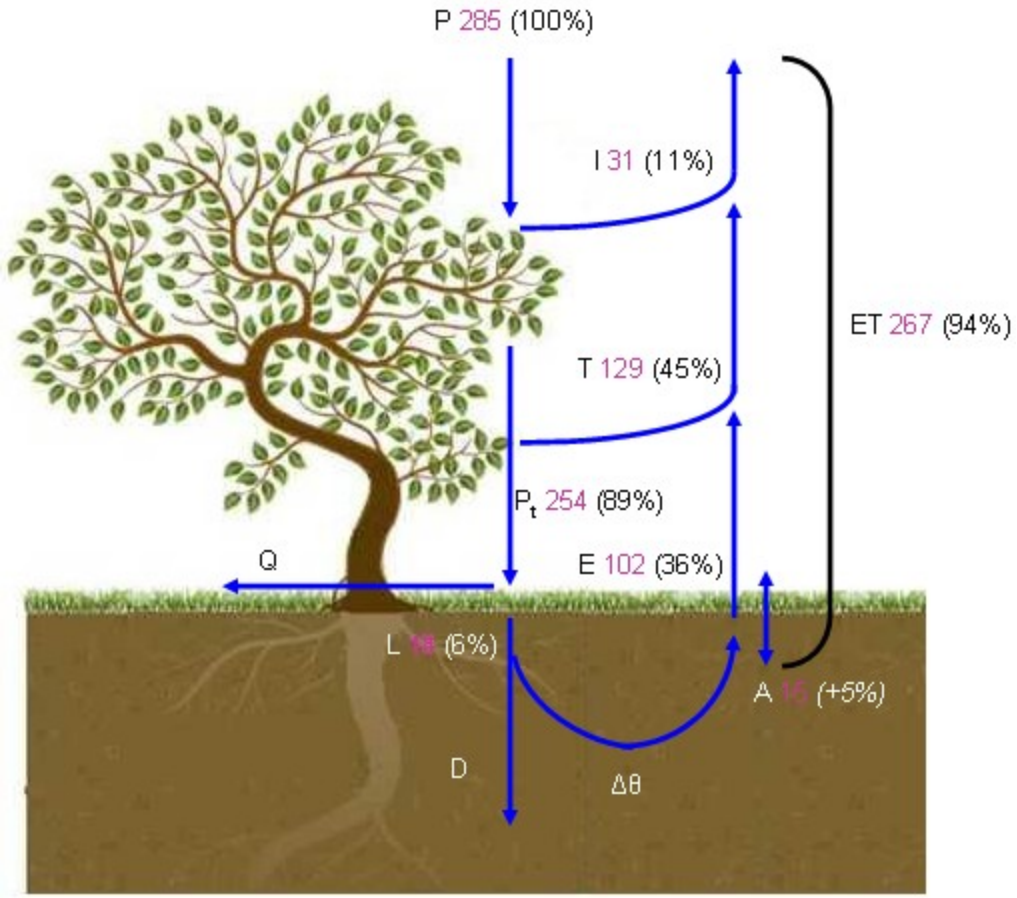

Figure 6.15: Components of the hydrological cycle for the Yatir forest. Values are in mm yr^{-1}; percentage from total precipitation is noted in brackets. Intercepted water on the canopy (I) is the difference between precipitation (P) and through-fall (P_t). Losses out of the system (L) were combined by runoff (Q), deep drainage (D) and soil water storage ($\Delta\theta$). The latter is considered a system loss on annual basis but is added to the cycle during the preceding years. Evapotranspiration (ET) is the combined flux of soil evaporation (E) tree transpiration (T) and I (ET=P-L=T+E+I). Soil adsorption (A) is balanced-out on these timescales but is estimated to add 5% to the precipitation inputs.

Chapter 7

Accompanying Report:

The isotopic composition of the water components at the Yatir Forest

7.1 Introduction

Stable isotope measurements offer valuable information on the sources and processes influencing ET and provide unique information regarding the biophysical controls on ecosystem gas exchange. Stable isotope techniques to scale and partition CO_2 and water fluxes are useful in terrestrial ecosystem studies (Wang and Yakir, 2000, Yakir and Sternberg, 2000, Lee and Veizer, 2003; Yepez *et al*., 2003, Ferretti *et al*., 2003 Williams *et al.*, 2004), enabling to better capture and interpret the dynamic changes in the sources and sinks of these fluxes.

Evaporation from soil and transpiration from plants each contribute unique isotopic signals to the water vapor in the ecosystem boundary layer and to the forest-atmosphere flux. Water evaporated from the soil is depleted in the heavy isotopes (^{2}H, ^{18}O) compared to liquid water at the evaporating surface of the soil as a result of kinetic and equilibrium fractionations (Craig and Gordon, 1965; Allison *et al*., 1983). Although the water in leaves is enriched in the heavy isotopes during transpiration because of these same fractionations, at steady-state the water transpired from leaf surfaces is isotopically similar to that taken up by the plant's roots (Flanagan *et al.*, 1991; Wang and Yakir, 1995). Since fractionation generally does not occur during uptake of water by roots (Yakir and Sternberg, 2000), the isotopic composition of vapor derived from soil evaporation and plant transpiration is very different and easily distinguished.

The isotopic composition of the evaporated vapor was modeled by Craig and Gordon (1965), specifying the factors affecting the isotopic ratio of the water:

$$\delta_E = \frac{\alpha_{eq}\delta_L - h\delta_a - \varepsilon_{eq} - (1-h)\varepsilon_k}{(1-h) + (1-h)\varepsilon_k/1000} \quad (7.1)$$

where δ(‰) is the normalized ratio of the heavy isotope of a sample ($R_{sample}/R_{standard}$), expressed in ‰, R is the ratio of $^{2}H/^{1}H$ or $^{18}O/^{16}O$, the standard is the IAEA Vienna Standard Mean Ocean water (V-SMOW), α_{eq} is the temperature dependant equilibrium fractionation factor (R_{vapor}/R_{liquid}), ε_{eq} is the equilibrium fractionation expresed as ε_{eq} = (1-α)x1000), ε_k is the kinetic fractionation associated with diffusion and h is the relative humidity of air normalized to the temperature of the evaporating surface.

Because ET is an integrated water flux, its' composition is influenced by the mixing of the contributing fluxes: transpired water, for which the isotopic composition resemble source water, and soil evaporation, which is depleted in the heavy isotopes in comparison to soil water:

$$F_{ET} = F_E + F_T \quad (7.2)$$

where F is the flux and subsripts ET, E and T stand for evapotranspiration, evaporation and transpiration, respectively. The isotopic mass balance of this system can be evaluated as:

$$F_{ET}\cdot\delta_{ET} = F_T\cdot\delta_T + F_E\cdot\delta_E \quad (7.3)$$

where δ is the isotopic composition and subscripts are as above. Ambient ecosystem air vapor will then have an isotopic composition which is a mixture of the background moisture and the combined ecosystem sources (E and T). These mass-balance relations can be utilized in the so-called "Keeling-plots" (Keeling, 1958), according to the linear relation derived from the above equations:

$$\delta_b = F_b(\delta_b - \delta_{ET})(1/F_e) + \delta_{ET} \quad (7.4)$$

where the subscripts b and e stand for background and ecosystem, respectively. For example, plotting changes in measured δ_e and in water vapor concentrations with height above the canopy (to a height in which $\delta_e=\delta_b$ and $C_e=C_b$) allow using the best fit line to estimate the Y intercept and therefore the δ value of the ET flux. Combined with measurements of ET (flux tower site), the two equation system (7.2 and 7.3) could be solved for E and T.

Based on similar methodology, Wang and Yakir (2000) combined the gradient approach mentioned above in a wheat field in order to partition ET into its components and showed that transpiration contributed most of ET (96.5-98.5%). Yepez *et al.* (2003) partitioned ET for understory and overstory vegetation and showed that understory transpiration accounted for 50% of the understory ET, 15% of the whole ecosystem ET and combined transpiration (overstory and understory) accounted for 85% of ET. Ferretti et al. (2003) demonstrated that T/ET was in the range of 60-100% for Colorado grassland, using an isotopic mass balance model between rain events. Williams *et al.* (2004) measured these relations in a semi-arid olive orchard and found that transpiration accounted for 100% of total ET prior to irrigation, but only 69–86% of ET during peak midday fluxes over a 5-day period following irrigation.

In the present study, isotopic composition of soil, leaf and atmospheric water vapor, accompanied the flux-partitioning methodology (Chapter 6) in order to partition ET. This could allow us to compare between the T/ET ratio and provide further insights into the dynamics of ecosystem fluxes and their sensitivity to environmental conditions.

7.2 Methods

During field measuring days, samples were collected routinely at noontime, for the analysis of the isotopic composition of $H_2{}^{18}O$. Ambient atmospheric ***water vapor*** at heights of 10 cm, 1 m, 5 m, 9 m, 13 m and 19 m (the latter is 9 m above the top of the canopy) were collected. Air was pumped for two hours at a rate of 1 L min^{-1} through low-absorption plastic tubes (Bev-a-Line) and water vapor was cryogenically collected in small Pyrex traps immersed in -80°C slurry of dry ice and Alcohol, as detailed in Wang and Yakir (2000). After sampling, the traps were sealed with taps and kept refrigerated. At the laboratory, the water was removed from the traps by distillation in a vacuum line (Wang and Yakir, 2000), sealed and kept refrigerated until analyzed for isotopic composition of $\delta^{18}O$ using isotope ratio mass-spectrometry (Barrie and Prosser, 1996). "Background" vapor was collected occasionally outside the forest, upwind of the flux tower site, at a height of 2 m. While H_2O concentrations were measured continuously at a height of 19m by the flux tower, vapor concentration during these occasional campaigns were measured with a stand-alone Infra-red Gas Analyzer (IRGA, LI-COR 6262) and recorded every 10 minutes.

Soil water was extracted from samples at depths of 0, -5, -10, -20, -30 cm and deeper if was possible. A new core was dug each field day from a relatively small, defined area, in order to maintain constant soil characteristics and in addition sample an uninterrupted profile. Samples from each depth were stored in glass Exetainers, sealed and refrigerated until analyzed. Then, water was extracted from the soil samples using a vacuum line and analyzed for $\delta^{18}O$ as above. ***Stem water*** indicating source water composition was analyzed from stem samples collected from two different but permanently-chosen trees. Leaf water (needles) of these two trees was also sampled. Stem and leaf materials were stored in glass Exetainers, sealed and refrigerated until analyzed. Water was extracted and analyzed as above.

Rain water was collected at the field into opaque glass bottles partially sealed with light-weight balls (enabling inflow of water and limiting evaporation). In each case circumstances enabled collection of this water during the 24 hours following a rain event,

three repetitions of rainwater were poured into Exetainers, sealed, refrigerated and analyzed for $\delta^{18}O$ composition.

In addition to measurements at the Yatir research site, seasonal campaigns were held during one year at two additional sites: the Judean hills ("Burma road") and the Carmel region ("Raqit"). Sites were chosen such that their height and vegetation type would be similar to that of Yatir, and the main varying parameter was precipitation. All sites are situated within forests dominated by the Aleppo pines (*Pinus halepensis* Mill.). Accordingly, the dynamics of the isotopic composition and flux contribution of each ecosystem source and their sensitivity to variations in precipitation could be questioned along the natural climatic gradient of Israel.

7.3 Results

The averaged $\delta^{18}O$ composition of all measured components for all measuring days (total 40 days) is presented in Figure 7.1. The average and standard deviations of each component indicates the range of values during all seasons. Relationships between measured components was be better observed when looking at specific days (Figure 7.2): stem water was similar to that of soil water at depth of ~15 cm, indicating tree water uptake probably occurred from this depth. In addition, soil water enrichment due to evaporation was observed between days.

Barely any variance was observed in profiles of vapor collected at different heights (less than 1‰). Variance was much larger when different measuring days were compared (up to 10‰). However, resemblance between vapor composition measured at Yatir and at Rehovot (Weizmann Institute) was observed (Figure 7.3).

Stem water indicative of source water show a seasonal trend, generally correlating with θ (Figure 7.4): $\delta^{18}O$ was most enriched at the end of summer, when θ was lowest, and started to deplete gradually following the rise of θ. Enrichment continued gradually throughout all summer season, even after θ was constantly low, raising again the assumption of deeper source water which was still in a drying process even at the end of summer.

Soil $\delta^{18}O$ demonstrated expected behavior (Figure 7.5): at the end of summer, soil was dry and soil water was enriched down to a depth of 30 cm. During the rain season, infiltration led to gradual depletion of soil water. In spring, surface soil water was enriched while deeper soil water was still depleted, due to higher θ at those depths (enrichment occur only at the evaporating surface).

Comparison between the three sites along the climatic gradient of Israel during the summer period (June 2004) shows high similarity of vapor composition, dominated by common background and less affected by ecosystem sources during this season (Figure 7.6). Soil water at the ground surface was depleted, due to low amounts of water in the pore spaces and high mixture with atmospheric vapor content. Variations between sites in the surface soil water composition can be attributed to soil type, which is least condense at the Carmel region and most condense at Yatir. Variations of stem water between sites resembled that of soil water at depth of 20 cm and at the surface. Leaf water was most enriched in the heavy isotopes at the Yatir site.

7.4 Future research

Preliminary work on this database has shown its applicability, but further analysis is needed. Ongoing investigation focuses on the trend and patterns of $\delta^{18}O$ in the different parts of the system and their relation to environmental conditions. The lack of an isotopic gradient within and above the canopy complicates flux partitioning based on mass balance and the gradient approach. However, it is suggested to differentiate the ET contribution from the ecosystem isotopic composition based on measurements of Yatirs' background or based on routine measurements conducted at the Weizmann Institute and Sde-Boker. Following, the partition of the ET flux can be executed, and comparison to flux-based partitioning (Chapter 6) will be enabled.

7.5 Figures

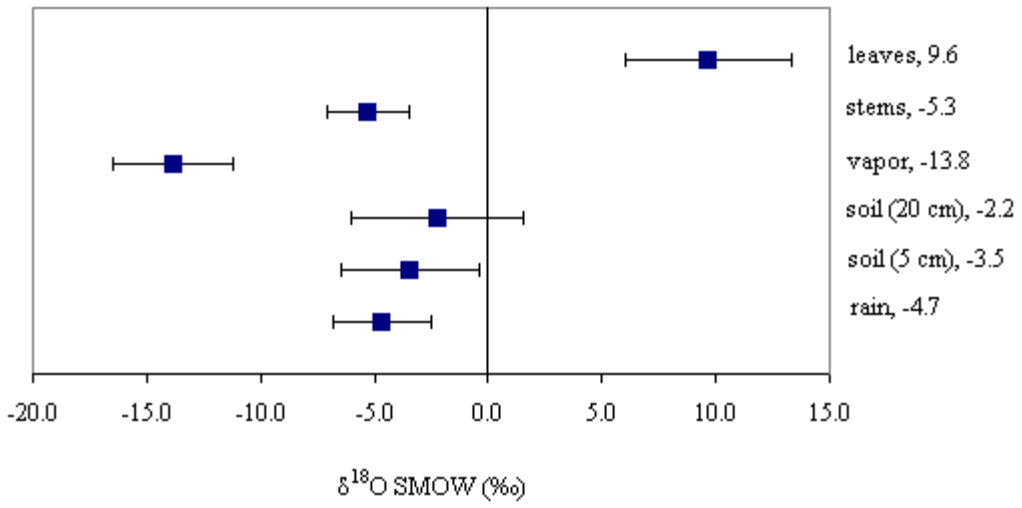

Figure 7.1: Averaged values of the isotopic composition during all research period (total of 40 days) of all measured components. Standard deviation is presented in bars, indicating the main value range of each component

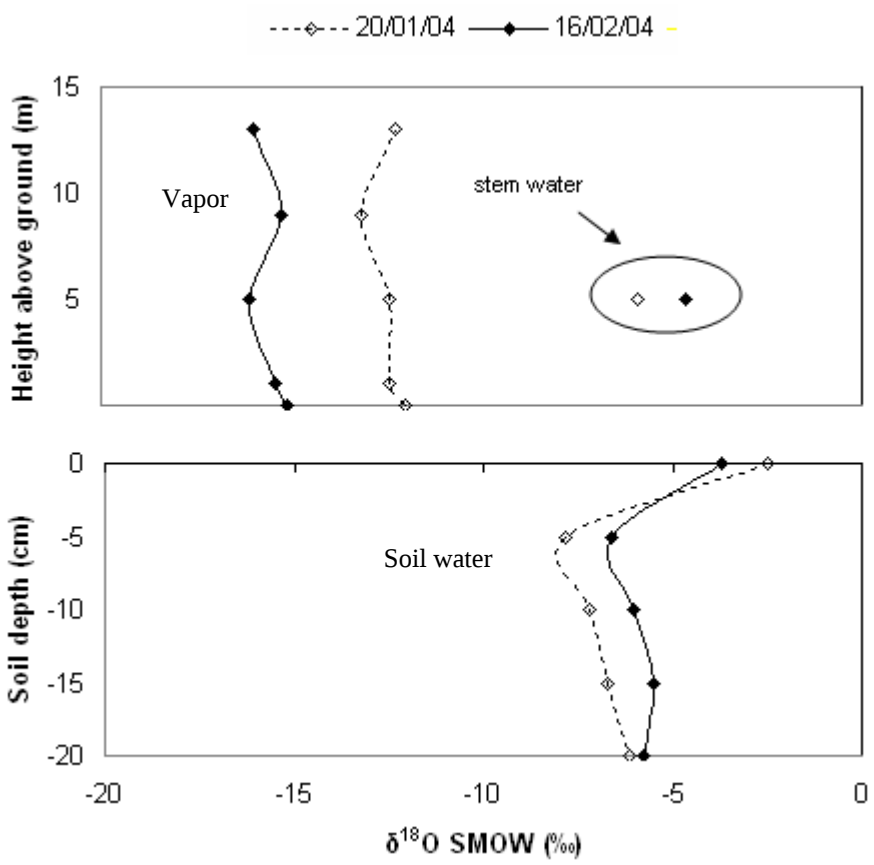

Figure 7.2: Vapor and soil profile during two measuring days. The soil water profile was enriched due to evaporation during this period. Stem water composition resembled that of soil water at depth of ~15 cm.

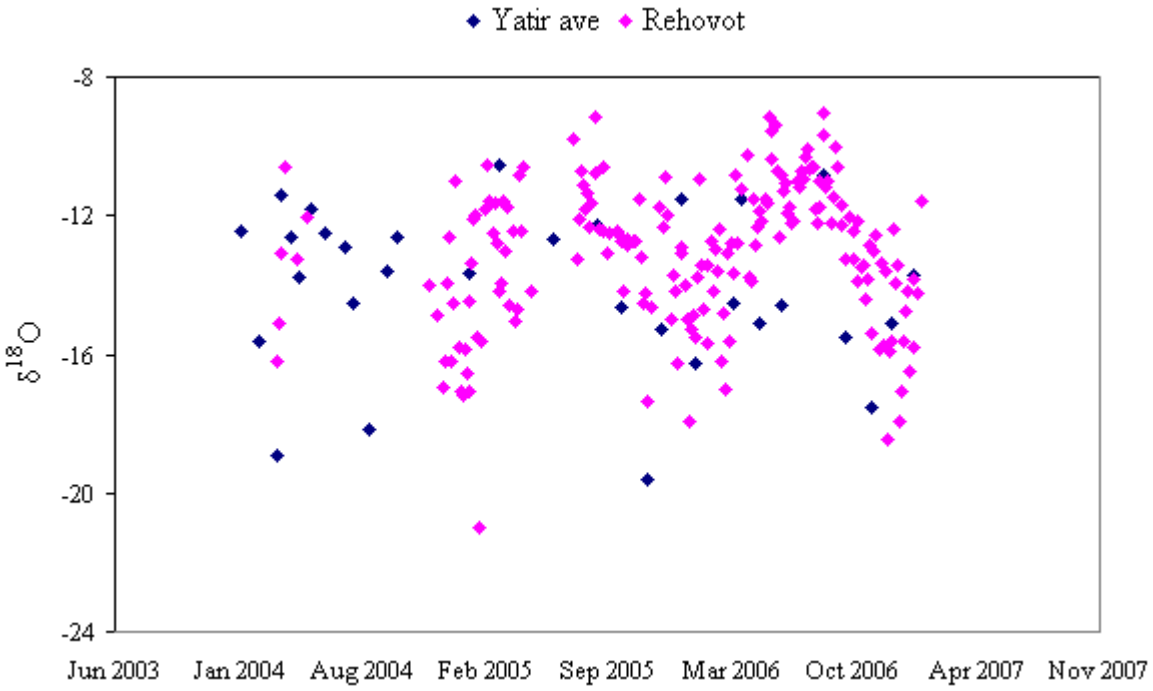

Figure 7.3: Compatibility between the vapor isotopic composition measured at Rehovot (Weizmann Institute) and Yatir forest. The continuous database of Rehovot measurements enables to identify a seasonal trend with enriched (higher) values during the summer season.

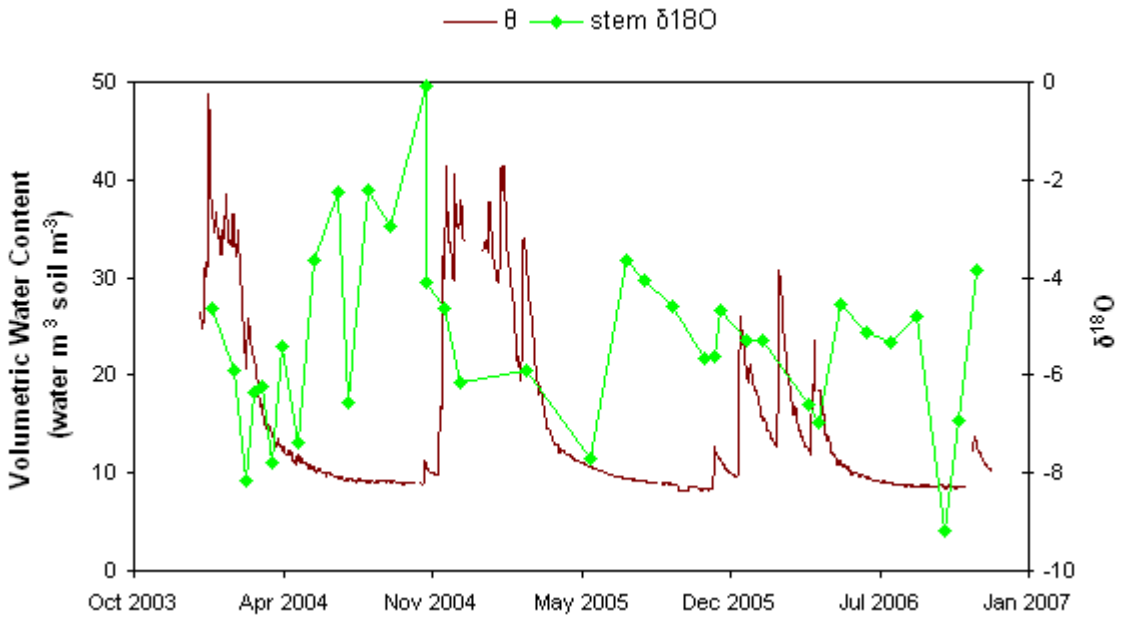

Figure 7.4: Seasonal trend of soil water content and stem water isotopic composition. Stem water was most enriched at the end of summer, when θ was lowest, and started to deplete gradually following the rise of θ. Enrichment continued throughout all summer season, even after θ was low and constant, raising the assumption of deeper source water which was still in a drying process even at the end of summer.

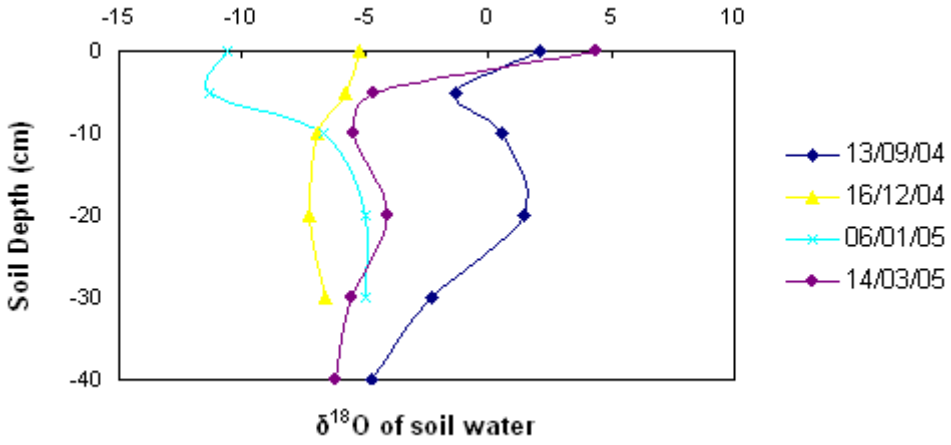

Figure 7.5: Soil profiles of $\delta^{18}O$ representing various seasons. At the end of summer (13/9/2004), the soil was dry and soil water was enriched down to a depth of 30 cm. During the rain season (16/12/2005 and 6/1/2005), infiltration leaded to gradual depletion of soil water. In spring (14/3/2005), surface soil water was enriched while deeper soil water was still depleted, due to higher θ at these depths.

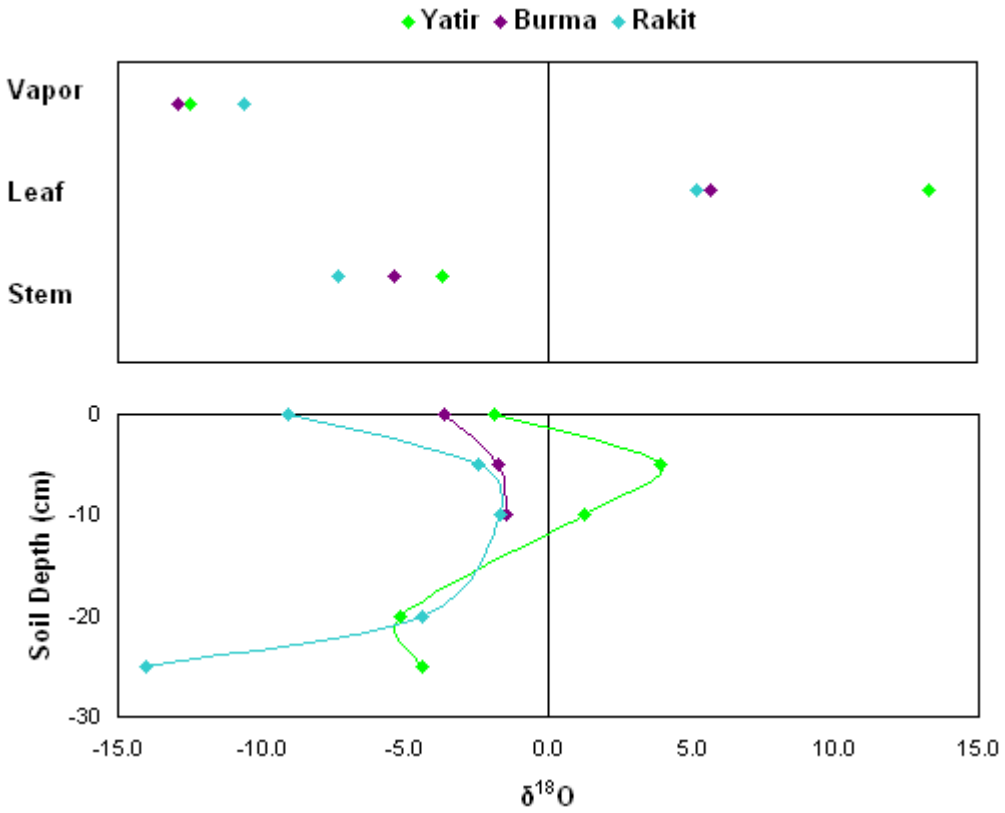

Figure 7.6: Comparison between the three sites along the climatic gradient of Israel during the summer period (June 2004). Surface soil water was depleted due to low water filled pore space and high mixture with atmospheric vapor. Relations between sites follow soil characteristics (most condense at Yatir, and least condense at Rakit, for which surface soil water equals vapor composition). Stem water composition resembled soil water at depth of 20-30 cm. Leaf water was most enriched at Yatir.

Summery and conclusions

- Measurements of soil evaporation fluxes (E) can be implemented utilizing the methodology developed in this research, based on a modified soil chamber connected to IRGA (LI-6400-09, LI-COR, USA). Testing against known water fluxes calculated from water loss (balance) showed high linearity, accuracy and repeatability for a large range of fluxes (-0.20 – 0.60 mm hr^{-1}). The calibration procedure defined a need to correct chamber fluxes by a factor of 2.66.
- Soil evaporation at Yatir forest was defined as a major component of the water cycle (102±8 mm yr^{-1}), accounting for approximately 42% of annual ET and reflecting the combined effects of an open forested canopy and small precipitation events with contribution to soil moisture mainly at superficial depths.
- The spatial variability of E between the 14 measured points was large (standard error of 5-54%, varying between measured days). Fluxes measured at exposed areas between trees where on average double those measured below trees.
- The spatial pattern of E was linked with those of radiation and soil water. Tree shading produced variations of up to 80% in PAR between sites. Soil moisture was lower at shaded areas during the wetting period (caused by intercepted precipitation and redistribution of localized runoff) and lower between trees during the drying season (caused by tree shading decreasing E rates).
- In light of the large measured heterogeneity, a simple average of the 14 measured points was not applicable for estimation of field E from point measurements of E. Up-scaling was preformed based on measured fluxes at shaded and at exposed areas and calculated forest floor shaded fraction (based on solar altitude and tree size), both varying daily.
- The effect of canopy design on soil evaporation was simulated and indicated that during tree growth from 2 to 15 m, a 50% decrease in E can be expected and a decrease in 60% is expected between stands of 100 and 600 trees ha^{-1}. This simple predictive tool can further provide estimations of water loss by E within forested ecosystems for management practices.
- Diurnal cycles of E were observed, with peak daily values around noon time (up to 0.20 mm hr^{-1}) and compatibility with measured trends of T and ET.

- The seasonal trend of E was characterized by high rates during early and late winter (a combination of high temperatures and high θ at the shallow soil layers; fluxes up to 0.80 mm d^{-1}) and low rates during mid-winter and summer (low temperatures or low θ, respectively; typical fluxes of 0.10 mm d^{-1})
- A good seasonal correlation was detected between E and environmental parameters (θ_5, R_n, VPD, T_a and WS), with soil moisture most significant during the wetting and drying season and R_n and T_a significant during the energy limited period (winter) and the dry summer. These relations were utilized in order to simulate E for non-measured days. Results indicated that derivation of E based on a constant function of PET and θ as preformed in some models is insufficient and will presumably produce major inaccuracies.
- As typical for arid and semi-arid climates, the precipitation at Yatir was characterized by small sporadic rain showers (82% of showers were below 5 mm). Usually, at least one large storm or a number of medium consecutive storms occurred (>60 mm) each year.
- Soils at Yatir are dense (~1.65 g cm^{-3}) and fined textured (28% clay, 41% silt). Accordingly, calculated water holding capacities of the soils were high (113 mm for the upper 40 cm) and infiltration rates were low (15-30 mm hr^{-1}).
- The combination of precipitation pattern and soil characteristics at the research site controlled the distribution of soil water content with depth: Superficial soil water content was increased even by small showers (but higher than 2 mm) having high occurrence throughout the rain season and enabling to maintain high moisture during the period November - June of all measured years. Soil moisture at depth was reliant on large and less common rain storms and therefore varied between years. High water holding capacities of the soil resulted in observed increase of soil moisture at depth only later in the season (January) but low evaporation at these depths enabled to maintain high levels of water content which sometimes prevailed all summer. Following years with deep infiltration, soil moisture storage was measured between years (up to 22 mm yr^{-1}).
- The annual trend of tree transpiration (T) measured by a collaborative research began to rise at mid-winter (January) and peaked during spring (March-April; up to 1.20 mm d^{-1}). This trend was well synchronized with the pattern of soil

moisture at depth of 30 cm, which is the depth of maximum root density. Annual T during the research period was 129±21 mm.

- The partial contribution of soil evaporation to the evapotranspiration flux behaved accordingly, with highest contribution during the wetting season, when E fluxes were high but T fluxes were still low (E/ET up to 0.80-0.90) and lowest during spring (0.27-0.37). At summer E and T were approximately equivalent.
- Soil adsorption (negative fluxes of E) was measured during the hours before sunrise and after sunset at the end of summer, when soil moisture was low (θ_5<0.10) and the amplitude of daily RH large (>40%). It was estimated that during the summer nearly half of daily E was contributed from this process. Annual values of adsorption were estimated to be in the range of 10-15 mm yr^{-1}, adding ~5% to P inputs. It is acceptable that adsorbed water cannot be utilized by trees, but can be significant for considerations of the energy budget and are also important for the sensitivity and accuracy of GCMs parameterizations.
- Closure of the hydrological balance for Yatir was obtained after defining the size and annual variation of the different components. Loses by deep drainage, runoff and temporarily stored soil moisture were calculated to be 18±25 mm yr^{-1}, accounting for approximately 6% of P.
- Similar to their effect on ET partitioning, precipitation pattern was found to control ecosystem production:
- Gross primary production (GPP) calculated for Yatir in a complementary research showed generally high compatibly with T, indicating the ecohydrological control of soil water on sequestration and biomass production.
- Ecosystem water use efficiency (WUE_e; NEE/ET) showed increased efficiencies with increased annual precipitation but better correlation when incorporating the effect of precipitation pattern (P/RD; RD- number of rain days). ET partitioning enabled to differentiate between the ecosystem and tree components and water use efficiency of the tree component (WUE_t; GPP/T) showed similar relations with P/RD. Exceptional was a year with low precipitation but condense storm events enabling deep infiltration and high transpiration fluxes, which were not accompanied by high tree production. It is therefore suggested, that under extreme dry conditions WUE is expected to decrease due to physiological stress effects.

- Current models for our region predict a decrease in P accompanied by intensification of the hydrological cycle, resulting in larger storms. According to our findings, this may at least partly compensate for the decrease in P and its potential adverse effects on forest productivity.

Appendixes 1

Soil profiles

Prior to the installation of TRIME soil water content sensors, pits were dug in the field both manually and with JVC tractors. Following are descriptions of the three cleavages revealed. Soil densities were determined from samples of known volumes. Soil texture was analyzed by Gilat Laboratories, KKL. Soil definitions were preformed with the assistance of Prof. Zinger, the faculty of agriculture, Hebrew University, Rehovot.

Pit 1

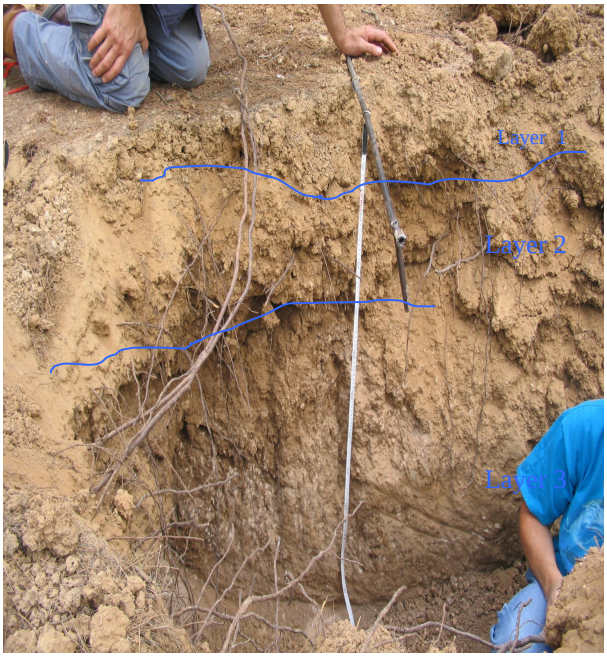

A

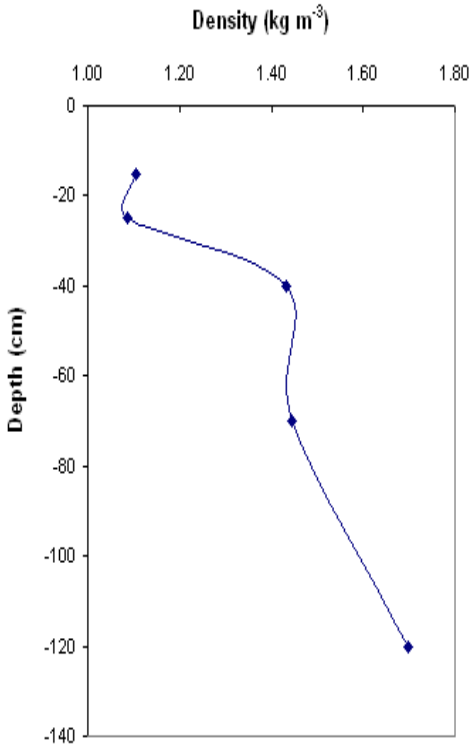

B

Figure 9.1.1: (A) The soil profile of Pit 1 and (B) The soil density. Location of samples for density tests were chosen according to position of TRIME sensors.

A B

Layer 1: 0-12 cm, unconsolidated, yellow - light brown, becomes powdery with touch and tends to spill. Density ~ 1.10 g cm^{-3}.

Layer 2: 12-50 cm, light brown, consolidated. Most roots were within this layer. Root density was highest at depth 30 cm. Aggregates of calcite were present. Soil density rose gradually until a maximum of 1.45 gr cm^{-3} at depth of 40 cm.
Average texture: 31% sand, 41% silt and 28% clay.

Layer 3 (Figure 9.1.2)*:* 50-135 cm, dark brown, very condense, many white calcite aggregates and few roots were present. Soil density rose gradually until a maximum of 1.70 g cm^{-3} at depth of 120 cm.
Average texture: 9% sand, 44% silt and 47% clay.

Bedrock was exposed at a depth of 130-135 cm. The rock was a light colored, crystalline limestone. No fractures were observed on the rock surface.

Figure 9.1.2: Palaeosol in Pit 1.

This horizon was defined as a palaeosol of fossil B horizon. The soil contained many fossil roots. Cutans (clay-covered particles) were observed, implying on deep leaching of

B horizon during wetter periods. No reduction effects were observed, indicating that this layer was never saturated for long periods.

Pits 2 and 3

Apparently homogeneous soil profile, light brown, consolidated, similar to layer 2 of pit 1 (layer 1 was not observed). Density was 1.45-1.65 g cm^{-3}, including the shallow soil (5 cm). Bedrock was exposed at a depth of 40 and 80 cm for pit 2 and 3, respectively.

Figure 9.1.3: Pit 2

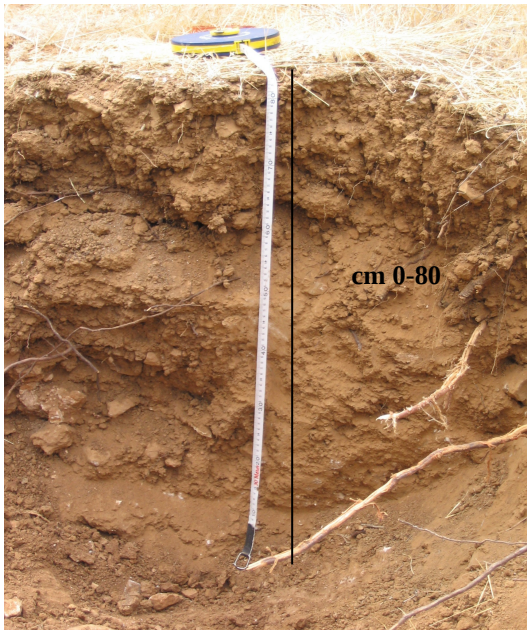

Figure 9.1.4: Pit 3

Appendix 2

Calibration, installation and calculation procedure for CS616 water content reflectometer, Campbell Scientific Inc.

Sensor description and technology

The CS616 (Figure 9.2.1) was designed to measure volumetric water content of soils or other porous media, derived from the probe sensitivity to the dielectric constant of the measured media. It consists of two 30 cm long stainless steel rods connected to a printed circuit board which is encapsulated in epoxy. A shielded four conductor cable is connected to the circuit board supplied power to produce pulse output and monitoring of the probe. The reflectometer connects directly to a data logger via its' single-ended analog inputs.

The CS616 is based on a high-speed electronic component configured as a multi-vibrator, which output is connected to the probe rods acting as a wave guides. The CS616 output is a square wave with amplitude of ±0.7 v with respect to system ground. A data logger control port is used to enable the CS616 for the amount of time required to make the measurement. Data logger instructions convert the probe square-wave output to travel time of the signal on the probe rods. Travel time ranges between 14 ms in air to 42 ms when immersed in water. The return of the reflection from the ends of the rods triggers a logic state change which initiates propagation of a new wave-front.

Accuracy and precision

The accuracy reported by the manufacture (Instruction Manual, Campbell Scientific Inc. 2/02) is ±0.03 θ for soils with bulk electrical conductivity lower than 0.5 dS m^{-1} and bulk density lower than 1.55 gr cm^{-3} for θ in the range of 0.00-0.50. Probe variability reported by the manufacture is ±1.50% for saturated soils. Chandler

et al (2004) tested a set of similar Campbell Scientific CS615 sensors, installed in pits up to 1 m depth. They calibrated the automated continuous measurements of the CS615 with periodical manual measurements executed with a TDR (Soil Moisture Equipment Inc.) over a two year period. For 10 sensors with paired TDRs', R^2 ranged between 0.93±0.02 to 1.00±0.01 with an average of 0.97, which is similar to the accuracy reported by the manufactures. This laborious procedure showed correlation between CS measurements and TDR are high but emphasized the need for site-specific and sensor-specific calibration.

Similar results were also obtained by this research: averaged daily standard deviation between the three sensors for a period of four years was ±2.63%. Deviation was even smaller when taking into account that the 25 m long cable of one of the sensors (SC616_1) was self assembled in order to cut expenses. Standard deviation between the other two sensors (for which cables were factory assembled) was ±1.08%.

Calibration and field installation

The output of the SC616 is the travel time or "output period" (ms). While for TDR technology a universal equation can be utilized in order to convert dielectric permittivity to θ (Topp *et al*., 1980), here a material-specific calibration procedure was required.

In order to achieve soil-specific equations, calibration was executed under laboratory conditions against known soil water content. Three 40 cm long and 10 cm diameter PVC columns were uniformly packed with soil samples taken from the field and oven dried at 105ºC until constant weight was observed. Original layering was preserved. The 30 cm long probes were inserted vertically into each column and connected to a Campbell CR10X data logger. The columns were placed inside an incubator to keep a constant temperature of 20ºC. This temperature was chosen as it is defined by the manufactures temperature correction equation as reference (Eq. 9.2.2). Measurements were conducted at intervals of one minute for each probe throughout the test. A known amount of distilled water was poured from the top of the column. After reaching a steady reading, the soil samples were weighted to insure no loss of water, following by an addition of a known amount of water. For such short periods and low θ it is obvious that water content in the soil sample was not homogeneous.

However, as long as the wetting front had not reached below the level of the probes (30 cm), all water should be detected by the probes, which measure the dielectric constant as an average over their whole length.

Differences between output periods of the three SC616 were small (Table 9.2.1) and the average standard error of the quadratic correlation calculated was ±3%, similar to that defined by the manufacture and Chandler *et al.* (2004). The last two stages were not included for definition of correlation coefficient as they exceed the range of θ defined by the manufacture.

The best fitted quadratic equation for the averaged output data was:

$$\theta = 0.1763 - 0.0227\tau + 0.0008\tau^2 \qquad (9.2.1)$$

where θ is the known soil water content (water m^3 soil m^{-3}) and τ is output period (milliseconds). The quadratic equation achieved was slightly different from the manufacture calibration equation. This was expected and attributed to the attenuation of the sensor response caused by the compact clayish soil of the Yatir field site (Figure 9.2.2).

The three CS616 sensors were installed vertically at the field, measuring θ representing averaged soil moisture for depth 0-30 cm. Sensors were positioned around the tower, at distances of ~20-25 m from it. After installation, soil samples were taken occasionally in order to define θ from weighted water content (gravimetric), and showed high agreement with SC616 results (Table 9.2.2). In addition, SC616 recordings were compared to measurements of θ conducted with a Neutron Probe measured by Ben-Gurion University, also showing high compatibility (Table 9.2.3).

Associated measurements of soil temperatures

CS616 measurements are sensitive to changes in soil temperatures and a temperature correction equation is supplied by the manufacture:

$$\tau_c = \tau_u + (20 - T)x(0.526 - 0.052\tau_u + 0.00136\tau^2_u) \qquad (9.2.2)$$

Where τ_c is the temperature-corrected output period (milliseconds), τ_u is the raw measured uncorrected output period (milliseconds) and T is the soil temperature (°C). The temperature correction effect increased with θ (Figure 9.2.3).

Soil temperature was measured with temperature probes (TMC6, Onset Computers, USA) connected to a data-logger (HOBO H8, Onset Computers, USA). Prior to installation, the accuracy of these temperature probes was tested in water tabs at the laboratory and probes readings were compared to a calibrated thermocouple for 8 points in the range 0°C (icy water) to 65°C. HOBO readings were found to be 0.75±0.16°C lower than reference, and standard deviation between the 8 sensors was ±0.20°C on average.

A system containing four probes was installed in the proximity of SC616_1 and SC616_3. At each location, soil temperature was measured at depths of 1, 5, 15 and 30 cm. The integrated average of soil temperature was calculated according to:

$$T_{ave}=[5xT(1\ cm)+14xT(5\ cm)+25xT(15\ cm)+16xT(30\ cm)]/60 \qquad (9.2.3)$$

Correcting θ according to measured soil temperature created a large diurnal trend that was overcome only when values were averaged for the whole day (Figure 9.2.4).

Calculation procedure

a) The averaged soil temperature for depth 0-30 cm was calculated from the temperature probes according to Eq. 9.2.3 for each 30 minute period.
b) The SC616 output period for the 30 minute values was corrected to the equivalent temperature according to Eq. 9.2.2.
c) The 30 minute temperature corrected output period was converted to θ according to Eq. 9.2.1, to fit Yatirs' soil.

Table 9.2.1: Laboratory results for obtaining soil-specific calibration equation. Known θ was compared to SC616 output period of each of the three sensors.

Cumulative Water Added (ml)	**Calculated θ (m^3 m^{-3})**	**Output Period (ms)**				
		SC 1	**SC 2**	**SC 3**	**Average**	**stdev**
0	0.00	16.17	16.26	16.42	16.28	0.13
150	0.06	19.34	19.75	19.75	19.61	0.24
300	0.13	22.93	24.85	22.6	23.46	1.22
450	0.19	25.88	27.26	25.79	26.31	0.82
600	0.25	28.2	29.58	27.73	28.50	0.96
900	0.38	32.86	33.88	33.63	33.46	0.53
1050	0.45	34.37	34.32	34.65	34.45	0.18
1200	0.51	35.45	36.02	35.62	35.70	0.29
1350	0.57	35.82	36.33	35.86	36.00	0.28

Table 9.2.2: Field measurements of soil water content comparing readings of SC616 and gravimetric measurements.

		θ (m^3 m^{-3})	
date	Sensor	gravimetric	SC616 readings
02/10/2003	SC_1	0.10	0.10
15/01/2004	SC_1	0.42	0.45
15/01/2004	SC_2	0.40	0.44
15/01/2004	SC_3	0.39	0.43
16/12/2004	SC_3	0.36	0.35
06/01/2005	SC_1	0.41	0.42

Table 9.2.3: Field measurements assuring compatibility between SC616 readings and measurements of θ with a Neutron Probe taken at different dates. Measurements with the Neutron Probe were conducted by the research group of Ben Gurion University. Values are averages of 7 pipes in the towers' area.

Date	θ (m^3 m^{-3}) Average SC616	Average Neutron Probe
09/10/2003	0.09	0.10
19/01/2004	0.37	0.39
26/01/2004	0.34	0.35
26/02/2004	0.30	0.32
05/07/2004	0.09	0.09
15/10/2004	0.08	0.08
09/12/2004	0.29	0.29

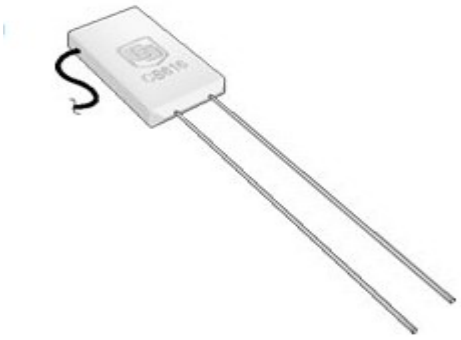

Figure 9.2.1: Campbell Scientific Inc. CS616 water content reflectometer. Rods are 30 cm long.

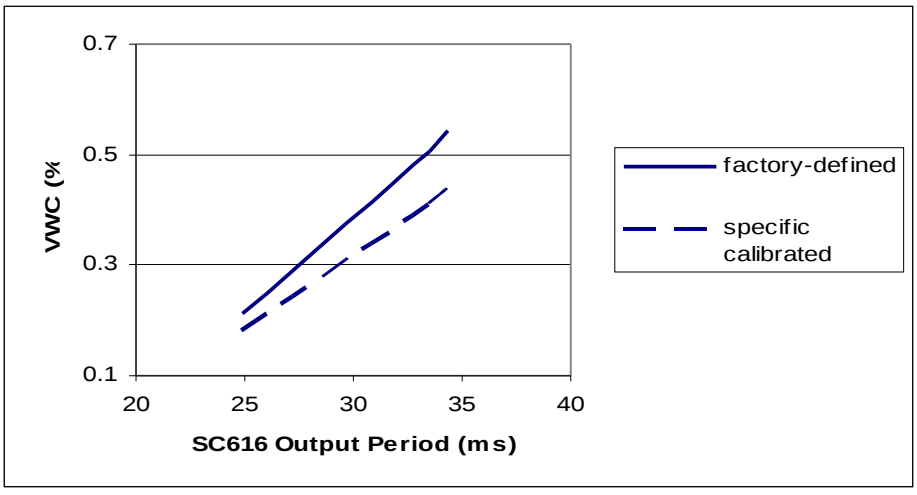

Figure 9.2.2: CS616 Response curves. Conversion of SC616 travel time output period (milliseconds) to θ (water m^3 soil m^{-3}). Yatir dense and high-clay content soil introduces a deviation of the converting equation (dashed line) in comparison to the factory defined equation (continuous line).

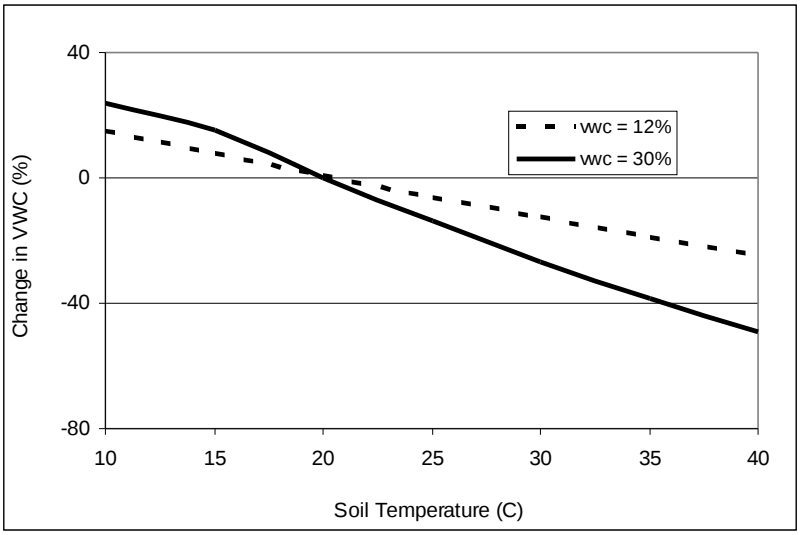

Figure 9.2.3: Effects of the temperature correction equation (9.2.2) on the value of θ. The difference between corrected and uncorrected θ increased with deviation from T_s=20°C and with soil moisture.

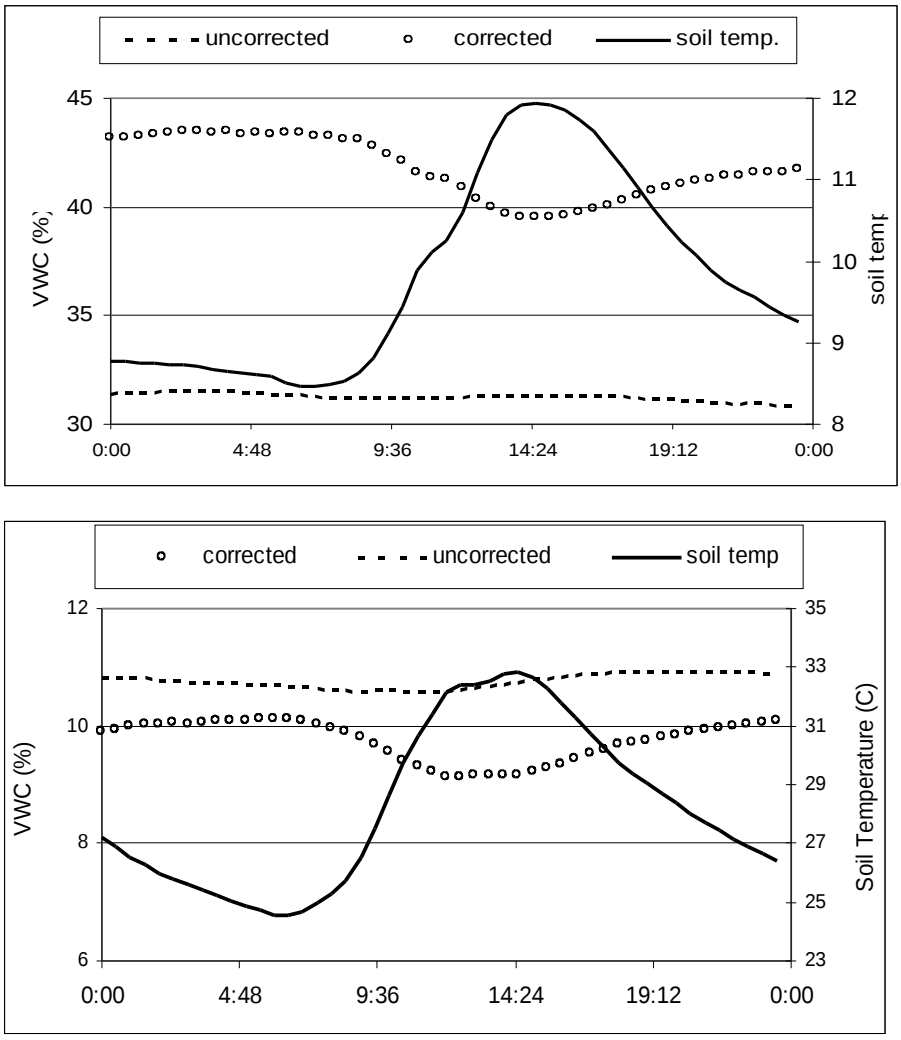

Figure 9.2.4: Diurnal cycles of soil temperature (continuous line) and θ (uncorrected to temperature in dashed lines, corrected to temperature in circles line) during a day with relatively dry soil (10/10/2003, lower graph) and a day with wet soils (20/12/2003, upper graph). The correction creates a diurnal cycle of θ not presented originally.

Appendix 3

Testing of TRIME intelligent soil water content sensors, IMKO Micromodultechnik GmbH

Sensor description and technology

TRIME (Time domain Reflectometry with Intelligent MicroElements) is based on the TDR-technique (Time Domain Reflectometry), and was developed to measure the dielectric constant of a material. The methodology is based on metal rods which are used as wave guides for the transmission of the TDR-signal. TRIME system generates a high frequency pulse (up to 1GHz) which propagates along the wave guides generating an electromagnetic field around the TRIME probe. At the end of the wave guides, the pulse is reflected back to its source. The resulting transit time (10 ps – 2 ns) and dielectric constant are dependent upon the moisture content of the material. IMKO has developed a patented measuring method which enables to measure the transit time with a resolution of 3 ps.

TRIME systems are unique in that all measurements and calculation procedures are executed directly within the sensor itself. Therefore, this system is not reliant on the cable length connecting between datalogger and sensor, satisfying our need to install sensors far from the power supply site. Data acquiring can be preformed via datalogger or PC interface. Two types of TRIME sensors are manufactured, differing in their dimensions and measuring volume (Figure 9.3.1). The smaller sensors (TRIME-IT) were needed for installation in the shallow soil (5 cm). The more robust sensors (TRIME-EZ) were installed at the deeper layers. The accuracy reported by the manufacture is ±1% for θ in the range of 0.00-0.40 and ±2% in the range of 0.40-0.70%.

Calibration and testing

TRIME measuring systems convert travel time to θ according to the standard universal calibration equation for mineral soils (Topp *et al*., 1980). This equation is applicable for soils in the range of:

- Clay content >50%
- Organic content >10%
- Bulk density in the range 1.1-1.7 g cm^{-3}.

Yatir soils falls within these limits, even though at some depth density approaches 1.7 g cm^{-3} and clay content approaches 50%.

Prior to field installation, TRIME readings were compared with water gravimetric measurements and other water content measuring devices. These tests showed repeatedly, that TRIME readings are satisfactory for low and high θ (0.00-0.10, 0.30-0.40) but up to 0.08 higher than other measurements for the middle ranged θ values. Other technologies were highly compatible with each other and with gravimetric measurements (Figure 9.3.2).

These results were sent to Imko, Germany. After some inquiry, the company found out that a wrong calibration equation was uploaded to the sensors (calibration of a material different than soil). As absolute values were forced at two points (0.02 and 0.41), the false equation caused a curve-like relation between actual θ and TRIME readings. Following, IMKO representatives came to Israel and uploaded the correct calibration parameters to each sensor. Comparisons carried on afterward in the laboratory and at field site were satisfactory and deviation from other soil water measuring techniques was below 2% (Figure 9.3.3).

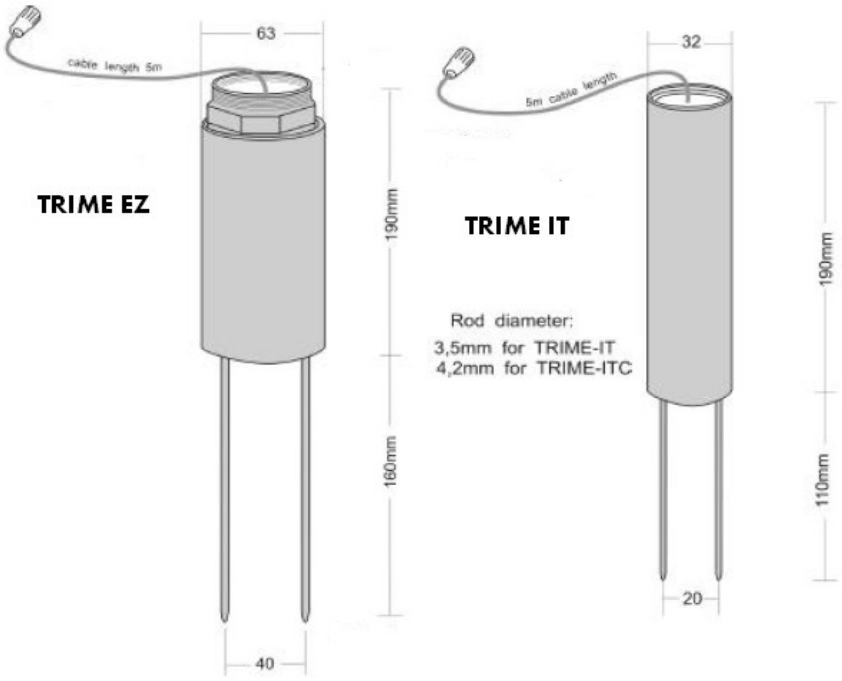

Figure 9.3.1: TRIME EZ and IT sensors.

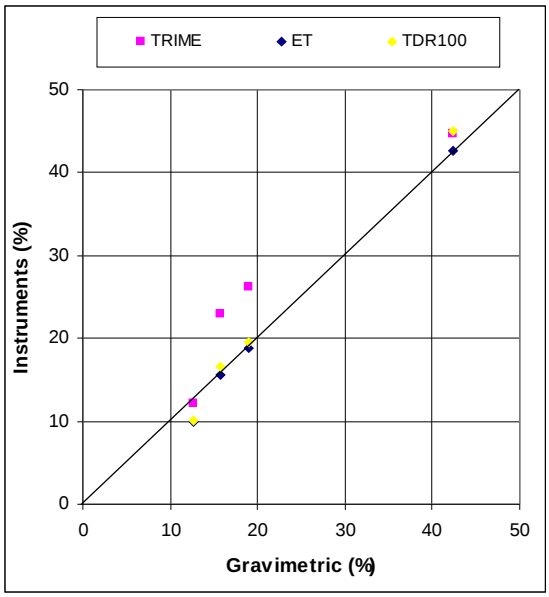

A

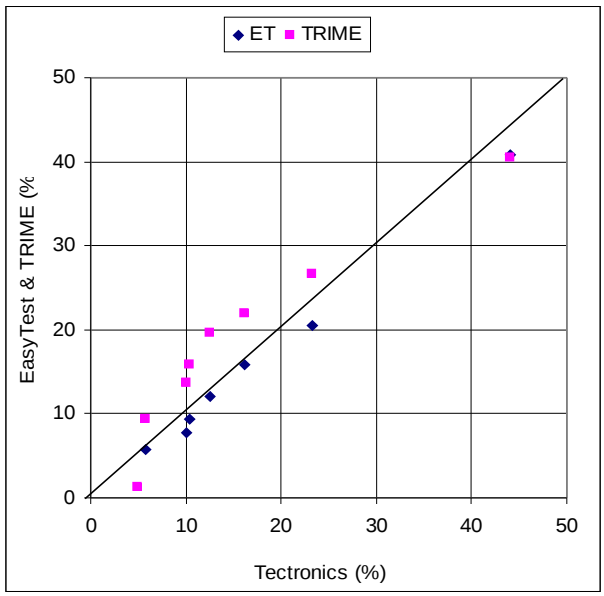

B

Figure 9.3.2: TRIME readings prior to sensor repair.

TRIME readings deviated in the medium-ranged values of θ in approximately 0.08 in comparison to other water content defining methods. This error was attributed to fail calibration parameters uploaded to the TRIME sensors.

Soil taken from Yatir site was oven dried until constant weight and divided to four samples with identical weight. The samples were packed into PVC containers of identical volume and distilled water was gradually added to reach θ of 0.13, 0.16, 0.19 and 0.42 . Three readings were taken with each instrument for every θ phase.

(A) TRIME, ET and TDR100 compared to gravimetrical measurements.

(B) TRIME and ET compared to Tektronics readings (regarded as true TDR).

TRIME intelligent soil water content sensor, IMKO Micromodultechnik, GmbH.

Easy Test (ET), Ltd., soil water and salinity monitoring device, Institute of Agrophysics, Polish Academy of Sciences.

TDR100, Campbell Scientific Inc., USA.

Tektronix. TDR cable tester.

A

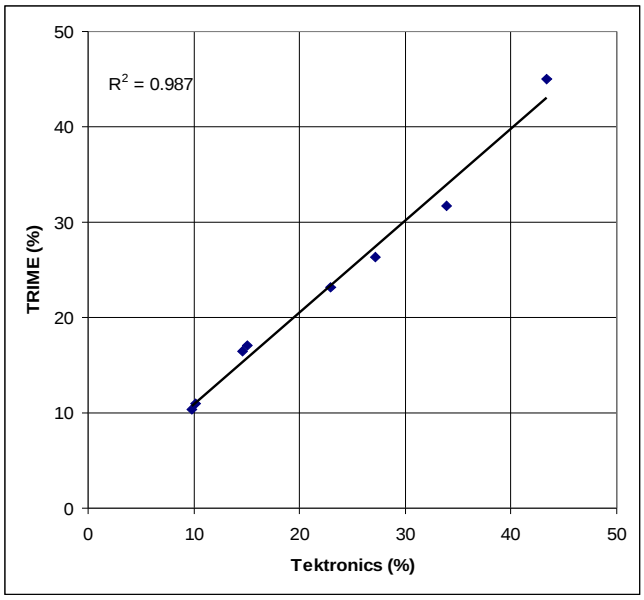

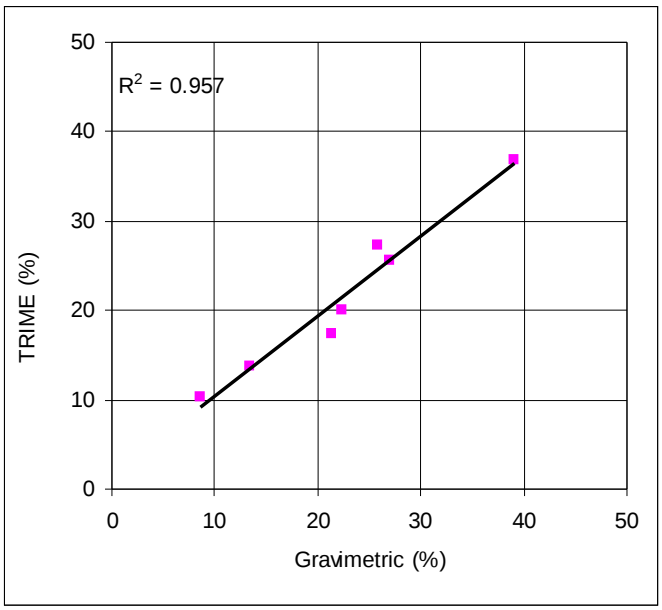

A

B

Figure 9.3.3: TRIME testing following sensor repair.

(A) TRIME compared to Tektronics readings in the lab.

(B) TRIME compared to gravimetric measurements. Samples were positioned at their terminal positions in the field.

Appendix 4

Equations for calculating shaded area according to solar altitude*

The solar declination δ (°) was calculated according to:

$$\delta = 23.45 \cdot \sin(DOY + 284) \cdot 360/365 \quad (9.4.1)$$

where DOY is the day of year (1-366).
The hour angle h (°) was calculated according to:

$$h = 360/24 \cdot (12 - T) \quad (9.4.2)$$

where T is the time of day (0-24). The hour angle was calculated daily for 12:00, which is the approximated standard time in which measurements of E were preformed.
Following, the solar altitude β (°) was calculated according to:

$$\sin\beta = \sin\lambda \cdot \sin\delta + \cos\lambda \cdot \cos\delta \cdot \cosh \quad (9.4.3)$$

where λ (°) is the latitude of Yatir (31°.249').
Crown length (CL) was calculated according to the averaged dimensions of the trees measured within the footprint (Table 2.1):

$$CL = \text{tree height} - \text{trunk height} \quad (9.4.4)$$

Shadow length (L) was calculated from the trigonometric ratio between β and tree CL:

$$L = CL/\tan\beta \quad (9.4.5)$$

L was not allowed to be lower than 4.6 m (crown width) or higher than 6.1 m (distance between trees), as above this length shadow coincide.
It was assumed that the area of the shade (S) was close to that of an ellipse:

$$S = \pi \cdot L/2 \cdot CW/2 \qquad (9.4.6)$$

where CW is the crown width (from average measured values, Table 2.1). The effect of the slope angle on the shadow area was neglected, as slopes within the footprint area are small.
Averaged shaded area was multiplied by the Yatir averaged tree density to define the forest floor shaded fraction (SF):

$$SF = S \cdot 300/10{,}000 \qquad (9.4.7)$$

* Eq. 1-3 from Jones, 1992.

References

Agam, N. and Berliner, P., R., 2006, Dew formation and water vapor adsorption in semi-arid environments — a review, Journal of Arid Environments 65: 572-590.

Agam, N., Berliner, P., R., Zangvil, A and Ben-Dor, E., 2004, Soil water evaporation during the dry season in an arid zone, Journal of Geophysical Research 109.

Aguilera, M., O. and Lauenroth, W., K., 1995, Influence of gap disturbances and type of microsites on seedling establishment, J. Ecol. 83: 87-97.

Allen, R., G., Pereira, L., S., Raes, D. and Smith, M., 1998, Crop evapotranspiration – guidelines for computing crop water requirements – FAO irrigation and drainage paper 56, FAO.

Allison, G., B., Barnes, C., J., Hughes, M., W., 1983, The distribution of deuterium and ^{18}O in dry soils 2. Exp. J. Hydrol. 64, 377–379.

Angert, A., Biraud, S., Bonfils, C., *et al*., 2005, Drier summers cancel out the CO_2 uptake enhancement induced by warmer springs, Proceedings of the National Academy of Sciences 102: 10823-10827.

Arnone, J. A., Obrist, D., 2003, A large daylight geodesic dome for quantification of whole-ecosystem CO2 and water vapour fluxes in arid shrublands, J. of Arid Environments 55: 629-643.

Aubinet, M., *et al*, 2000, Estimates of the annual net carbon and water exchange of forests: the EUROFLUX methodology, Advances in Ecological Research, vol. 30, Academic Press.

Baker, J. M. and Spaans, E. J. A., 1994, Measuring water exchange between soil and atmosphere with TDR-microlysimetry, Soil Sci., 158: 22-29.

Baldocchi, D. and Harley, P., 1995, Scaling CO_2 and water exchange from leaf to canopy-2, Plant, Cell and Environment, 18, 1157-1173.

Baldocchi, D. D. and Vogel, C. H, 1996, Energy and CO_2 flux densities above and below a temperate broad-leaved forest and a boreal pine forest, Tree Physiology 16: 5-16.

Baldocchi, D. D., Law, B. E. and Anthoni, P. M., 2000, On measuring and modeling energy fluxes above the floor of a homogeneous and heterogeneous conifer forest, Agricultural and Forest Meteorology 102: 187-206.

Baldocchi, D., Falge, E., Gu, L. *et al*., 2001, FluxNet: A new tool to study the temporal and spatial variability of ecosystem scale carbon dioxide, water vapor and energy flux densities, Bulletin Of The American Meteorological Society 82: 2415-3434.

Bar-Massada, A., Carmel, Y., Even Tzur, G., Grunzweig, J. And Yakir, D., 2006, Assessment of temporal changes in aboveground forest tree biomass using aerial photographs and allometric equations, Canadian Journal of Forest Research 36: 2585-2594.

Barrie, A. and Prosser, S., J., 1996, Automated analysis of light-element stable isotopes by isotope ratio mass spectrometry, Mass Spectrometry of Soils, Boutton, T., W. and Yamasaki, S. (Editors), Marcel Dekker Inc., 1-46.

Beerling, D., J. and Woodward, F., I., 1995, Leaf stable carbon isotope composition records increased water-use efficiency of C_3 plants in response to atmospheric CO_2 enrichment, Functional Ecology, 9, 394-401.

Belk, E., L., Markewitz, D., Rasmussen, T., C., Maklouf Carvalho, E., J., Nepstad, D., C. and Davidson, E., A., 2007, Modeling the effects of throughfall reduction on soil water content in a Brazilian Oxisol under a moist tropical forest, Water Resources Research 44.

Belnap, J., Welter, J., R., Grimm, N., B., Barger, N. And Ludwig, J., A., 2005, Linkages between microbial and hydrologic processes in arid and semiarid watersheds, Ecology 86(2): 298-307.

Ben-Asher, A. D., Matthias, A. D. and Warrick, A. W., 1983, Assessment of evaporation from bare soil by Infarred Thermometry, Soil Sci. Soc. Am. J. 47:185-191.

Bitan, A., and Rubin, S., 1991, Climatic atlas of Israel for physical and environmental planning and design, Ramot Publishers, Tel Aviv University, Tel Aviv.

Bonachela, S., Orgaz F., Villalobos, F. and Fereres E., 2001, Soil evaporation from drip-irrigated olive orchards, Irrigation Science 20: 65-71.

Boulet, G., Braud, I. and Vauclin, M., 1997, Study of the mechanisms of evaporation under arid conditions using a detailed model of the soil-atmosphere continuum: Applications to the EFEDA I experiment, Journal of Hydrology 193:114-141.

Braud, I., Noilhan, P., B., Bessemoulin, P., Mascart, P., Haverkamp, R. and Vauclin, M., 1993, Bare-ground surface heat and water exchanges under dry conditions: observations and parameterization, Boundary-Layer Meteorology 66: 173-200.

Breshears, D., D., Nyhan, J., W., Heil, C., E. and Wilcox, B., P., 1998, Effects of woody plants on microclimate in a semiarid woodland: soil temperature and evaporation in canopy and intercanopy patches, International Journal of Plant Science 159(6): 1010-1017.

Brugnoli, E., Scartazza, A. *et al*, 1998, Stable Isotopes, BIOS Scientific Publishers Limited, Bosher A. (Editor), 133-146.

Buckley, T. H, Farquhar, G. D. and Mott, K. A., 1999, Carbon-water balance and patchy stomatal conductance, Oecologia 118: 132-143.

Campbell, G., 1985, Soil Physics with BASIC, Transport Models for Soil-Plant Systems, Elsevier, New York.

Chandler, D. G., Seyfried, M. M. and McNamara, J. P., 2004, Field calibration of Water Content Reflectometers, Soil Sci. Soc. Am. J. 68: 1501-1507.

Chanzy, A. and Bruckler, L., 1993, Significance of soil surface moisture with respect to daily bare soil evaporation, Water Resources Research 29(4): 1113-1125.

Chen, F. and Dudhia J., 2001, Coupling an advanced land surface – hydrology model with the Penn State –NCAR MM5 modeling system part I: Model implementation and sensitivity, Mon. Weather Rev., 129, 569– 585.

Clark, I. and Fritz, P., 1997, Environmental Isotopes in Hydrology, CRC Press, 29.

Cohen, Y., 1994, Thermoelectric methods for measurement of sap flow in plants, Stenhill, G. (Ed.), Advances in Bioclimatology, Vol. 3, Springer, Heidelberg, Germany, pp. 63-88.

Craig, H. and Gordon, L. I., 1965, Deuterium and oxygen-18 variations in the ocean and the marine atmosphere, Proceedings of the Conference on Stable Isotopes in Oceanographic Studies and Paleotemperatures, Tongiorgi E. (ed.), Laboratory of Geology and Nuclear Science.

Cramer, W. *et al*, 2001, Global response of terrestrial ecosystem structure and function to CO_2 and climate change: Results from six dynamic global vegetation models, Global Change Biology, 7, 357-373.

Davidson, E. A., Savage, K., Verchot, L. V. and Navarro, R., 2002, Minimizing artifacts and biases in chamber-based measurements of soil respiration, Agricultural and Forest Meteorology 113: 21-37.

Denmead, O. T., 1984, Plant physiological methods for studying evaporation: problems of telling the forest from the trees, Agric. Water Manage. 8: 167-189.

Denmead, O., T., Dunin, F., X., Wong, S., C. and Greenwood, E., A., N., 1993, Measuring water use efficiency of Eucalypt trees with chambers and micrometeorological techniques, Journal of Hydrology 150: 649 664.

Diawara, A., Loustau, D. and Berbigier, P., 1991, Comparison of two methods for estimating the evaporation of a Pinus pinaster (Ait.) stand: sap flow and energy balance with sensible heat flux measurements by an eddy covariance method, Agricultural and Forest Meteorology 54: 49-66.

Dugas, W., A.., Reicosky, D., C. and Kiniry, J., R., 1997, Chamber and micrometeorological measurements of CO_2 and H_2O fluxes for three C_4 grasses, Agricultural and Forest Meteorology 83: 113- 133.

Dunin, F., X. and Greenwood, E., A., N., 1986, Evaluation of the ventilated chamber for measuring evaporation from a forest, Hydrological Processes 1(1): 47-62.

Ehleringer, J., R. and Cerling, T., E., 1995, Atmospheric CO_2 and the ratio of intercellular to ambient CO_2 concentrations in plants, Tree Physiology, 15, 105-111.

Farquhar, G., D., O'Leary, M., H, and Berry, J., L., 1982, On the relationship between carbon isotope discrimination and the intercellular carbon dioxide concentration in leaves, Australian Journal Of Plant Physiology, 9, 121-137.

Ferretti, D. F., Pendall, E., Morgan, J. A., Nelson, J. A., LeCain, D. and Mosier, A. R., 2003, Partitioning Evapotranspiration fluxes from a Colorado grassland using stable isotopes: seasonal variations and ecosystem implication of elevated atmospheric CO_2, Plant and Soil 254: 291-303.

Field, C., B., Jackson, R., B. and Mooney, H., A., 1995, Stomatal responses to increased CO_2: implications from the plant to the global scale, Plant, Cell and Environment, 18, 1214-1225.

Flanagan, L., B., Comstock, J., P., Ehleringer, J., R., 1991. Comparison of modeled and observed environmental influences on the stable oxygen and hydrogen isotope composition of leaf water in Phaseolus vulgaris L. Plant Physiol. 96, 588–596.

Forestel, H., 1996, Hydrogen and Oxygen isotopes in soil water: use of ^{18}O and D in soil water to study the soil-plant-water system, Mass Spectrometry of Soils, Boutton, T., W. and Yamasaki, S. (Editors), Marcel Dekker Inc., 285-310.

Garratt, J., R., 1993, Sensitivity of climate simulations to land surface and atmospheric boundary layer treatments – a review, Journal of Climatology 6: 419-449.

Gervois, S., Ciais, P., Brisson, N., *et al*., 2008, Carbon and water balance of European croplands throughout the 20th century, Global Biochemical Cycles 22.

Gockede, M., Foken, T., Aubinet M., *et al*., 2007, Quality control of CarboEurope flux data – Part I: Footprint analyses to evaluate sites in forest ecosystems, Biogeosciences Discussions 4: 4025–4066.

Granier, A., Breda, N., Biron, P. And Villette, S., 1999, A lumped water balance model to evaluate duration and intensity of drought constraints in forest stands, Ecological Modeling 116: 269-283.

Granier, A., Reichstein, M., Breda, N., *et al*., 2007, Evidence for soil water control on carbon and water dynamics in European forests during the extremely dry year: 2003, Agricultural and Forest Meteorology 143: 123-145.

Grau, A., 1995. A closed chamber technique for field measurement of gas exchange of forage canopies, New Zealand J. Agric. Res. 38: 71-77.

Greenwood, E., A., N. and Beresford, J., D., 1979, Evaporation from vegetation in landscapes developing secondary salinity using the ventilated-chamber technique, Journal of Hydrology 42: 369-382.

Grelle, A., Lundberg, A., Lindroth, A., Moren, A. and Cienciala, E., 1997, Evaporation components o a boreal forest: variations during the growing season, Journal of Hydrology 197: 70-87.

Groisman, P., Y., Knight, R., W., Karl, T., R., *et al*., 2004, Contemporary changes of the hydrological cycle over the contiguous United States: trends derived from in situ observation, Journal of Hydrometeorology 5: 64-85.

Grunzweig, J. M., Lin, T., Rotenberg, E., Schwartz, A. and Yakir, D., 2003, Carbon sequestration in arid-land forest, Global Change Biology 9: 791-799.

Guo Yu Qiu, Ben-Asher, J., Yano, T. and Momii, K.,1999, Estimation of soil evaporation using the differential temperature method, Soil Sci. Soc. Am. J., 63.

Guswa, M., A., 2002, Models of soil moisture dynamics in ecohydrology: A comparative study, Water Resources Research 38.

Healy, R., W., Striegl, R., G., Russell, T., F., Hutchinson, G., L. and Livingston, G., P., 1996, Numerical evaluation of static-chamber measurements of soil-atmosphere gas exchange: identification of physical processes, Soil Sci. Soc. Am. J. 60: 740-747.

Hetherington, A., L. and Woodward, F., I., 2003, The role of stomata in sensing and driving environmental change, Nature 424: 901-908.

Hillel, D., 1972, Soil and water; physical principles and processes, Academic Press.

Houghton, J., T., Jenkins, G., J. and Ephraums, J., J. (Editors), 1990, Climate Change, The IPCC Scientific Assessment, Cambridge University Press.

Hutchinson, G. L. and Livingston, G. P., 2001, Vents and seals in non-steady-state chambers used for measuring gas exchange between soil and the atmosphere, Eur. J. Soil Sci. 52:675-682.

Huxman, T., Wilcox, B., P., Breshears, D., D., *et al*, 2005, Ecohydrological implications of woody plant encroachment, Ecology 86: 308-318.

IPCC 2007, IPCC Climate Change: The Physical Science Basis.

Iritz, Z., Lindroth, A. and Gardenas, A., 1997, Open ventilated chamber system for measurements of H_2O and CO_2 fluxes from the soil surface, Soil Technology 10: 169-184.

Jackson, R., B., Canadell, J., Ehleringer, J. R., Mooney, H., A., Sala, O., E. and Schulze, E., D., 1996, A global analysis of root distributions for terrestrial biomes, Oecologia 108: 389-411.

Jacquemin, B. and Noilhan, J., 1990, Sensitivity study and validation of a land surface parameterization using the HAPEX-MOBILHY data set, Boundary-Layer Meteorology 52: 93-134.

Jenerette, G., D. and Lal, R., 2005, Hydrologic sources of carbon cycling uncertainty throughout the terrestrial-aquatic continuum, Global Change Biology 11: 1873-1882.

Jones, H., G., 1992, Plants and microclimate, Cambridge University Press.

Jones, S. B., Wraith, J. M. and Or, D., 2002, Time domain reflectometry measurement principles and application, Hydrological Processes 16: 141-153.

Katata, G., Nagai, H., Ueda. H., Agam, N. and Berliner, P., R., 2007, Development of a land surface model including evaporation and adsorption processes in the soil for the land–air exchange in arid regions, Journal of Hydrometeorology 8: 1307-1324.

Kauppi, P., E., Ausubel, J., H., Fang, J., *et al*, 2006, Returning forests analyzed with the forest identity, Proceedings of the National Academy of Sciences 103: 17574-17579.

Keeling, C., D., 1958. The concentration and isotopic abundance of atmospheric carbon dioxide in rural areas. Geochim. Cosmochim. Acta 13, 322–334.

Kelliher, F. M., Lloyd, J., Arneth, A. *et al*., 1998, Evaporation from a central Siberian pine forest, J. Hydrol. 205: 279-296.

Kite, G., W. and Droogers, P., 2000, Comparing evapotranspiration estimates from satellites, hydrological models and field data, Journal of Hydrology 229, 1-2.

Kosmas, C., Marathianou, M., Gerontidis, St., Detsis., V., Tsara., M. and Poesen, J., 2001, Parameters affecting water vapor adsorption by the soil under semi-arid climatic conditions, Agricultural Water Managements 48:61-78.

Kramer, P. J. and Boyer, J. S., 1995, Water Relations of Plants and Soils, Academic Press.

Kurk, S. and A., Small, E., E., 2004, Dynamics of evapotranspiration in semiarid grassland and shrubland ecosystems during the summer monsoon season, central New Mexico, Water Resources Research (40).

Kurk, S. and A., Small, E., E., 2007, Soil moisture variations and ecosystem-scale fluxes of water and carbon in semiarid grassland and shrubland, Water Resources Research 43.

Kurpius, M., R., Panek, J., A., Nikolov, N., T., McKay, M. and Goldstein, A., H., 2003, Partitioning of water flux in a Sierra Nevada ponderosa pine plantation, Agricultural and Forest Meteorology 117: 173–192.

Kutilek, M. and Nielsen, D. R., 1994, Soil Hydrology, Catena GeoEcology Publications.

Kuuluvainen T. and Pukkala T., 1989, Simulation of within-tree and between-tree shading of direct radiation in a forest canopy: effect of crown shape and sun elevation, Ecological Modelling 49: 89-100.

Lai, C., T., Katul, G., Oren, R., Ellsworth, D. and Schafer, K., 2000, Modeling CO_2 and water vapor turbulent flux distributions within a forest canopy, Journal Of Geophysical Research-Atmospheres, 105, 26333-26351.

Laronne, J., B., Alexandrov, Y., Chocron, M., Guertin, D., G. and Goodrich, D., C., 2007, Reducing runoff / soil erosion by afforestation in a semi arid area, report to LALC.

Law, B., E., Falge, E., Gu, L., *et al*., 2002, Environmental controls over carbon dioxide and water vapor exchange of terrestrial vegetation, Agricultural and Forest Meteorology 113: 97-120.

Lee, D. and Veizer, J., 2003, Water and carbon cycles in the Mississippi River basin: Potential implications for the Northern Hemisphere residual terrestrial sink, Global Biogeochemical Cycles, 17(2): 1-17.

Liu, H., J., Cohen, S., Tanny, J., Lemcoff, J., H. and Huang, G., 2008, Transpiration estimation of banana (Musa sp.) plants with the thermal dissipation method, Plant Soil 308:227–238.

Mahfouf, J., F. and Noilhan, J, 1991, Comparative study of various formulations of evaporation from bare soil using in situ data, Journal of Applied Meteorology 30: 1354-1359.

Martens, S., N., Breshears, D., D., Meyer, C., W., 2000, Spatial distributions of understory light along the grassland - forest continuum: effects of cover, height and spatial pattern of tree canopies, Ecological Modeling 126: 79-93.

Maseyk, K., 2006, Ecophysiological and phonological aspects of *Pinus halepensis* in an arid-Mediterranean environment, Thesis for the degree Doctor of Philosopy, Weizmann Institute of Science.

Maseyk, K., Grunzweig, J., M., Rotenberg, E. and Yakir, D., 2008, Respiration acclimation contributes to high carbon-use efficiency in a seasonally dry pine forest, Global Change Biology 14(7): 1553-1567.

McLeod, M., K., Daniel, H., Faulkner, R., Murison, R., 2004, Evaluation of an enclosed portable chamber to measure crop and pasture actual evapotranspiration at small scale, Agricultural Water Management 67: 15–34.

Milly, P., C., D., Wetherald, R., T, Dunne, K., A., and Delworth, T., L., 2002, Increasing risk of great floods in a changing climate, Nature 415: 514-517.

Moldrup, P., Olesen, T., Gamst, J., Schjønning, P., Yamaguchi, T. and Rolston, D., E., 2000, Predicting the Gas Diffusion Coefficient in Repacked Soil: Water-

Induced Linear Reduction Model, Soil Science Society of America Journal (64):1588-1594.

Monteith, J., L., 1981, Evaporation and surface temperature, Quarterly Journal of the Royal Meteorological Society, 107.

Monteith, J., L., 1988, Does transpiration limit the growth of vegetation or vise versa? Journal of Hydrology 100: 57-68.

Morecroft, M., D., Taylor, M., E. and Oliver, H., R., 1998, Air and soil microclimates of deciduous woodland compared to an open site, Agricultural and Forest Meteorology 90: 141-156.

Moreira, M. Z., Scholz, F. G. *et al.*, 2003, Hydraulic lift in a neotropical savanna, Functional

Nicolau, J., M., Sole-Benet, A., Puigdefabregas, J. and Gutierrez, L., 1996, Effects of soil and vegetation on runoff along a catena in semi-arid Spain, Geomorphology 14: 297-309.

Ninari, N. and Berliner, P., R., 2002, The role of dew in the water and heat balance of bare loess soil in the Negev Desert: quantifying the actual dew deposition on the soil surface, Atmospheric Research, 64.

Nobel, P. S., 1999, Plant Physiology, Academic Press.

Noy-Meir, I., 1973, Desert ecosystems: environment and producers, Annual Review of Ecology and Systematic 4: 25-51.

Ohmura, A. and Wild, M., 2002, Is the hydrological cycle accelerating? Sience 298:1345-1346.

Pales, J., C. and Keeling, C., D., 1965, Concentration of atmospheric carbon dioxide in Hawaii, Journal of Geophysical Research 70(24): 6053.

Parmesan, C., and Yohe, G., 2003, A flobally coherent fingerprint of climate change impact across natural systems, Nature 421: 37-42.

Parton, W., Holland, E., Del Grosso, S., *et al*., 2001, Generalized Model for NOx and N_2O emissions from soils, Journal of Geophysical Research 106: 17,403-17,419.

Penman, H., L., 1948, Natural evaporation from open water, bare soil and grass, Proc. R. Soc. Lond. A 193: 120-145.

Philip, J., R., 1957, Numerical solution of equations of the diffusion type with diffusivity concentration – dependent, Aust. J. Phys. 10: 29-42.

Pickering, N.B., Jones, J.W. and Boote, K.J., 1993. Evaluation of the portable chamber technique for measuring canopy gas exchange by crops. Agric. For. Meteorol. 63: 239-254.

Pierrehumbert, R., 2002, The hydrological cycle in deep-time climate problems, Nature 419: 191-198.

Porporato, A., D'Odorico, P., Laio, F., Ridolfi, L. and Rodriguez-Iturbe, I., 2002, Ecohydrology of water-controlled ecosystems, Advances in Water Resources 25: 1335-1348.

Pumpanen, J. Kolari, P, Ilvesniemi, H., *et al.*, 2004, Comparison of different chamber techniques for measuring soil CO_2 efflux, Agricultural and Forest Meteorology 123: 159-176.

Ramirez, D., A., Bellot, J., Domingo, F. and Blasco, A., 2007, Can water responses in *Stipa tenacissima* L. during the summer season be promoted by non-rainfall water gains in soil? Plant Soil 291: 67-79.

Rana, G. and Katerji, N., 2000, Measurement and estimation of actual evapotranspiration in the field under Mediterranean climate: a review, European Journal of Agronomy, 13, 125-153.

Reichstein, M., Tenhunene, J., D. *et al*., 2002, Severe drought effect on ecosystem CO_2 and H_2O fluxes at three Mediterranean evergreen sites: revision of current hypotheses?, Global Change Biology, 8, 999-1017.

Reichstein, M., Viovy, N., Granier, A., *et al*., 2005, Europe-wide reduction in primary productivity caused by the heat and drought in 2003, Nature 437: 529-533.

Reicosky, D., C., Sharratt, B, S., Ljungkull, J., L. and Baker, D., G., 1983, Comparison of alfalfa evapotranspiration measured by weighing lysimeter and a portable chamber, Agricultural Meteorology 28(3): 205-211.

Robinson, D., A., Jones, S., B, *et al*., 2003, A review of advances in dielectric and electrical conductivity measurement in soils using Time Domain Reflectometry, Vadose Zone Journal, 2, 444-475.

Rodriguez-Iturbe, I., 2000, Ecohydrology: A hydrologic perspective of climate-soil-vegetation dynamics, Water Resources Research 36: 3-9.

Roupsard, O., Bonnefond, J.M., Irvine, M., 2006, Partitioning energy and evapo-transpiration above and below a tropical palm canopy, Agricultural and Forest Meteorology 139: 252-268.

Salvucci, G., D., 1997, Soil and moisture independent estimation of stage-two evaporation from potential evaporation and albedo or surface temperature, Water Resources Research 33(1): 111-122.

Schafer, K., V., R., Oren, R., Lai, C., T. and Katul, G., G., 2002, Hydrologic balance in an intact temperate forest ecosystem under ambient and elevated atmospheric CO_2 concentrations, Global Change Biology, 8, 895-911.

Schiller, G. and Cohen, Y., 1995, Water regime of a pine forest under a Mediterranean climate, Agriculture and Forest Meteorology, 74, 181-193.

Schiller, G. and Cohen, Y., 1998, Water balance of Pinus halepensis Mill. afforestation in an arid region, Forest Ecology and Management, 105, 121-128.

Schlesinger, W. H, Reynolds, J. F. *et al*., 1990, Biological feedbacks in global desertification, Science 247: 1043-1048.

Schmugge, T. J., and. Andre J., C., 1991, Land surface evaporation — measurement and parameterization, Springer-Verlag, NewYork.

Scott, R. L., Shuttleworth, W. J., Keefer, T. O. and Warrick, A., W., 2000, Modeling multiyear observations of soil moisture recharge in the semiarid American Southwest, Water Resources Research 36: 2233-2247.

Scott, R., L., Huxman, T., E., Cable W., L. and Emmerich, W., E., 2006, Partitioning of evapotranspiration and its relation to carbon dioxide exchange in a Chihuahuan Desert shrubland, Hydrological Processes 20: 3227–3243.

Seyfried, S. and Wilcox, B., P., 1995, Scale and the nature of spatial variability: field examples having implication for hydrologic modeling, Water Resources Research, 31.

Seyfried, M., S., Schwinning, S., Walvoord, M., A., Pockman, W., T., Newman, B., D., Jackson, R., B. and Phillips, F., M., 2005, Ecohydrological control of deep drainage in arid and semiarid regions, Ecology 86(2): 277-287.

Shachnovich, Y., Berliner, P., R. and Bar P., 2008, Rainfall interception and spatial distribution of throughfall in a pine forest planted in an arid zone, Journal of Hydrology 349: 168- 177.

Sharon, D., 1972, The spottiness of rainfall in a desert area, Journal of Hydrology, 17, 161-175.

Shuttleworth, W., 2007, Putting the 'vap' into evaporation, Hydrology and Earth System Sciences 11: 210-244.

Simonin, K., Kolb, T., E., Montes-Helu, M. and Koch, G., W., 2007, The influence of thinning on components of stand water balance in a ponderosa pine forest stand during and after extreme drought, Agricultural and Forest Meteorology 143: 266-276.

Smith, S., T., Travis, E., H. *et al.*, 2000, Elevated CO_2 increases productivity and invasive species success in an arid ecosystem, Nature, 408, 79-81.

Sprintsin, M., Karnieli, A., Berliner, P., Rotenberg, E., Yakir, D. and Cohen, S., 2007, The effect of spatial resolution on the accuracy of leaf area index estimation for a forest planted in the desert transition zone, Remote Sensing of Environment 109: 416-428.

Stannard, D., I. and Weltz, M., A., 2006, Partitioning evapotranspiration in sparsely vegetated rangeland using a portable chamber, Water Resources Research 42.

Steduto, P., Cetinkoku, O., Albrizio, R. and Kanber, R., 2002, Automated closed-system canopy-chamber for continuous field-crop monitoring of CO_2 and H_2O fluxes, Agricultural and Forest Meteorology 111: 171-186.

Swanson, R., H. and Whitfield, D., W., A., 1981. A numerical analysis of heat pulse velocity theory and practice, J. Exp. Bot. 32: 321-239.

Topp, G. C., Davis, H. L. and Annan, A. P, 1980, Electromagnetic determination of soil water content: measurements in coaxial transmission lines, Water Reas. Res. 16: 574-582.

UNEP, 1992, World Atlas of Desertification, UNEP.

Van Wijk, M., T., Dekker, S., C., Bouten, W., Kohsiek, W. and Mohren, G., M., J., 2001, Simulation of carbon and water budgets of a Douglas-fir forest, Forest Ecology and Management, 145, 229-241.

Verhoef, A., Diaz-Espejo, A., Knight, J., R., Villagarcia, L., and Fernandez, J. E., 2006, Adsorption of water vapor by bare soil in an olive grove in southern Spain, Journal of Hydrometeorology 7(5):1011-1027.

Wang, K., Wang, P., Li, Z., Cribb, M. and Sparrow, M., 2007, A simple method to estimate actual evapotranspiration from a combination of net radiation, vegetation index, and temperature, Journal of Geophysical Research 112.

Wang, X., F., Yakir, D., 1995. Temporal and spatial variations in oxygen-18 content of leaf water in different plant species. Plant Cell Environ. 18, 1377–1385.

Wang, X., F. and Yakir, D., 2000, Using stable isotopes of water in evapotranspiration studies, Hydrological Processes, 14, 1407-1421.

Waring, R., H. and Schlesinger, W., H., 1985, Forest Ecosystems, Academic Press.

Webb, R. S. and Rosenzweig, C. E., 1993, Specifying land surface characteristics in general circulation models: soil profile data set and derived water-holding capacities, Global Biochem. Cycles, 7:97-108.

Williams, D., G., Cable, W., Hultine, K., *et al*., 2004, Evapotranspiration components determined by stable isotope, sap flow and eddy covariance techniques, Agricultural and Forest Meteorology 125: 241-258.

Wilson K., B., Hanson, P., J. and Baldocchi, D., D., 2000, Factors controlling evaporation and energy partitioning beneath a deciduous forest over an annual cycle, Agricultural and Forest Meteorology 102: 83–103.

Wilson, K., B., Hanson, P., J., Mulholland, P., J., Baldocchi, D., D. and Wullschleger, S., D., 2001, A comparison of methods for determining forest evapotranspiration

and its components: sap-flow, soil water budget, eddy covariance and catchment water balance, Agricultural and Forest Meteorology 106: 153–168.

Wullschleger, S, Meinzer, F., C. and Vertessy, R., A., 1998, A review of whole-plant water use studies in trees, *Tree Physiology* 18, 499-512.

Wythers K. R., Lauenroth W. K., Paruelo J. M., 1999, Bare-soil evaporation under semiarid field conditions, Soil Sci. Soc. Am. J. 63 (5): 1341-1349.

Yair, A. and Danin, A., 1980, Spatial variations in vegetation as related to the soil moisture regime over an arid limestone hillside, Northern Negev, Israel. *Oecologia*, 47.

Yair, A. and Raz-Yassif, N., 2004, Hydrological processes in a small arid catchment: scale effects of rainfall and slope length, Geomorphology 61: 155-169.

Yakir, D. and Stenberg, L., S., L., 2000, The use of stable isotopes to study ecosystem gas exchange, Oecologia, 123: 297-311.

Yang, Z., Dickinson, L., R., E., Shuttleworth, W., J. and Shaikh, M., 1998, Treatment of soil, vegetation and snow in land surface models: A test of the Biosphere-Atmosphere Transfer Scheme with the HAPEX-MOBILHY, ABRACOS and Russian data, J. Hydrol. 212–213: 109–127.

Yepez, E. A., Williams, D. G., Scott, R. L. and Lin, G., 2003, Partitioning overstory and understory Evapotranspiration in a semiarid savanna woodland from the isotopic composition of water vapor, Agricultural and Forest Meteorology 119: 53-68.

Yepez, E. A., Williams, D. G., Scott, R. L. and Lin, G., 2003, Partitioning overstory and understory Evapotranspiration in a semiarid savanna woodland from the isotopic composition of water vapor, Agricultural and Forest Meteorology 119: 53-68.

Zhang, L., Dawes, W., R. and Walker, G., R., 2001, Response of mean annual evapotranspiration to vegetation changes at catchment scale, Water Resources Research 37: 701-708.